Dissertation

submitted to the

Combined Faculties for the Natural Sciences and for Mathematics

of the Ruperto-Carola University of Heidelberg, Germany

for the degree of

Doctor of Natural Sciences

Presented by

MSc Taslima Nahar

Born in: Tangail, Bangladesh

Oral-examination: 19.10.2017

ROLE OF THE LIM-DOMAIN PROTEINS LPP AND ZYXIN IN HYPERTENSION-INDUCED CARDIOVASCULAR REMODELING

Referees

Prof. Dr. Markus Hecker

Prof. Dr. Thomas Wieland

Table of Contents

List of figures

List of abbreviations

ACF	Adult cardiac fibroblast	LATS	Large Tumor Suppressor Kinase 1
ACLP	Aortic carboxypeptidase like protein	LIM	Lin11, Isl-1, Mec-3
AP-1	Activator protein 1	LIMD1	LIM domain-containing protein 1
APEG-1	Aortic preferentially expressed protein-1	LPA2	Lysophosphatidic acid-2
Ang II	Angiotensin II	MEF2C	Myocyte enhancer factor-2 C
CFBs	Cardiac fibroblasts	Mena	Mammalian Enabled
CMs	Cardiomyocytes	MGP	Matrix gla protein-1
CO	Cardiac output	MLL	Mixed lineage leukaemia
CRBP-2	Retinol-binding protein-2	miRISC	miRNA-mediated silencing complex
CRP-2	C-reactive protein-2	mmHg	Millimeter of mercury
DAPI	4', 6-diamidino-2-phenylindole	MMP	Matrix metalloproteinase
DOCA	Deoxycorticosterone acetate	MRTFA	Myocardin related transcription factor-A
DDR 2	Discoidin domain receptor 2	NES	Nuclear export signal
EC	Endothelial cells	NF-kB	Nuclear factor-κB
ECG	Electrocardiogram	PAGE	Polyacrylamide gel electrophoresis
ECM	Extracellular matrix	PDGF	Platelet derived growth factor
EF	Ejection fraction	PALX	parasternal long axis view (PLAX)
EFs	Embryonic fibroblasts	pRB	Retinoblastoma protein
Ena	Enabled	PRR	Proline-rich region
FA	Focal adhesion	SDS	sodium dodecyl sulfate
FBs	Fibroblasts	SMA	Smooth muscle α-actin
FCS	Foetal bovine serum	SM-MHC	Smooth muscle myosin heavy chain
FS	Fractional shortening	STAT1	Signal transducer and activator of transcription-1
FSP-1	Fibroblast specific protein -1	SV	Stroke volume
GFP	Green fluorescent protein	TIMPs	Tissue inhibitors of metalloproteinase
HMGA2	High mobility group A2	TGF-β	Transforming growth factor beta
HR	Heart rate	TNF-α	Tumor necrosis factor alpha
IBF	Interfaculty Biomedical Facility	TRIP6	Thyroid receptor interacting partner 6
ICAM-1	Intercellular adhesion molecule-1	tTG 2	Tissue transglutaminase 2
IF	Immunofluorescence	VASP	Vasodilator stimulated phosphoprotein
IGF-1	Interferon gamma 1	VSMC	Vascular smooth muscle cells
IL-1β	Interleukin 1 beta	WHO	World Health Organization
JNK	c-Jun N-terminal kinases	WTIP	Wilm's tumor protein 1-interacting protein
ko	knockout	YAP	Yes Associated Protein

Zusammenfassung

Bluthochdruck (Hypertonie), also ein chronischer und dauerhafter Anstieg des Blutdrucks, ist ein beeinflussbarer Risikofaktor z. B. für die koronare Herzkrankheit, den hämorrhagischen Schlaganfall oder eine terminale Niereninsuffizienz. Trotz der wichtigen pathophysiologischen Rolle der Hypertonie sind die zellulären Mechanismen beim Entstehen der Erkrankung noch unklar. Während der Hypertonie sind die glatten Gefäßmuskelzellen (*vascular smooth muscle cells*, VSMCs) einer erhöhten Wandspannung ausgesetzt. Dies führt zu einem Wechsel des Phänotyps der VSMCs, um dem übermäßigen Anstieg der Wandspannung entgegenzuwirken und schließlich den Tonus des Gefäßes wieder herzustellen. Auf zellulärer Ebene führt eine übermäßige Dehnung zur Translokation des als Mechanotransducer fungierenden Proteins Zyxin von den fokalen Adhäsionen zu den Stressfasern und zu einem gewissen Teil auch in den Zellkern, wo es indirekt über MRTF-A (*myocardin-related transcription factor-A*) die Expression mechanosensitiver Gene reguliert. Aus 3 Monate alten Zyxin-Knockout (Zyxko)-Mäusen isolierte VSCMs zeigten *in vitro* einen synthetischen Phänotyp. Dagegen wiesen nur sehr alte (18 Monate), mit Desoxycorticosteron-Azetat (DOCA)-Salz behandelte Zyxko-Mäuse einen deutlichen vaskulären Phänotyp auf, der z. B. durch einen fehlenden Blutdruckanstieg, einen niedrigeren Widerstandsindex, d. h. dem Widerstand in den periphären Blutgefäßen, und eine veränderte Zusammensetzung der extrazellulären Matrix (*extracellular matrix*, ECM) charakterisiert ist. Die Altersabhängigkeit des *in vivo*-Phänotyps lässt einen kompensatorischen Einfluss anderer Proteine mit LIM-Domäne aus der Zyxin-Familie vermuten.

Deshalb wurde zunächst analysiert, ob LPP (*lipoma preferred partner*) oder TRIP6 (*thyroid receptor interacting partner 6*) beim Bluthochdruck-induzierten arteriellen Umbauprozess den Verlust von Zyxin kompensieren kann. Wie Zyxin transloziert auch LPP, aber nicht TRIP6 bei supra-physiologischer Dehnung *in vitro* von den fokalen Adhäsionen vor allem an die Aktin-Stressfasern und in den Nukleus. Interessanterweise nimmt in den Arterien sehr alter Zyxko Mäuse nur LPP auf Proteinebene ab. Aus 3 Monate alten Lppko-Mäusen isolierte VSMCs glichen funktionell dem synthetischen Phänotyp von aus gleichaltrigen Zyxko-Mäusen isolierten VSMCs. Auch wenn die VSMCs junger (3 Monate) Lppko-Mäuse bei einer experimentell induzierten Hypertonie keinen synthetischen Phänotyp aufweisen, könnte der verminderte Widerstandsindex auf eine vaskuläre Dysfunktion bereits in diesem jungem Alter hinweisen. Die Überexpression von LPP in VSMCs aus Zyxko-Mäusen oder Zyxin in VSMCs aus Lppko-Mäusen konnte den Verlust der jeweiligen anderen Funktion vollständig kompensieren und den kontraktilen VSMC-Phänotyp wieder herstellen. Diese Ergebnisse charakterisieren Zyxin als neuen Regulator des Phänotyp-Wechsels bei VSMCs während des Bluthochdruck-induzierten arteriellen Umbaus, wobei LPP Zyxin unterstützen kann, um diesen Wechsel zu verhindern.

Anders als VSCMs reagieren terminal differenzierte Kardiomyozyten (*cardiomyocytes*, CMs) auf arterielle Hypertension durch eine Vergrößerung der Zelle und normalisieren so die Wandspannung nach dem Gesetz von Laplace. Der auf diese kompensatorische Hypertrophie folgende Verlust von CMs und die übermäßige Ablagerung von ECM-Proteinen durch kardiale Fibroblasten (cadriac fibroblast, CFBs) führen zu einer kardialen Dysfunktion. Der Mechanotransducer Zyxin wird offenbar

für das Überleben der CMs benötigt. Zweites Ziel dieser Arbeit war daher zu analysieren, wie sich das Fehlen von Zyxin auf die kardiale Funktion bei DOCA-Salz induzierter experimenteller Hypertonie auswirkt. Tatsächlich zeigten 12 Monate alte Zyxko-Mäuse eine möglicherweise auf eine exzessive kardiale Fibrose und die daraus resultierende Versteifung des Herzens zurückzuführende kardiale Dysfunktion. Um diesen Befund zu bestätigen, wurde ein kardiales Fibrose-Modell etabliert, bei dem 3, 6 und 12 Monate alte Zyxko- und Wildtyp (WT)-Mäuse über eine implantierte osmotische Minipumpe mit einer hohen Dosis Angiotensin II (Ang II) oder physiologischer Salzlösung behandelt wurden. In diesem Modell zeigten 3 Monate alte, unbehandelte Zyxko-Mäuse im Vergleich zu gleichaltrigen Kontrolltieren eine verminderte diastolische, aber unveränderte systolische Funktion. Durch die Behandlung mit Ang II verschlechterte sich die systolische kardiale Funktion fortschreitend mit steigendem Alter der Versuchstiere, was mit einer altersabhängigen verstärkten Kollagen-Einlagerung im Herzen einherging. Der Einfluss von Ang II auf die interstitielle und perivaskuläre kardiale Fibrose war in WT-Mäusen gleichen Alters deutlich weniger ausgeprägt, was auf eine fortschreitende restriktive Kardiomyopathie in Zyxko-Mäusen in diesem Modell hinweist.

Um für die ausgeprägte kardiale Fibrose in Zyxko-Mäusen verantwortliche Schlüsselmoleküle zu identifizieren, wurde die Expression pro-fibrotischer Gene in adulten kardialen Fibroblasten (*adult cardiac fibroblasts*, ACFs) von Zyxko- oder WT-Mäusen untersucht, die *in vitro* mit TGF-β1 (*transforming growth factor-β1*) stimuliert wurden. Die starke Expression von CTGF (*connective tissue growth factor*), Kollagen I und III sowie der Lysyloxidase (LOX) in den ACFs der Zyxko-Mäuse unterstützt die Vermutung, dass die kardialen Fibroblasten zur verstärkte Ausbildung von Narbengewebe in den Herzen dieser Tiere beitragen. Da LOX durch die Vernetzung von Kollagen die Bildung unlöslicher Kollagen-Ablagerungen im Herzen verstärkt, ist es möglich, dass dies zusammen mit der erhöhten Synthese von Kollagen I und III maßgeblich für die Entstehung der übermäßigen kardialen Fibrose und somit auch für die kardiale Dysfunktion der Zyxko-Mäuse verantwortlich ist. Ob die Altersabhängigkeit dieses kardialen Phänotyps ähnlich wie die des vaskulären mit der funktionellen Kompensation zwischen Zyxin und LPP in den CFBs oder in den CMs selbst verbunden ist, muss noch untersucht werden. Dennoch ist es wahrscheinlich, dass ein Fehlen von Zyxin zu einer veränderten CM-ECM-Interaktion führt, die die Apoptose von Kardiomyocyten und in Folge oder parallel eine übermäßige kardiale Fibrose fördert und damit zu der beschriebenen kardialen Dysfunktion in adulten Zyxko-Mäusen beiträgt.

In dieser Studie konnten die LIM-Domänen-Proteine Zyxin und LPP als redundante und protektive Moleküle identifiziert werden, die in VSMCs den kontraktilen Phänotyp aufrechterhalten und so dazu beitragen, die Entwicklung eines Hypertonie-induzierten arteriellen und möglicherweise kardialen Remodellings zu verhindern. Der zeitliche Unterschied beim Auftreten der durch die experimentelle Hypertonie induzierten Phänotypen (vaskulär und kardial) könnte auf die unterschiedliche Häufigkeit von Zyxin bzw. LPP in den jeweiligen Zellen der betrachteten Gewebe zurückzuführen sein. Daher könnten Untersuchungen von alten Lppko und Lpp/Zyx Doppelknockout-Mäusen weiteren Aufschluss über ihre mögliche funktionelle Kompensation im Rahmen eines Hypertonie-induzierten Umbauprozesses geben.

Summary

Hypertension, a chronic and persistent increase in blood pressure, is a modifiable risk factor for, e.g. coronary heart disease, hemorrhagic stroke and end-stage renal failure. Despite the pathophysiological importance of hypertension, understanding of the cellular mechanisms at the onset of this disease remains elusive. During hypertension, vascular smooth muscle cells (VSMCs) are exposed to increased wall stress. This promotes a phenotype shift of the VSMCs to overcome the undue rise in wall stress and eventually reinstate vascular tone. At the cellular level, excessive stretch induces translocation of the mechanotransducer protein zyxin from focal adhesions to stress fibers and to some extent to the nucleus where it indirectly via myocardin-related transcription factor-A (MRTF-A) fine-tunes the expression of mechanosensitive genes. VSMCs isolated from 3-months old zyxin knockout (Zyxko) mice showed a synthetic phenotype. In contrast, only deoxycorticosterone acetate (DOCA)-salt treated very old (18-months) Zyxko mice revealed a prominent vascular phenotype exemplified by failure to develop hypertension, a lower resistivity index, i.e. peripheral resistance, and an altered composition of the extracellular matrix (ECM). The age dependency of the *in vivo* phenotype argues for a possible compensation by other LIM-domain proteins of the zyxin family.

Therefore, the first aim was to analyze whether LPP (lipoma preferred partner) or TRIP6 (thyroid receptor interacting partner 6) might compensate for the loss of zyxin in hypertension-induced arterial remodeling. Like zyxin, LPP but not TRIP6 *in vitro* translocated from focal adhesions predominantly to actin stress fibers as well as to the nucleus upon exposure to supraphysiological stretch. Interestingly, only the level of LPP protein significantly declined in arteries of very old Zyxko mice. VSMCs isolated from 3-months old Lppko mice functionally mimicked the synthetic phenotype of VSMCs isolated from age-matched Zyxko mice. Although young Lppko mice (3 months old) failed to reveal a synthetic VSMC phenotype in experimental hypertension, their significantly lower resistivity index may point to the presence of some vascular dysfunction at this young age. Overexpression of either Lpp in Zyxko VSMCs or Zyx in Lppko VSMCs fully compensated for their alternate loss of function in restoring the contractile VSMC phenotype. Hence, these findings characterize zyxin as a novel regulator of the phenotypic shift of VSMCs during hypertension-induced arterial remodeling with LPP capable of reinforcing zyxin in preventing this shift to occur.

Distinct from VSMCs, terminally differentiated cardiomyocytes (CMs) respond to arterial hypertension by increasing their cell size hence thickness of the ventricular wall (hypertrophy) thereby normalizing wall stress according to the law of Laplace. Following this compensatory CMs hypertrophy, loss of CMs as well as excessive deposition of ECM proteins by cardiac fibroblasts (CFBs) causes cardiac dysfunction. The mechanotransducer zyxin seems to be important for CMs

survival. Therefore, the second aim of this work was to study the consequences of the loss of zyxin for cardiac function in DOCA-salt induced experimental hypertension. In fact, 12 months old Zyxko mice showed cardiac dysfunction possibly due to excessive cardiac fibrosis and the resulting stiffening of the heart. To corroborate this finding, a cardiac fibrosis model, where 3, 6 and 12 months old Zyxko and wild type (WT) mice are treated with a high dose of angiotensin II (Ang II) or saline delivered through implanted osmotic mini pumps, was established. In this model, untreated 3 months old Zyxko mice presented with a reduced diastolic but preserved systolic function as compared to age-matched WT mice. Upon Ang II treatment, systolic cardiac function progressively deteriorated in the Zyxko mice with age and this was paralleled by a prominent age-dependent rise in collagen deposition in the heart. The effects of Ang II on both interstitial and perivascular cardiac fibrosis were significantly less pronounced in age-matched WT mice, indicative of the development of a progressive restrictive cardiomyopathy in the Zyxko mice in this model.

To identify key molecule(s) responsible for the profuse cardiac fibrosis in Zyxko mice, pro-fibrotic gene expression profiles were studied in adult cardiac fibroblasts (ACFs) isolated from Zyxko or WT mice that were exposed *in vitro* to transforming growth factor-β1. Prominent expression of connective tissue growth factor, collagens I and III as well as lysyl oxidase (LOX) by the Zyxko ACFs supports the notion that CFBs account for the excessive formation of scar tissue in the heart of these animals. Since LOX augments the formation of insoluble collagen deposits in the heart, namely by cross-linking them, it might be together with the enhanced synthesis of collagens I and III primarily responsible for the exaggerated cardiac fibrosis and hence cardiac dysfunction in the Zyxko mice. Whether the age-dependency of this cardiac phenotype is like the vascular phenotype related to a functional compensation between zyxin and LPP in the CFBs or even CMs remains to be determined. Nonetheless, it is likely that the lack of zyxin leads to an altered CM-ECM interaction facilitating CM apoptosis and in turn or in parallel excessive cardiac fibrosis hence contributing to the observed cardiac dysfunction in adult Zxyko mice.

In summary, the findings of this study characterize the LIM-domain proteins zyxin and LPP as redundant protective molecules that help to maintain the contractile VSMC phenotype and thus contribute to impeding the development of hypertension-induced arterial and possibly cardiac remodeling. The temporal difference in the appearance of two distinct hypertension-induced phenotypes (vascular and cardiac) might be attributed to the differential abundance of zyxin and LPP in the respective tissue-resident cells contributing to the pathogenesis. Therefore, analysis of old Lppko as well as Lpp/Zyx double-knockout mice has the potential to shed more light on their possible functional compensation in the context of hypertension-induced cardiovascular remodeling processes.

1 Introduction

1.1 Hypertension: A silent killer

Blood is pumped, with each heartbeat to all parts of the body through the arterial blood vessels. Thus, blood pressure is established by the force of blood pushing against the walls of these blood vessels. The peak pressure that is developing during the beating of the heart, i.e. when the volume of blood ejected from the left ventricle travels down the arterial system, is called systolic blood pressure whereas the resting pressure that is observed between the heart beats is called diastolic blood pressure. Mean arterial pressure is regulated by cardiac output and the total peripheral resistance in the vessel[1]. According to the world health organization (WHO) hypertension is a pathophysiological condition in which the blood vessels experience persistently elevated pressure. Persistent elevation of systolic blood pressure greater than 140 mmHg and diastolic blood pressure greater than 90 mmHg are considered as clinical hypertension[2]. On its own, arterial hypertension is asymptomatic and in about 5% of cases, a specific (organ-related) cause can be found for the elevated blood pressure, known as secondary hypertension. However, for the remaining 95% of cases no etiology can be defined, hence this condition is referred to as primary hypertension. Chronic hypertension is a chief risk factor for the development of ischemic heart disease and stroke, which remained the number 1 and 2 leading causes of death globally in the last 15 years[3].

1.2 Induction of cardiovascular remodeling during hypertension

Hypertension induces the transmural pressure difference that elicits circumferential wall stress according to the law of Laplace[4]. This increased wall stress can induce maladaptive, i.e. pathophysiological remodeling processes in the heart, arterial or even venous blood vessel wall by an interplay of tissue-resident cells such as endothelial cells (EC), vascular smooth muscle cells (VSMC), cardiomyocytes (CMs) or cardiac fibroblasts (CFBs) with some contribution by infiltrating leukocytes.

1.2.1 Remodeling of the blood vessel wall: VSMCs in focus

Typically, an artery consists of three structural layers, namely intima, media and adventitia. Endothelial cells are longitudinally arranged in the intima and VSMCs are circumferentially arranged in the media together with connective tissue. Both layers get separated by an internal elastic lamina. The adventitia contains many components, including, in most cases, sympathetic nerves, considerable amounts of collagen, and fibroblasts[2]. VSMCs are dynamic, multifunctional cells that

contribute to arterial remodeling through numerous processes, including cell growth (hyperplasia and/or hypertrophy), apoptosis, elongation of cells, reorganization of cells, and/or altering composition of the extracellular matrix (ECM)[5]. The primary functional property of an arterial blood vessel is to maintain a certain lumen diameter, which determines vascular resistance (according to the Poiseuille's law) and hence blood flow to the downstream organs or organ substructures. Arterial hypertension typically causes a chronic rise in wall stress imposing an enhanced cyclic strain on the VSMCs, which triggers a shift in their phenotype switching from a quiescent, contractile state to a proliferative and synthetic state. This phenotype switching finally establishes VSMC hypertrophy or hyperplasia in the vascular wall, depending on the size of the arterial blood vessel, thereby increasing wall thickness to counter-balance the rise in wall stress (Figure 1.1 A,B)[6–8]. The differentiated and contractile VSMCs express a broad repertoire of genes such as smooth muscle α-actin (SMA), smooth muscle myosin heavy chain (SM-MHC), smooth muscle myosin light chain (SM-MLC), calponin, smooth muscle α-tropomyosin, smoothelin, desmin and vinculin (Figure 1.1 C)[5,9,10].

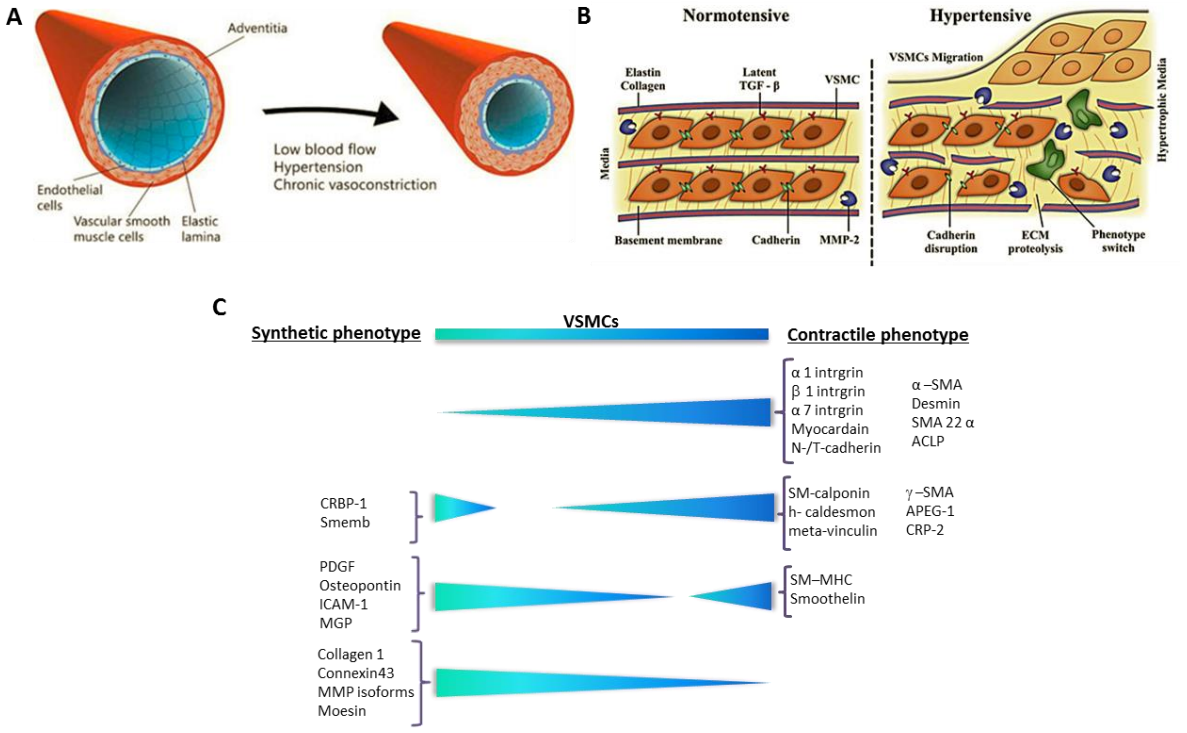

Figure 1.1 Hypertension induced arterial remodeling

(A) Inward eutrophic remodeling of small arteries can be triggered by low blood flow, chronic vasoconstriction, and hypertension. (B) Schematic representation of a cross section of the arterial vessel wall in normotension and hypertension, respectively. Arterial remodeling is characterized by thickening of the wall where switching of the VSMC phenotype (dedifferentiation) and remodeling of the ECM take place. (C) Schematic representation of expression levels of genes associated with a particular SMC phenotype (adapted from[10–12]). Abbreviations: ECM, extracellular matrix; SMA, smooth muscle α-actin; ACLP, aortic carboxypeptidase-like protein; APEG-1, aortic preferentially expressed protein-1; CRP-2, c-reactive protein-2; SM-MHC, smooth muscle myosin heavy chain; CRBP-2, retinol-binding protein-2; PDGF, platelet derived growth factor; ICAM-1, intercellular adhesion molecule-1; MGP, matrix gla protein-1; MMP, matrix metalloproteinase.

The phenotype shift of VSMCs in small resistance-sized arteries is characterized by a marked reduction in expression of VSMC-selective differentiation marker genes (Figure 1.1 C)[9,10] together with increased proliferation, migration, and synthesis of extracellular matrix components.

1.2.2 Remodeling of the heart: cardiac fibroblasts in focus

Increased biomechanical stress during hypertension (pressure overload) induces hypertrophy of the cardiomyocytes which in turn increases thickness of the wall of the left ventricle to neutralize the increased wall stress[13]. Terminally differentiated cardiomyocytes (CMs) respond to pressure-overload stress by enlarging their size rather than proliferation because of their incapability to reenter the cell cycle. This pro-hypertrophic response is accompanied by enhanced protein synthesis as well as higher organization of the sarcomeric structure. As part of this process, a wide range of transcriptional and posttranslational events occur, including re-expression of fetal genes, the so-called pro-hypertrophic gene program.

At the early stage of hypertension this pro-hypertrophic response of the CMs is considered adaptive, ultimately to diminish wall stress and to decrease oxygen demand. However, in fact this remodeling process is maladaptive because it impairs adequate fractional shortening of the CMs and in parallel hampers diffusion of oxygen from the nearby capillaries, thus causing early systolic dysfunction of the left ventricle. Moreover, when pressure overload due to arterial hypertension persists, cardiac remodeling eventually is sped up, resulting in a more severe dysfunction ultimately leading to heart failure[14]. CMs apoptosis is much enhanced while the proliferating cardiac fibroblasts differentiated to myofibroblasts secrete large amounts of ECM proteins to replace the dead myocardium by scar tissue. This surplus of ECM protein deposition around the blood vessels (perivascular) and throughout the interstitium causes a stiffening of the heart that enhances CMs apoptosis and the subsequent fibrosis even further and ultimately results in a condition that is referred to as hypertrophic or restrictive cardiomyopathy and will inevitably lead to heart failure (Figure 1.2). Moreover, cardiac fibrosis disrupts the coordination of myocardial excitation-contraction coupling in both systole and diastole to promote arrhythmia[15–17].

Fibroblasts (FBs), morphologically flat and spindle shaped cells with multiple projections, comprise the largest cell population in the myocardium. A variety of cell surface markers has been identified for both FBs and cardiac fibroblasts (CFBs), i.e. vimentin, discoidin domain receptor 2 (DDR-2) or fibroblast-specific protein 1 (FSP-1), although their specificity for these cells has been repeatedly challenged[18]. In chronic hypertension, CFBs can differentiate into myofibroblasts, which are more mobile and contractile with a greater synthetic ability to produce ECM proteins (Figure 1.2).

Myofibroblasts are present in the myocardium only following cardiac injury as the healthy myocardium is devoid of them[17,19]. These cells are defined according to their dual functions: fibroblast-like in terms of ECM synthesis and smooth muscle myocyte-like in terms of migration. Although, similar to CFBs, myofibroblasts are also non-excitable cells but express a number of smooth muscle cell markers such as SMA, SM-MHC, vinculin and paxillin[15,20,21].

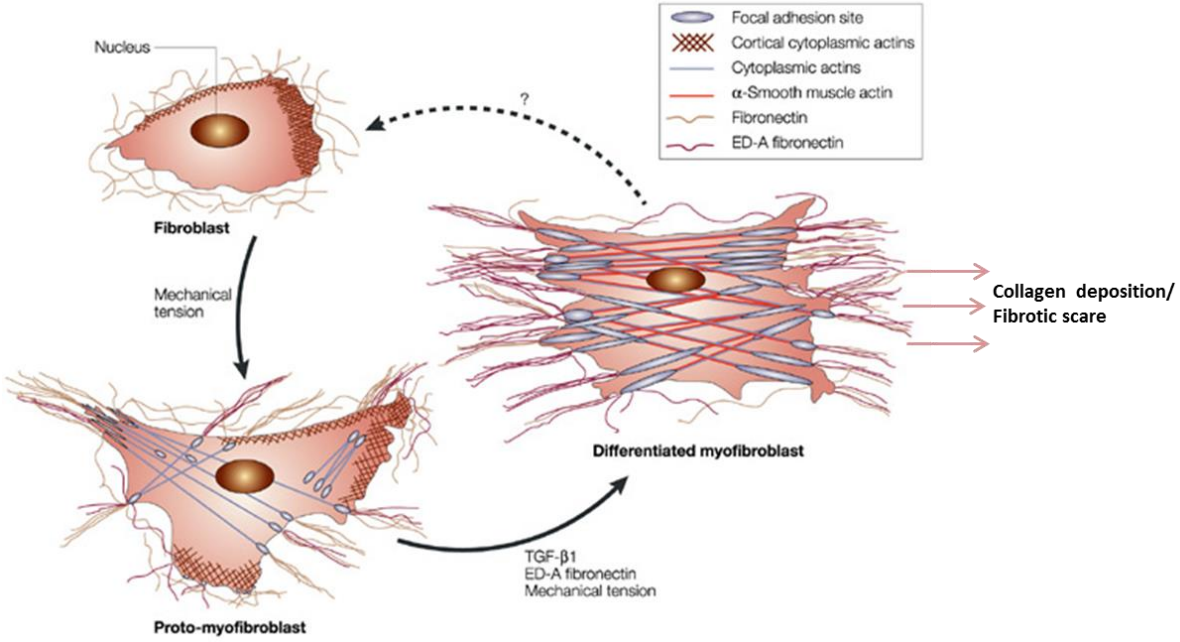

Figure 1.2 Transdifferentiation of fibroblasts to myofibroblasts during hypertension
A supraphysiological rise in wall stress triggers the differentiation of fibroblasts into proto-myofibroblasts and finally to myofibroblasts. Myofibroblasts are characterized by their expression of α-smooth muscle actin and well developed stress fibers; they primarily contribute to scar tissue formation (adpated from[17]).

In the setting of pathological stress, the source of this highly active fibroblast might include resident fibroblasts, adult epicardial cells undergoing endothelial-to-mesenchymal transition, and circulating collagen-secreting bone marrow-derived cells[22]. Myofibroblast-mediated collagen turnover is regulated by autocrine and paracrine factors generated within the myocardium and by endocrine hormones derived from the circulation. Transforming growth factor-β1 (TGF-β1) induces this process to reinforce collagen expression, whereas IL-1β prevents differentiation of CFBs to myofibroblasts[23,24]. In the myocardium, this transdifferentiation induces ECM turnover in favor of increased synthesis and accumulation of ECM proteins to replace lost myocytes and/or interrupt myocyte–myocyte interactions, resulting in an overall deterioration of cardiac function (Figure 1.2)[20].

1.2.3 Remodeling of the extracellular matrix: in the arterial vessel wall and in the myocardium

The arterial vessel wall is an active, flexible, and integrated dynamic organ made up of cellular (ECs, VSMCs, and FBs) and non-cellular (ECM) components, which undergo reorganization in response to pathophysiological stimuli. This structurally determined change in lumen diameter is designated vascular remodeling and medial VSMCs play a pivotal role therein[5,25]. In the media, these cells are surrounded by and embedded into different ECM proteins including collagen, elastin and proteoglycans that are organized into a highly ordered network. During remodeling, activated VSMCs degrade and breach the surrounding ECM to support their migration and release of growth factors. Quantitative, topographic or both changes in ECM composition alter medial VSMC-ECM interaction, resulting in a rearrangement of both VSMCs and ECM proteins, and hence a restructured arterial vessel wall[26,27]. In arterial hypertension, induction of collagen and elastin synthesis by VSMCs combined with a reduced degradation of these matrix proteins results in stiffening of the arterial vessel wall[28]. Additionally, the receptors for these ECM proteins such as integrins also contribute to the remodeling process by perceiving and subsequent transduction of the signals into the recipient tissue-resident cells[29]. Moreover, tissue transglutaminase-2 (tTG-2) could be involved in the remodeling process by mediating interactions between integrins and ECM proteins[30,31]. Matrix metalloproteinases (MMPs), a family of zinc and calcium dependent endopeptidases, are able to degrade collagen, elastin, and other extracellular molecules. The activity of MMPs is regulated by conversion of the inactive pro-form to the active form as well as inhibition by specific tissue inhibitors of MMPs (TIMPs). While MMP1 and 13 are collagenases, MMP2 and 9 are gelatinases; in contrast MMP3 rather has a broad spectrum of activity[32]. MMP2 and MMP9 play a pivotal role in vascular remodeling by controlling VSMC migration[12,33].

In hypertensive heart disease, altering the composition and degree of crosslinking of the ECM is a key component of cardiac remodeling, where disintegration of the ECM affects the structural integrity as well as function of the left ventricle[34]. In contrast, excessive production, accumulation and crosslinking of ECM proteins, e.g. cardiac fibrosis, results in stiffening of the myocardium distorting left ventricular architecture and function[35]. Myocardial stiffness is largely attributed to changes in type I and III fibrillar collagens secreted from the myofibroblasts as pro-collagens and eventually assembled into the mature collagen fibers. A number of growth factors/mitogens such as angiotensin II (Ang II), TGF-β1, insulin like growth factor-1 (IGF-1), and tumor necrosis factor-α (TNF-α) may act synergistically to regulate collagen turnover by the myofibroblasts[20,36]. It has been shown that lysyl oxidase (LOX)-dependent collagen crosslinking is a prerequisite for the development of cardiac fibrosis and systolic dysfunction in different pathological situations[37,38].

Moreover, an imbalance in the ratio of MMPs to their inhibitors, TIMPs, has significance for the progression of systolic dysfunction, hence stresses the importance of studying both ECM degradation mechanisms and those that underlie ECM synthesis[39]. Counterintuitively, degradation of collagen was shown to accelerate synthesis of the ECM itself[40,41]. Hence, MMP activation reinforces cardiac fibrosis by taking part in a vicious circle in which ECM degradation promotes ECM protein synthesis and thus scar tissue formation[20].

1.3 Mechanotransduction: focal adhesions (FA) in focus

Intramural cells sense their local chemomechanical environment and remodel the ECM to provide suitable compliance and sufficient strength[42,43]. The dynamic process by which cells convert a mechanical stimulus into biochemical events is known as mechanotransduction. At the cellular level, mechanical forces are crucial in regulating cytoskeletal organization, gene expression, proliferation and survival[44,45]. Effects of physical forces on cellular activity are most apparent in blood pressure regulation, the endothelial cells response to fluid shear stress and remodeling of bone[44,45]. Intracellular actin bundles are mechanically linked to integrins on the cell surface and the ECM through multi-protein structures known as focal adhesions (FAs)[46]. FAs serve as molecular bridges that coordinate a variety of environmental stimuli and facilitate communication between the ECM and the cytoskeleton[47]. Formation of these structures requires tension generated by cellular actomyosin networks, resisted by a substratum of sufficient stiffness (Figure 1.3 A). Hence, the assembly rate, size and functional impact of FAs depend on the contractile capacity of the cytoskeleton, composition of the ECM, integrin activation and avidity, and further specifics of the microenvironment[48,49]. Within FAs, mechanotransduction could be propagated either via increased integrin clustering or alterations in the conformation of certain force-sensitive components like zyxin, paxillin, talin, vinculin and Ena/VASP (Figure 1.3 B)[50,51].

1.4 Zyxin as a mechanotransducer

Zyxin, a 82 KDa LIM domain containing protein found in FAs, regulates actin polymerization[51–53]. It has been shown that a reduction in cellular traction force leads to disassembly of FAs by inducing the molecular unbinding kinetics of zyxin but not that of its binding partner vinculin[54]. Cyclic stretch, an *in vitro* model resembling one important aspect of arterial hypertension, induces the phosphorylation mediated translocation of zyxin into nucleus (Figure 1.4)[55]. Herein, zyxin can interact with DNA and act as a transcription factor to regulate the expression of mechanosensitive genes (Figure 1.4)[56,57]. Another possibility is that zyxin may stabilize actin dynamics and thus prevent transcriptional co-activators such as myocardin-related transcription factor-A (MRTF-A) from

entering the nucleus and interacting with serum response factor (SRF) to alter mechanosensitive gene expression, e.g. in VSMCs exposed to cyclic stretch[58].

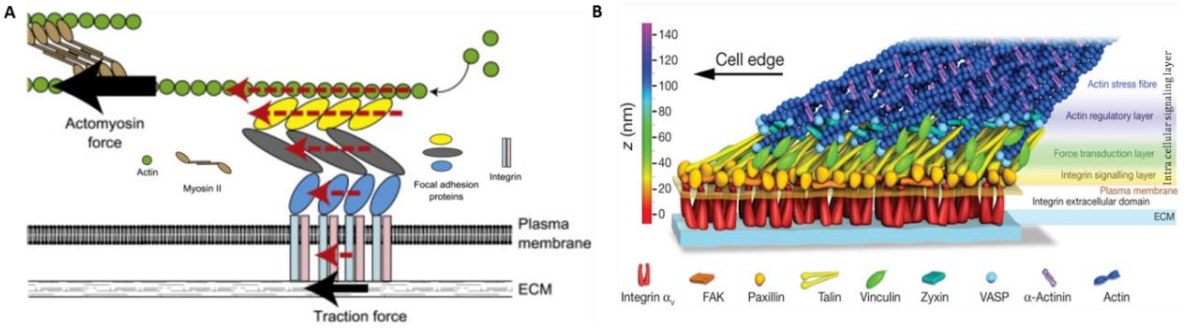

Figure 1.3 Structural and molecular organization of focal adhesions

(A) Focal adhesions are multi-layer arrangements of different proteins connecting the ECM with the cortical actin cytoskeleton. Formation of focal adhesions is dependent on the tension generated by cortical actin cytoskeleton and the traction force generated by the ECM. (B) Integrins establish attachment of the cortical actin cytoskeleton to the ECM at the matrix receptor binding site of focal adhesions. The intracellular domain contains 3 functional layers: (i) the intracellular signaling layer consisting of focal adhesion kinase and intracellular integrin domains, (ii) the force transduction layer consisting of proteins like zyxin, paxillin, talin, vinculin and Ena/VASP, and (iii) the actin regulatory layer essentially composed of actin filaments and myosin (adapted from[50]).

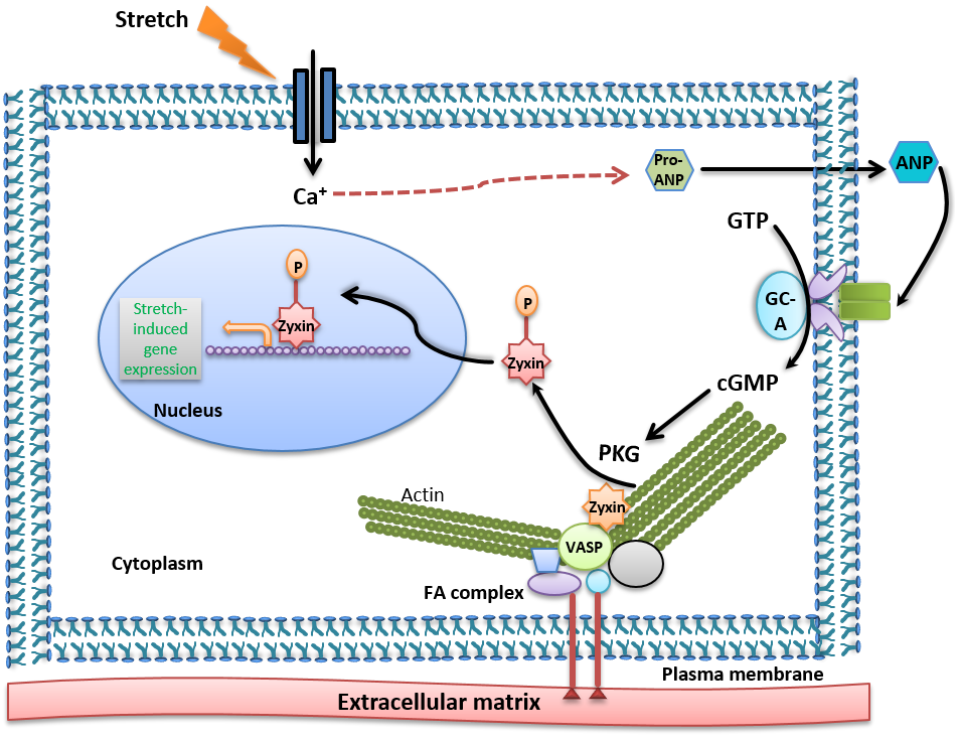

Figure 1.4 Mechanism for the stretch-induced phosphorylation and translocation of zyxin from focal adhesions to nucleus in endothelial cells

Cyclic stretch causes a diacylglycerol/TRPC3 mediated rise in intracellular calcium that triggers the release of ANP which in turn stimulates particulate guanylyl cyclase and subsequently protein kinase G (PKG). PKG phosphorylates zyxin at serine-142 thus enabling its translocation to the nucleus where it acts (in this particular case) as a transcription factor (adapted from[55]).

1.5 The zyxin family of LIM-domain containing proteins

The LIM-domain consists of approximately 55 amino acids with 8 highly conserved residues and, is present in a wide variety of eukaryotic proteins but absent in prokaryotes. The LIM-domain was identified as a common cysteine-rich sequence in a small group of homeodomain transcriptions factors, Lin11, Isl-1, Mec-3 (LIM), and named after their origin[59]. The LIM-domain is devoid of intrinsic catalytic activity, however, it can function as adaptor, competitor, auto inhibitor or localizer for other protein. LIM-domain containing proteins together with partner proteins can regulate various biological processes including actin cytoskeletal dynamics, integrin-dependent adhesion and signaling, cell-fate determination, neuronal guidance as well as tissue-specific gene expression[59,60]. According to sequence similarity, LIM-domain containing proteins can be classified into four broad categories (Figure 1.5). The zyxin family belongs to the 'LIM actin associated' category and consists of 7 members: ajuba, LIM domain-containing protein 1 (LIMD1), LIM-domain containing preferred translocation partner in lipoma (LPP), migfilin, thyroid receptor interacting partner 6 (TRIP6), wilms tumor protein 1-interacting protein (WTIP) and zyxin. All proteins in this family have an N-terminal proline-rich region (PRR), three highly conserved LIM-domains at their C-terminus and other non-LIM domains which take part in association with other proteins[59].

1.5.1 Ajuba

Ajuba harbors a functional nuclear export signal (NES) at the pre-LIM region which facilitates the shuttling of this protein from cell-cell contacts to the nucleus to modulate cell growth and differentiation[61]. Ajuba can promote meiotic maturation of *Xenopus* oocytes through the induction of MAPK activity[62]. Ajuba knockout mice lack any obvious phenotype. Nevertheless, primary embryonic fibroblasts (EFs) isolated from this mice exhibited reduced migration[63]. Recently, ajuba has been shown to be involved in metastasis of esophageal squamous cell carcinoma by upregulating MMP10 and MMP13[64]. In addition, ajuba can either limit Hippo regulation via YAP-LATS or represses the expression of tumor suppressor genes via JAK1/STAT1 to support cell proliferation[65,66].

1.5.2 LIMD1

LIMD1 contains a leucine-rich NES within its pre-LIM region which accounts for its nuclear localization. LIMD1 is involved in cell anchoring via focal adhesions and some breast tumors reveal an altered LIMD1 expression[67,68]. LIMD1 can serve as tumor suppressor by interacting with the retinoblastoma protein (pRB)[69].

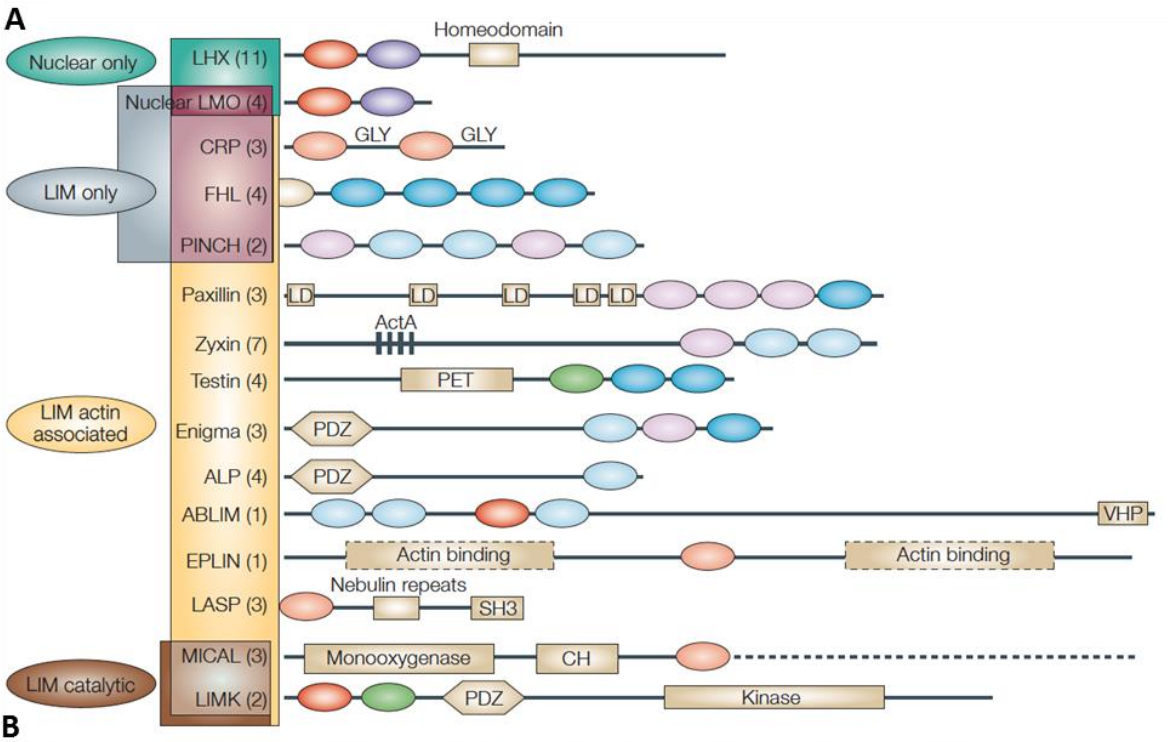

LHX	LMO	CRP	FHL	PINCH	Paxillin	Zyxin	Testin	Enigma	ALP	LASP	MICAL	LIMK	Other
ISL1 LHX4	LMO1	CRP1	ACT	PINCH	HIC5	Ajuba	Dyxin	Cypher	ALP	LASP	MICAL	LIMK1	ABLIM
ISL2 LHX5	LMO2	CRP2	FHL1	PINCH2	Leupaxin	LIMD1	LMO6	ENH	CLP-36	LIM-nebulette	MICAL-like	LIMK2	EPLIN
LHX1 LHX6	LMO4	CRP3	FHL2		Paxillin	LPP	RILP	Enigma	Mystique	NRAP	MIRAB		LMO7
LHX2 LHX9	LMOX		FHL3			Migfilin	Testin		RIL				Sciellin
LHX3 LMX1a						TRIP6							ZNF185
LMX1b						WTIP							
						Zyxin							

Figure 1.5 Classification and domain structures of LIM domain containing proteins
(A) LIM domain families are classified into four groups according to sequence similarity and homology within the LIM sequence. The domain structures of the founding member and/or the best characterized example are shown for each family of LIM domain containing proteins. The number of known members of each family is indicated in parentheses. Individual LIM domains are shown as colored ovals. Dashed lines indicated that scale is not preserved. (B) A list of the identified members of each LIM domain containing protein family. Abbreviations: CH, calponin homology; GLY, glycine-rich region; PDZ, postsynaptic density-95, Discs large, zona occludens-1; PET, prickle, espinas and testin; SH3, Src-homology-3; VHP, villin head piece. (Adapted from[59]).

1.5.3 WTIP

WTIP (WT1-interacting protein) was identified as a binding partner of WT1 (Wilms' tumor gene protein 1), a zinc finger transcription factor, and can regulate glomerular podocyte differentiation by shuttling between focal adhesions and the nucleus. It contains three C-terminal LIM domains and a pre-LIM prolin-rich region in which the NES is located. In normal glomeruli, WTIP is part of a multiprotein complex in podocyte foot processes. After injury, WTIP translocates to the nucleus where it co-localizes with WT1 and represses WT1-dependent gene expression[70]. Moreover, together with ajuba and LIMD1, WTIP has been proposed to be involved in microRNA mediated gene silencing through the miRISC complex[71].

1.5.4 Migfilin

Migfilin contains an N-terminal region with binding sites for filamin, a central prolin-rich region in which a vasodilator-stimulated phosphoprotein (VASP) binding site has been identified, and a C-terminal LIM region which mediates the interaction with other proteins. Migfilin can also travel from the cytoplasm to the nucleus in a calcium dependent manner[72]. By interacting with different partner proteins this adapter protein can modulate cell shape and motility[73,74] as well as cardiac development[75]. In response to pressure overload, migfilin knockout mice hearts showed less hypertrophy and fibrosis[76]. Downregulation of migfilin was observed in VASP depleted breast cancer cells which in turn inhibited tumor spheroid invasion[77].

1.5.5 TRIP6/ZRP-1

Thyroid hormone receptor interacting protein 6 (TRIP6), also known as zyxin-related protein-1 (ZRP-1), contains a NES, multiple transactivation domains (one overlaps with sequences of the NES) and a nuclear targeting sequence both in the PRR and in the LIM-domains[78]. Three different isoforms of TRIP6 have been described and the shortest form has been termed nuclear isoform of TRIP6 (nTRIP6)[79]. According to its localization both in focal adhesions and in the nuclear compartment, TRIP6 has also been proposed as a molecule that transmits signals between adhesion sites and the nucleus[78,80]. TRIP6 was demonstrated to be essential for stress fiber formation through reorganizing of the cortical actin cytoskeleton via modulation of Rho GTPase[81]. Moreover, TRIP6 interacts with p130Cas family member of signal transduction through SH2 domain to regulate cellular motility[82,83]. Depending on the interacting transcription factor, TRIP6 can function either as a transcriptional co-activator or co-repressor. During cancer-associated inflammatory response and tumorigenesis, TRIP6 can associate with the lysophosphatidic acid-2 (LPA-2) receptor, and serve as a co-activator for several transcription factor like nuclear factor-κB (NF-κB) as well as c-Jun N-terminal kinases (JNK), i.e. the activator protein-1 (AP-1) pathway[84]. In addition, nTRIP6 can serve as a co-activator for NF-κB, AP-1 or myocyte enhancer factor-2 C (MEF2C) to regulate different cellular responses[79,85]. It was found to be a selective co-activator for AP-1 dimers containing Fos[86], and has been associated with proteins ensuring telomere protection[87].

1.5.6 LPP

The Lpp (lipoma preferred partner) gene was identified first as the most frequent translocation partner of the HMGA2 (high mobility group A2) gene in lipomas and later in a number of other soft tissue tumors[88,89]. However, in acute monoblastic leukaemia, the Lpp gene was shown to act as a

translocation partner of the MLL (mixed lineage leukaemia) gene[90]. Like TRIP6, the LPP protein contain a NES located at the leucine-rich pre-LIM region and can shuttle from focal adhesions to the nucleus where it displays transcriptional activation capacity[91]. It has been demonstrated that within the nucleus LPP acted as a coregulatory protein to enhance the transactivation potential of PEA3, a regulatory region associated with tumorigenesis as well as embryogenesis[92]. The localization of LPP to FAs is largely mediated by the LIM-domains rather than the pre-LIM region which harbors the α-actinin and VASP binding sites[93]. LPP has occasionally been observed along stress fibers[94] and a specific region within the pre-LIM region is required for their this actin stress fibers targeting[95].

In 2003, two independent studies reported LPP as a novel smooth muscle cell (SMC) marker[96,97]. Later, it was found that LPP was also involved in the regulation of vascular SMC migration in an *in vitro* model for vascular injury[98]. In SMCs, LPP expression can be mediated by an alternative promoter that is regulated by serum response factor/myocardin[99]. It has been suggested that LPP expression could be regulated by non-canonical Wnt signaling and might be involved in Rho kinase 2-dependent signaling pathways in human iliac vein SMCs[98]. In zebrafish, LPP has been shown to interact with the Wnt/PCP protein Scrib to regulate cell migration and intercalation during convergence and extension movement in early embryonic development[100]. Moreover, LPP can positively regulate invadopodia formation to enhance breast cancer metastasis by binding to the Src substrate ErbB2[101,102]. Surprisingly, Lpp knockout (Lppko) mice do not exhibit any defect during embryonic development and are viable[103]. They reach adulthood without displaying any obvious macroscopic or microscopic abnormalities possibly due to functional redundancy among the closely related members belonging to the zyxin family of LIM protein (Figure 1.6)[103]. However, an aberrant Mendelian inheritance was observed in heterozygous mating which could be explained by the partial embryonic lethality in knockout females[103].

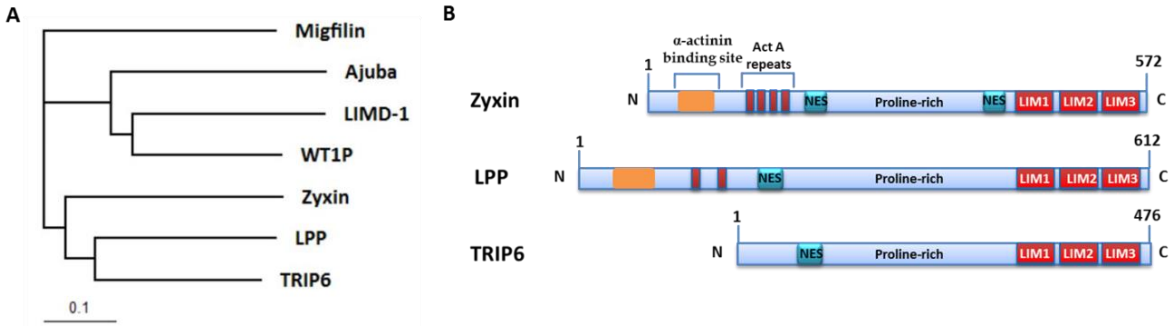

Figure 1.6 Evolutionary relationship and similarity in the domain structure among the zyxin family of LIM domain-containing proteins

(A) Cladogram of a phylogenetic tree for members of the zyxin family. Full-length protein sequences were obtained from Entrez Protein Database (National Center for Biotechnology Information (NCBI), and their sequences were aligned and phylogenetic tree was constructed using the web tool CLUSTAL Omega. The phylogenetic tree was visualized with TreeView (version 1.6.6, 2001). Scale bar represents 0.1 amino acid substitution per site. (B) Scheme of the subdomain structure of the most closely related zyxin family member i.e.

zyxin, LPP and TRIP6. All proteins contain a C-terminal cysteine-rich portion composed of 3 LIM domains and an N-terminal proline-rich domain. Both LPP and zyxin also harbor an α-actinin binding motif and 2 or 4 Act A repeats which facilitate the binding of Ena/VASP family proteins. In contrast, TRIP6 is relatively shorter and devoid of the binding site for α-actinin and VASP (adapted from[91]).

1.5.7 Zyxin

Zyxin, the founding member of the family, is a phosphoprotein that localizes at focal adhesions and along actin filaments[104]. Zyxin contains four proline-rich repeats that serve as binding sites for Mena (mammalian Ena) and VASP in the pre-LIM region and three zinc finger containing LIM domains (for interaction with the DNA) at the C-terminus. Depending on the species, zyxin contains one or more leucine-rich nuclear export signals[105]. Several lines of evidences suggest that zyxin plays an important role in localizing members of the Mena/VASP family to sites of cell adhesion[106]. Zyxin has been shown to be involved in the assembly of the actin cytoskeleton as well as in the maintenance and repair of actin stress fibers to retain mechanical homeostasis[107]. Moreover, zyxin can regulate endothelial cell exocytosis through reorganizing the local actin network as, e.g. during the release of von Willebrand factor (VWF) from Weibel–Palade bodies (WPB)[108]. Moreover, it has been shown that exposure to cyclic stretch causes dissociation of zyxin from focal adhesions both in ECs and VSMCs to either associate with actin stress fibers or to accumulate in the nucleus where it can act as a transcription factor[55–57,109]. Thus, zyxin can regulate the expression of a vast majority (90%) of mechanosensitive genes, e.g. in VSMCs, hence strongly affecting their cell cycle regulation, mitogenesis and contractile capacity[58]. In fact, VSMCs isolated from zyxin knockout (Zyxko) mice revealed a shift from the contractile to the synthetic phenotype which could be attributed to an increased RhoA activity and persistence of myocardin related transcription factor-A (MRTF-A) in the nucleus[58].

Although zyxin is ubiquitously expressed in mice both during embryonic development and in adulthood, mice that lack zyxin are viable, fertile and do not show any discernible abnormalities[110]. It was therefore suggested that the absence of a phenotype in Zyxko mice might be accredited to a possible functional overlap between zyxin and a closely related member of the zyxin family of LIM domain-containing proteins (Figure 1.6)[110]. Reinforcing this assumption adult Zyxko mice only revealed the same synthetic phenotype as VSMCs isolated from 3-months old Zyxko mice when subjected to experimental arterial hypertension. While a cardiac phenotype (systolic dysfunction) was unmasked at 12 months of age, the vascular phenotype (poor myogenic response) only became apparent at 18 months of age[111] . This age-dependency argued for a possible functional redundancy mediated by other members of the zyxin family of LIM-domain-containing proteins, namely LPP and TRIP6.

1.6 Aims of the thesis

By considering the aforementioned findings in assigning a role for zyxin in experimental hypertension, two main aims were devised for this doctoral thesis.

1. The first focus was to analyze the presumed functional redundancy among the most closely related members of zyxin family of LIM-domain-containing proteins, i.e. LPP and TRIP6, in hypertension-induced arterial remodeling.
   i. In the first part of the study, expression levels of these two potential compensators were analyzed in selected arterial blood vessels derived from Zyxko mice of different age. Moreover, their responses to cyclic stretch were analyzed and compared to that of zyxin.
   ii. Next, analysis of the phenotype of mice lacking LPP or TRIP6 was considered. However, so far a mouse lacking TRIP6 is not available and the data obtained for TRIP6 in stretched VSMCs did not reveal a major role for this protein as a potential mechanotransducer. Lppko mice, on the other hand, proved viable but similar to Zyxko mice revealed no phenotype at baseline. Therefore, the role of LPP in VSMC function was analyzed *in vitro* by focusing on three major aspects of the contractile VSMC phenotype, i.e. migration, proliferation and contractile capacity. In addition, Lppko mice were subjected to deoxycorticosterone acetate (DOCA)-salt induced experimental hypertension, and both their vascular and cardiac phenotype studied by a combination of telemetry-based blood pressure recording and high resolution ultrasound imaging of the heart and the conduit arteries.
   iii. Finally, the potential of zyxin and LPP to compensate for their alternate loss of function was analyzed *in vitro* by overexpression of zyxin in Lppko VSMCs and *vice versa* of LPP in Zyxko VSMCs.
2. Secondly, the previously observed cardiac phenotype of Zyxko mice in DOCA-salt induced experimental hypertension should be corroborated in a second model of experimental hypertension where cardiac fibrosis dominates despite a comparable pressure overload.
   i. To achieve this goal, 3, 6 and 12-months old Zyxko mice as well as age-matched wild type (WT) mice were subjected to a high dose treatment with angiotensin II, delivered by osmotic mini-pumps implanted in these animals, followed by characterization of their cardiac phenotype essentially as described before.
   ii. Finally, in search for key mediators and cells responsible for developing the prominent cardiac fibrosis in Zyxko as compared to WT mice, adult cardiac fibroblasts were isolated from the hearts of these animals and analyzed *in vitro* for their capacity to express pro-fibrotic gene products at baseline and following exposure to transforming growth factor-β1 (TGF-β1).

2 Materials

2.1 Consumables

Materials	Supplier
Bacterial culture tubes	Sarstedt
BioFlex® Culture plate (collagen type-1 coated)	Flexcell International Corporation
Cell culture dishes	TPP
Cell culture flasks (T25, T75)	Sarstedt
Cell culture plates	Sarstedt, Greiner
Cell scraper	Sarstedt
Cover slips for microscopy	Thermo Scientific
Filter papers	Munktell
Microscope slides	Thermo Scientific
PCR tubes	Sarstedt
Pipette tips	Sarstedt
Plastic pipettes	Sarstedt
PVDF transfer membranes	Immobilon®-P (Merck Millipore)
Safe lock tubes	Sarstedt
Sterile filters	GE Healthcare
U-bottom 96 well plate	Greiner

2.2 Equipment's

Equipment	Supplier (Model)
Autoclave	Tuttnauer (5050 EL)
Bacterial incubator	New Brunswick Scientific (Innova 4230)
Balance	Sartorius (BP121S)
Centrifuge	Hettich Zentrifugen (Universal 32)
CODA-tail cuff	Kent Scientific Corporation
CO_2 incubator	New Brunswick Scientific (Innova CO-170)
	Heraeus Instruments (BB-16)
	Thermofisher Scientific (Heracell™ VIOS 160c)
Cooling plate	Leica (EG1140C)
Cooling centrifuge	HERMLE (Z323K)
Confocal microscope	Olympus (IX81)
Flexercell system	Flexcell® International (FX-5000)
GentleMACS C Tubes	Miltenyi Biotec (130-093-237)
GentleMACS dissociator	Miltenyi Biotec (130-093-235)
High resolution ultrasound	VisualSonics (Vevo2100)
Heating block	HLC-Haep Labor Consult (HBT-1131)
Heating chamber	Memmert (U40)
Laminar flow	Heraeus (HS18 Hera safe)
Light cycler	Roche (LightCycler 1.5)

Equipment	Supplier (Model)
Light microscope	Wild Heerbrugg (M5-51845)
	Carl zeiss (Axiovert 25, invrted)
	Olympus (CKX41, inveretd)
Luminescent image analyzer	GE healthcare (ImageQuant LAS 4000 mini)
MACS smart strainers	Miltenyi Biotec (130-098-462)
Magnetic stirrer	Janke & Kunkel GmbH (IKAMAG)
Microtome	Microm International GmbH (HM430)
	Leica RM 2125 RT
Mini centrifuge	Biozym (SPROUT™)
NanoDrop	PeQlab BiotechnologieGmb (H ND-1000)
Nitrogen tank	Air Liquide (Arpege 140)
Nucleofector®	Amaxa (Nucleofector® II)
Paraffin embedding system	Leica (EG1120)
PCR cycler	Biometra (Thermocycler)
Peristaltic pump	TSE systems (Ismatec Reglo)
pH meter	Inolab (pH 720)
Plate reader	BIO-TEK (PowerWave XS)
Power supply for gel chamber	BIORAD (PowerPac HC)
Radio telemetry	DSI (PA-C10)
Rotor gene	Qiagen (Rotor gene Q)
SDS-PAGE chamber	BIORAD (Mini-Protean)
Silicon block	Flexi PERM (Sarstedt)
Sonicator	dr. hielscher GmbH (UP50H)
Stereomicroscope	Heerbrugg (Wild M650)
Table top centrifuge	Heraeus Pico 21
Table top cooling centrifuge	Hettich Zentrifugen Mikro22R
Transfer chamber	BIORAD Mini-Protean
Transilluminator	BIORAD Gel Doc™
Universal power supply	Biometra powerpack
Vortex	Scientific Industries Inc.Vortex-2 Genie
Water bath	Dinkelberg analytics E11

2.3 Materials for surgery and ultrasound imaging

Material	Supplier (Ref no.)
Anaesthetic pump	Datex Ohmeda (Isotec5)
Angiotensin II acetete	Bachem (H-1705)
Cannula	B Braun Venofix® (25G)
Cannulation forceps	F.S.T (11251-33)
Deoxycorticosterone acetate (DOCA)	Innovative Research of America (M121)
Electrode cleanser	Dr. Schumacher GmbH (Cleanisept® wipes)
Electrode gel	Leonhard Lang GmbH (Skintact®)
Eye cream	Bayer (Bepanthen)

Material	Supplier (Ref no.)
Forceps and tweezers	F.S.T (Dumont, 11251-35)
Hair removal cream	Veet ultra (sensitive skin)
Isoflurane	Baxter (HDG9623)
Microvessel clips	Aesculap (FD562R)
Osmotic mini pump	Charles River Laboratories (Alzet, 1002)
Physiologicla saline	B. Braun
Rectal lubricant	Parker laboratories (Aquagel®)
Re-gel syringe	DSI (276-0038-001)
Remadyle (50mg/ml)	Pfizer GmbH
Silk	F.S.T (18020-60)
Skin antiseptic spray	Schülke & Mayr GmbH (Kodan tinktur forte)
Skin antiseptic cream	Mundipharma GmbH (Betaisodona Salbe)
Spring scissor (straight blade)	F.S.T (15000-00)
Surgical suture	Ethicon (G-6, 30 cm 6-0 Perma-hand Seide)
Syringe	BD-plastipak (Luer-lok™, 20 ml)
Syringe	BD-plastipak (Luer, 1 ml)
Tissue glue	3M™ Vetbond™
Ultrasound gel	Dahlhausen (PZN 8825881)

2.4 Chemicals and reagents

Chemicals / reagents	Supplier
Agar	Roth
Agarose	Sigma
Ampicillin	Sigma Aldrich
APS	Roth
Bacto-tryptone	BD
Boric acid	Sigma Aldrich
Bio-Rad protein assay (Bradford)	BIORAD
BSA	Sigma
Calcium chloride	Merck
Casein	Sigma
Calcium acetate	Roth
Chemiluminescence substrate	LuminataTM Forte (Merck Millipore)
Collagenase Type 2 (Lot: 43D14200A)	Worthingon
Competent cells	Invitrogen
DABCO	Sigma
DAKO® pen	Dako Denmark
DAPI	Invitrogen
Disodium hydrogen phosphate	Roth
DNA ladder	Thermo Scientific
DTT	Roth
Deoxyribonuclease I	Worthington

Chemicals / reagents	Supplier
EDTA	AppliChem
EGTA	Roth
Ethidium bromide	Roth
FCS	Gibco
Fungizone	Gibco
Gelatin	Merck
Glucose	Merck
Glycine	Sigma Aldrich
Glycerol	VWR
Hanks BSS	Gibco
HEPES	Sigma
KCl	AppliChem
LB-Broth	Sigma (L3022)
Leupeptin A	Sigma
L-glutamine	25030 Life technologies
Loading dye	Roti®-load 1Roth
Lysis buffer	Cytoskeleton
Methanol	Sigma Aldrich
Methyl cellulose	Sigma (M-0512)
Mowiol 4-88	Fluka
M-MLV reverse transcriptase	Promega
Nonidet-P-40	Fluka
Oligo dT	Promega
Paraformaldehyde	Sigma
Paraffin	Paraplast® PlusTM Leica
Pefabloc	Fluka
Penicillin	Gibco
Pepstatin A	Sigma
Polyacrylamide	Roth
Potassium dihydrogen phosphate	Riedel- de Haën
PBS	Life technologies
RNAlater (RNA stabilization reagent)	Qiagen
SOC medium	Invitrogen
SDS	Serva
Sodium fluoride	Riedel- de Haën
Sodium chloride	Sigma Aldrich
Sodium hydroxide	Sigma Aldrich
Sodium hydrogen carbonate	J.T.Baker
Sodium orthovanadate	Sigma
Streptomycin	Gibco
TEMED	Roth
Trypsin	Gibco
Triton-X 100	Sigma
Taq polymerase	Bioron

Chemicals / reagents	Supplier
Tris hydrochloride	Roth
Tween 20	Roth
Xylene	Sigma Aldrich
Yeast extract	Carl Roth
Zinc acetate dihydrate	Roth
Zinc chloride	Merck

2.5 Kits

Product	Supplier (Catalog number)
Basic nucleofector kit (SMC)	Lonza (VPI-1004)
DQ-gelatin	Thermofisher (EnzCheck, D12054)
Maxiprep kit	Macherey-Nagel (740424.10)
NucleoSpin® RNA extraction kit	Macherey-Nagel (740955)
Neonatal heart dissociation Kit	Miltenyi Biotec (130-098-373)
Neonatal cardiac fibroblast isolation Kit	Miltenyi Biotec (130-101-372)
QIAprep spin miniprep kit	Qiagen (27104)
QIAprep Plasmid midi kit	Qiagen (12143)
QuantiTect SYBR Green® kit	Qiagen (204243)
RNAeasy mini kit	Qiagen (74104)
Sensiscript RT kit	Qiagen (205211)
TOPO Mammalian Expression Vector Kit	Invitrogen (K36020)

2.6 Oligonucleotides

Gene	Primer sequence
Primers used for genotyping	
Zyxin WTR	5’ – TGGACGAAGTTTCCGTGTGTTG– 3’
Zyxin WTF	5’ – TACAAGGGCGAAGTCAGGGCGAGTG– 3’
Zyxin NEOF	5’ – GACCGCTTCCTCGTGCTTTAC– 3’
LPP Lacz F	5’ – GCATCGAGCTGGGTAATAAGCGTTGGCAAT– 3’
LPP Lacz R	5’ – GACACCAGACCAACTGGTAATGGTAGCGAC– 3’
LPP KOSB F	5’ – TTCCAGTTTCTCAGCTTAG– 3’
LPP KOSB R	5’ – CTGGACTATTGCTTGGTGAC– 3’
Primers used for cloning	
Zyxin F	5’ – GGCCATGGCGGCCCCCCGC– 3’
Zyxin R	5’ – TCAGGTCTGGGCTCTAGCGGAGTG– 3’
LPP F	5’ – GGCCATGTCTCACCCATCTTG– 3’
LPP R	5’ – CTACAGGTCAGTGCTTGCCT– 3’
Primers used for quantitative real time PCR	
Mouse RPL32	For 5’ – GGGAGCAACAAGAAAACCAA – 3’ Rev 5’ – ATTGTGGACCAGGAACTTGC -3’

Human/mouse Gapdh	For 5’ – GACCACAGTCCATGCCATCACTGC– 3’
	Rev 5’ – ATGACCTTGCCCACAGCCTTGG– 3’
Mouse TRIP6	For 5’ – TACAAGTGTGAGGAGTGTGGG– 3’
	Rev 5’ – TGAGAGCTCTTGGATACGCC– 3’
Mouse LPP	For 5’ – ACCCTACAAGCCACGTCCCC
	Rev 5’ – GGTGGCTGCTGTGGAAT
Mouse LOX	For 5’ – CAGCCACATAGATCGCATGGT– 3’
	Rev 5’ – GCCGTATCCAGGTCGGTTC– 3’
Mouse CTGF	For 5’- CGAAGCTGACCTGGAGGAA–3’
	Rev 5’ – TTGGCGATTTTAGGTGTC–3’
Mouse Col I α1	For 5’ – GAGCGGAGAGTACTGGATCG–3’
	Rev 5’ – TACTCGAACGGGAATCCATC–3’
Mouse Col III α1	For 5’ – TGGTCCTCAGGGTGTAAAGG–3’
	Rev 5’ – GTCCAGCATCACCTTTTGGT–3’
Mouse Itgb1	For 5’ – TGGCAACAATGAAGCTATCGTG–3’
	Rev 5’ – GTAGGACAGTCTGGAGTCTCCACA–3’

2.7 Antibodies

Antibody	**Application, Dilution, Supplier**
Primary antibody used in this study	
Rabbit polyclonal anti-zyxin, B71	WB, 1:1000
	ICC 1:250, Prof. Mary Beckerle, USA
Rabbit polyclonal anti-PCNA	IHC, 1:200, Abcam #ab2426
Mouse monoclonal anti-beta actin	WB, 1:5000, Abcam #ab6276
Rabbit polyclonal anti-tubulin	WB, 1:1000, Cell signaling #2144
Rabbit polyclonal anti-histone H3	WB, 1:3000, Abcam #ab1791
Rabbit polyclonal anti-Ki67	IHC, 1:200, Abcam #ab16667
Mouse monoclonal anti-LPP	ICC, 1:200, Abcam # ab211682
Rabbit polyclonal anti-LPP	WB 1:1000, Atlas antibodies # HPA011133
	IHC, 1:200, Atlas antibodies # HPA011133
Rabbit polyclonal anti-TRIP6, B65	WB 1:1000, Prof. Mary Beckerle, USA
	IHC, 1:200, B65, affinity purified
Mouse monoclonal anti-SMA	ICC, 1:200, Abcam # 7817
Rabbit polyclonal anti-SMA	ICC, IHC, 1:200, Abcam # 5694
Rabbit monoclonal anti-calponin	ICC, IHC, 1:200, Abcam # 46794
Rabbit polyclonal anti-LOX	ICC, IHC, 1:200, Abcam # 31238
Rabbit monoclonal anti-GAPDH	WB, 1:5000, Cell signaling #2118
Secondary antibody used in this study	
Cy2-conjugated donkey IgG (H+L)	ICC 1:100 Dianova
Cy3-conjugated donkey IgG (H+L)	ICC 1:100 Dianova
Cy5-conjugated donkey IgG (H+L)	ICC 1:100 Dianova
Rabbit Goat IgG peroxidase	WB 1:5000 Sigma # A6154

Mouse Goat IgG peroxidase	WB 1:5000 Sigma # A4416

2.8 Growth media

Media	Purpose	Composition
Growth medium	Isolation of VSMCs	DMEM (1x) + GlutaMaxTM-I + 5% FCS +Penicillin/Streptomycin/Fungizone
Growth medium	Propagation of VSMCs	DMEM (1x) + GlutaMaxTM-I + 15% FCS +Penicillin/Streptomycin/Fungizone
Growth medium	Propagation of ACFs	DMEM (1x) + GlutaMaxTM-I + 10% FCS +Penicillin/Streptomycin/Fungizone
DMEM-methocell	Spheroid preparation	1.2% Methyl cellulose + DMEM (1x) + GlutaMaxTM-I + 30% FCS +Penicillin/Streptomycin/Fungizone
Luria-Bertani (LB) agar	Propagation of bacteria	1.5 % (w/v) Agar in LB medium + 50 µg/ml ampicillin
Luria-Bertani (LB) medium	Propagation of bacteria	1.0 % (w/v) Bacto-tryptone + 0.5 % (w/v) Yeast extracts + 1.0 % (w/v) NaCl

2.9 Buffers and solutions

Buffer	Composition
Blocking buffer for ICC/IHC	0.25 % Casein + 0.1 % BSA + 15 mM NaN_3 + 50 mM Tris, pH 7.6
Blocking buffer for WB	5 % milk powder or Blotto® in TBST
Collagenase solution (Type 2)	2% (w/v) solution in PBS
DNase I solution	0.5% (w/v) solution in PBS
Lysis buffer (whole cell lysates)	10 mM HEPES, pH 7.9 + 10 mM KCl + 0.1 mM EDTA + 0.1 mM EGTA + 0.1 M DTT

	+ 50 µM Pefabloc + 25 µM Protease inhibitors mix
Lysis buffer I for nuclear extraction	10 mM HEPES, pH 7.9 + 10 mM KCl + 0.1 mM EDTA + 0.1 mM EGTA + 0.15 % Nonidet-P-40 Supplement fresh with + 20 mM Na_3VO_4 + 15 mM NaF + 1 mM DTT + 1 mg/ml pefabloc + 12 µg/ml Protease inhibitor mix
Lysis buffer II for nuclear extraction	20mM HEPES + 400 mM NaCl + 0.01 mM EDTA + 0.01 mM EGTA + 0.15 % Nonidet-P-40 Supplement fresh with + 20 mM Na_3VO_4 + 15 mM NaF + 1 mM DTT + 1 mg/ml pefabloc + 12 µg/ml Protease inhibitor mix
Membrane stripping buffer	0.2 M NaOH
Mounting medium for ICC/IHC	0.1 M Tris HCl, pH 8,5 + 10 % Mowiol 4-88 + 25 % Glycerin + 2.5 % DABCO
Phosphate-buffered saline (PBS)	8.0 g NaCl + 0.2 g KCl + 1.44 g Na_2HPO_4 + 0.2 g KH_2PO_4, in 1 liter H_2O
Pefabloc	15 mM HEPES buffer, pH 7,4 + 4 % Pefabloc-SC
Protease inhibitor mix (PIM)	1 % Pepstatin-A in 20 % DMSO + 80 % 15 mM HEPES, pH 7,4 + 1 % Leupeptin in 20 % DMSO
Ringer's solution	154 mM NaCl, + 5.6 mM KCl + 2.4 mM $CaCl_2$, + 6 mM $NaHCO_3$ + 5.6 mM Dextrose, + 30 mg/l Sodium nitroprusside

	+ 27 mg/l Adenosine
Running buffer for SDS-PAGE	25 mM Tris HCl, pH 8.3 + 192 mM Glycine + 0.1% SDS
5x TBE buffer	450 mM Tris + 450 mM Boric acid + 20 mM EDTA, pH 8.0
Tris-buffered saline (TBS)	6.1 g Tris (0.5 M) + 8.75 g NaCl (1.5 M) in 1 liter H_2O
TBST	0.05 % Tween-20 in TBS
Transfer buffer	25 mM Tris HCl, pH 8.3 + 192 mM Glycine
Zinc fixative	0.1 M Tris HCl, pH 7.4 + 3.2 mM $Ca(CH_3COO)_2(H_2O)$ + 22.8 mM $Zn(CH_3COO)_2.2H_2O$ + 35.9 mM $ZnCl_2$

3 Methods

3.1 Animal experiments

All animal studies were performed with permission of the Regional Council Karlsruhe and in conformance with the Guide for the Care and Use of Laboratory Animals published by the US National Institute of Health (NIH publication No. 85-23, revised 1996). C57Bl6/J wild type (WT) mice were purchased from Charles River laboratories. Zyxko[110] and Lppko[103] mice (at least 10 times back crossed on the C57Bl6/J background) were bred and housed in the Interfaculty Biomedical Facility (IBF) of Heidelberg University. Mice were housed in plastic cages with hard wood chips as bedding, under controlled conditions of 12 hour dark-light cycles. They all received standard pellet diet and water ad libitum. Mice were euthanized in CO_2 chambers.

3.2 Methods using isolated cells

3.2.1 Cell isolation and culture

3.2.1.1 Isolation of mouse vascular smooth muscle cells (VSMCs)

To isolate the mouse VSMCs, the thoracic aorta was isolated, cleared from surrounding fat and cut into small fragments. After washing with Hank's Balanced Salt Solution (HBSS), these fragments were transferred to one well of a 6-well plate containing 1.4 ml of SMC growth medium (DMEM: SMC growth medium 2 in 1:1 ratio) supplemented with 5% FBS and containing 250 µl collagenase solution (1%). The arterial fragments were incubated overnight at 37 °C for better digestion and the medium was replaced with fresh SMC growth medium without collagenase on next day. Upon reaching the 70-80% of cell confluency, the cells were trypsinized and centrifuged for 5 minutes at 1000 rpm. The cell pellet was suspended in DMEM medium containing 15% FCS, antibiotics and fungicide for further propagation and experimentation.

3.2.1.2 Monolayer culture of VSMCs (2D cell culture)

Isolated VSMCs were seeded in T25 or T75 flasks and propagated with DMEM containing 15% FCS and supplemented with antibiotics and fungizone. For the experiments, cells were either seeded on plastic plates or collagen type I-coated BioFlex® culture plates. Cells were allowed to grow in a CO_2 incubator (5%) at 37 °C. Cells cultured up to maximum three passages were used for the experiments to avoid artifacts due to prolong sub-culture of smooth muscle cells.

3.2.1.3 Culturing of VSMCs in 3D spheroid

DMEM with 30% FCS containing antibiotic and fungizone was mixed with methylcellulose (stock, 1.2% methylcellulose in DMEM basal medium) in a ratio of 4:1[112]. To form spheroid, VSMCs were seeded in U-bottom 96-well plates (3000 cells/well) in DMEM-methylcellulose medium and incubated O/N at 37 °C. Cell spheroids were further allowed to grow for 48 hours prior to harvest for specific purposes.

3.2.1.4 Isolation and culture of cardiac fibroblast from adult mouse heart

For isolation of adult cardiac fibroblasts (ACFs), the heart was isolated from euthanized animal and the atrium was removed. The remaining ventricular parts of the heart were washed several times with cold PBS to remove red blood cells and cell debris. The heart was chopped in fine pieces and incubated with the digestion solution from neonatal heart dissociation kit for 10 min at 37 °C without shaking. From this digested heart, single cell suspension was prepared by using GentleMACs dissociator. After sieving the cell suspension from any undigested part, the cell pellet was collected by centrifuging. This cell pellet was then sorted for cardiac fibroblast by magnetic-activated cell sorting (MACS) using neonatal cardiac fibroblast isolation kit according to the provided protocol. Isolated ACFs were then seeded in a gelatin coated 6-well plate with DMEM medium containing 10% FCS and antibiotics. ACFs were allowed to grow till 70-80% confluency and used within 3-5 days.

3.2.2 Biomechanical stretch protocol

According to Laplace's law, wall tension in a blood vessel is dependent on transmural pressure, radius of the vessel and wall thickness. As it is difficult to expose cultured VSMCs to a transmural pressure gradient, an easier, reproducible way of mimicking wall tension *in vitro* is to increase its radial component. Biochemical stretch method is routinely used to mimic an increase in circumferential wall tension during hypertension[55,113]. VSMCs were seeded on collagen I-coated BioFlex® culture plate and were exposed to 15% cyclic elongation at 0.5 Hz with a sinusoidal profile using a Flexercell®FX-5000™ strain unit for specific time periods depending on the experimental design. However, cyclic stretch generated in this model is not a reflection of the pulsatile nature of blood flow in the body.

3.2.3 Transfection

A Nucleofector™ technology (LONZA) was used for transient transfection of expression plasmids in VSMCs according to the manufacturer's instructions. $2x10^6$ cells were transfected with 4 µg of

plasmid DNA using the preset program U025 for primary smooth muscle cells. A GFP expressing construct (Lonza) was used as a control for all transient transfection experiments. After 48 hours of transfection, the cells were analyzed. The transgenic expression was confirmed by immunofluorescence and Western blot analysis.

3.2.4 Immunofluorescence (IF) analysis

3.2.4.1 Fixation and IF analysis of monolayer 2D culture of VSMCs

Cells were either fixed with 4 % PFA (15 min, at room temperature, RT) or ice cold methanol (10 min, at –20 °C) depending on the experiment. The fixed cells were permeabilized with 0.1% Triton X-100 for 10 minutes and incubated with casein blocking solution for 30 minutes. Thereafter, cells were incubated with primary antibodies (diluted in the blocking solution) for 2 hours at RT or overnight at 4 °C. The cells were washed with PBST to remove excess unbound antibodies and incubated with secondary antibodies (conjugated with Cy2, Cy3, Cy5) for 1 hour at RT. After washing with PBS, the cells were incubated with nuclear staining dye DAPI (4', 6-diamidino-2-phenylindole) for 5 minutes, washed with PBS and mounted on cover slips with mowiol. Images were obtained using an IX81 confocal microscope equipped with a IX-DSU disk unit and analyzed with ImageJ.

3.2.4.2 Fixation, paraffin embedding and IF analysis of 3D spheroid culture of VSMCs

After 48 hours of culturing (3000 cells/spheroid), spheroids were harvested and fixed with zinc fixative for O/N at 4 °C. Subsequent rehydration steps were followed by serial incubation in 70%, 85%, 96% ethanol and isopropanol and finally embedded in the paraffin wax[112]. The paraffin embedded spheroids were sectioned in 5 µm thickness and deparaffinized after O/N drying at 37 °C. Deparaffinized spheroid sections were then incubated with blocking buffer and finally with primary antibody for 2 hour at RT or overnight at 4 °C. After washing off the nonspecifically bound primary antibody, fluorescent probes conjugated secondary antibodies were incubated for 1 hour at RT. Finally, the spheroid sections were mounted with mowiol using cover slips. Images were taken with IX81 confocal microscope and analyzed with the ImageJ.

3.2.5 Molecular biology methods

3.2.5.1 Isolation of RNA from cultured cells

Total RNA was isolated using a RNA extraction kit according to manufacturer's instructions. Cells were briefly washed with ice-cold Hanks PBS solution and lysed with 350 µl lysis buffer containing

1% β-mercaptoethanol. The RNA was eluted in 30-35 µl of RNase-free water. The concentration and quality of the RNA was determined using a spectrophotometer (NanoDrop ND-1000).

3.2.5.2 Reverse transcription

Reverse transcription of the isolated RNA was carried out using Omniscript RT Kit according to the supplied protocol. Briefly, 500 ng of the RNA template and 0.1 M Moloney murine leukemia virus reverse transcriptase (M-MLV RT) were mixed with oligo dT primer in a volume of 20 µl and incubated at 42°C for 50 minutes for first strand cDNA synthesis. The resultant cDNA (20 µl) was diluted 1:5 or 1:10 with Dnase-free water for conventional and real time PCR, respectively.

3.2.5.3 Standard PCR

Standard PCR has been used to amplify gene sequences for cloning or mice genotyping. The PCR reaction mixture (containing cDNA, dNTP, MgCl2, taq-polymerase with 10x reaction buffer in 50 µl volume) was placed in an automatic thermocycler.

3.2.5.4 Quantitative real time polymerase chain reaction (real time PCR)

Real time PCR was performed by using the QuantiTect SYBR Green® kit. Briefly, 5 µl cDNA, 1 µl each of forward and reverse primers (10-20 µM), 3 µl of RNase-free water, and 10 µl of SYBR Green were added to obtain a final reaction volume of 20 µl. Different annealing temperatures were used for specific primer pairs. The quantification of changes in gene expression was done using the (delta) (delta) Ct method[114](based on the number of cycles required for crossing a certain threshold of detection). Expression levels of all the experimental genes were normalized using the reference gene RPL32 (60S ribosomal protein L32).

3.2.5.5 Expression plasmids

For mouse zyxin expression plasmid, a full-length PCR fragment including the first stop codon (positions 305 to 1999; NM_011777, from cDNA prepared from VSMCS) was sub-cloned into the pcDNA™6.2/N-EmGFP-GW TOPO® 5.9-kb vector, with the TOPO cloning reaction according to the manufacturer's recommendations. For the mouse LPP expression plasmid, the same principle was used with a full length PCR fragment including the first stop codon (Positions 551 to 2392; NM_178665.5, from cDNA prepared from VSMCS). Positive constructs were sequenced and used for transient overexpression experiments. In both cases, 2 µl of the TOPO vector containing the PCR fragment was transformed in Top10FTM competent bacterial cells. 50 and 100 µl of transformed

bacterial cells were plated on sterile LB-agar plates with ampicillin. Bacterial colonies were allowed to grow overnight at 37 °C. Transformed colonies were randomly picked and inoculated in LB medium with antibiotics and let them grow overnight at 37 °C with shaking. Plasmids were purified using the QIAPrep® Spin Miniprep kit according to manufacturer's instructions. The proper orientation of the insert was verified by restriction digestion and sequencing. For the correct plasmids, the corresponding bacterial colonies were further propagated and a concentrated plasmid DNA was prepared by QIAPrep® Maxiprep kit.

3.2.6 Biochemical methods

3.2.6.1 Total protein extraction

Cells were washed with ice-cold HBSS and 100 µl of whole cell lysis buffer was added to each well of a 6-well plate. Cells were then scraped off and collected into 1.5 ml tubes placed on ice. 2.5 µl of Triton X-100 was added for each 50 µl of lysis buffer and incubated for 10 minutes. The resulting lysate was centrifuged at 12,000×g for 15 minutes at 4 °C to remove any debris. The lysate was either snap frozen and stored at -80 °C or used for further analysis. The protein concentration was measured using a Bradford assay (Bio-Rad) with a colorimetric plate reader.

3.2.6.2 Nuclear protein extraction

To determine the sub-cellular localization of proteins, the cell lysate was separated into cytosolic and nuclear fractions[58]. VSMCs were lysed using lysis buffer I for nuclear extraction. The lysates were centrifuged (12,000×g at 4 °C for 15 minutes) and the supernatant (cytosolic fraction) was collected. The residual pellet containing the nuclear fraction was washed twice with ice-cold Hanks buffer, dissolved in 40 µL lysis buffer II and sonicated 2 times for 5 seconds at 50 Watts on ice. After centrifugation (12,000×g at 4 °C for 15 minutes), the supernatant containing the nuclear fraction was collected.

3.2.6.3 Immunobloting

Protein samples were separated by sodium dodecyl sulfate polyacrylamide gel electrophoresis (SDS-PAGE). Separating gels were prepared depending on the size of the proteins of interest. Proteins were denatured by addition of sample loading buffer followed by heating at 95°C for 10 minutes. The proteins were then separated in gel and transferred into a PVDF membrane (pre-activated with methanol, 10 minutes at RT). After the transfer, the membrane was incubated with blocking buffer

for 1 hour, followed by incubation with primary antibody overnight at 4 °C. After brief wash of membrane with TBST, secondary antibody (conjugated to horseradish peroxidase) incubation was done for 1 hour at room temperature. Finally, the membrane was washed with TBS and the proteins were detected by chemiluminescence based method using an 'ImageQuant LAS 4000 mini' imaging system. Densitometric analysis was done with the help of ImageJ.

3.2.7 Functional assays using cultured cells

3.2.7.1 Migration analysis by wound healing assay in 2D cell culture of VSMCs

Mouse VSMCs (5×10^4 cells/well) were seeded in 12-well plastic plates with a silicon block in the middle of the well. Upon reaching the cell confluency around 70-80%, the silicon block cell growing hindrance was gently removed. Light microscopic images were taken at the beginning and 24 hours later (at same spots on both days). The distance between the cell borders was measured by ImageJ.

3.2.7.2 Proliferation assay by counting DAPI-positive nuclei in 2D cell culture of VSMCs

VSMCs isolated from same animal were seeded in two 6-well plastic plates (2×10^4cells/well) and allowed to attach (6 hours). Immediately after attachment, the cells in one plate were fixed (T0) while the other was fixed 72 hours (T72) after the attachment. Cells were fixed with 4 % PFA and stained with DAPI. Images were taken and analyzed with ImageJ.

3.2.7.3 Migration by spheroid invasion assay in 3D cell culture of VSMCs

A modification of the spheroid angiogenesis assay was used to measure the invasion of VSMCs into a collagen gel as previously described[112,115]. To form spheroid, VSMCs were seeded in U-bottom 96-well plates (500 cells/well) in growth medium containing methylcellulose and incubated O/N at 37 °C. The spheroids were then suspended into a gel containing rat tail collagen-type-I and 1 ml of the resultant mixture was plated in one well of a 24-well plates and allowed to polymerize at 37 °C for 30 minutes. 100 µL of DMEM medium (containing 30% FCS) was added over the gel surface. 24 hours later light microscopic images of the spheroids were taken and the number of sprouts and cumulative length was measured. For each genotype, at least 20-25 spheroids were analyzed per experiment.

3.2.7.4 Analysis of proliferation and contractile properties of VSMCs in 3D cell culture

To study the proliferation nature of the VSMCs in 3D spheroid culture, the paraffin embedded spheroid sections (5 µm thick) were immunoflurescently labeled with Ki67 and DAPI. From captured confocal images Ki67-positive DAPI nucleus were counted. For contractile properties of the VSMCs in 3D spheroid culture, sections were stained for alpha smooth muscle actin (α-SMA), calponin and DAPI.

3.2.7.5 Analysis of matrix metalloproteinases (MMP) activity of VSMCs in 2D and 3D cell culture

MMP activity was measured in the fixed cells by DQ-gelatin assay (EnzChek). Normally, in DQ-gelatin, the fluorescence intensity is intramolecularly quenched and can be revealed after proteolytic degradation (Figure 3.1). In 2D monolayer cell culture, VSMCs were serum starved for 24 hours and fixed with ice cold methanol at -20°C. Fixed cells were then incubated with DQ-gelatin at 37 °C for 1 hour. Thereafter, these cells were further immunostained with either MMP9 or MMP2. Zinc fixed paraffin embedded spheroid sections were incubated with DQ-gelatin at 37 °C for 2 hours and further stained for either MMP9 or MMP2[116]. Nucleus was counter stained with DAPI.

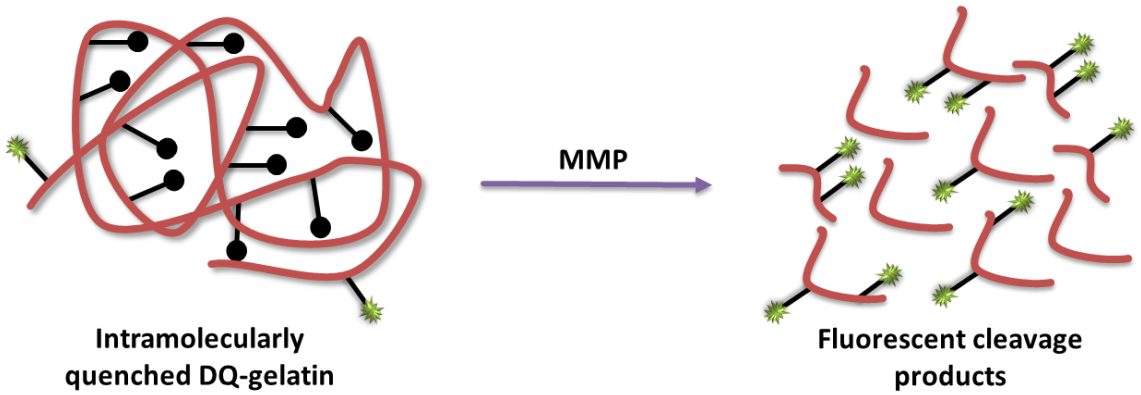

Figure 3.1 Principle of MMP activity detection via DQ-gelatin assay
The degree of MMP activity is determined by the extent of fluorescence intensity revealed upon hydrolysis of the labeled and quenched substrate provided in the DQ-gelatin assay kit.

3.3 In vivo methods

Experimental hypertension was induced in WT, Lppko and Zyxko mice to study the remodeling processes in the heart and vasculature. All animal experiments were approved by the local ethics committee (Ethics approval G 217/14 and G 60/15).

3.3.1 Induction of experimental hypertension

3.3.1.1 Induction of hypertension by DOCA-salt

The DOCA-salt model is a renovascular volume-overload model which induces an increase in blood pressure by retention of sodium and water in the kidneys[117]. Briefly, 3 months old (young) WT and Lppko mice were anaesthetized using isoflurane. After removing the hair from back, the skin was disinfected and a small incision was made for a paravertebral pocket. The DOCA-salt pellet (50 mg) was placed inside the pocket. The pellets contained a biodegradable matrix which released the active ingredient in a sustained manner over a period of 21 days. The incision was closed with sutures and the animal was allowed to regain consciousness. The body temperature of the animal was maintained at 37 °C during the entire procedure. In order to complement the effect of DOCA-salt on blood pressure, the drinking water was supplemented with 1% w/v (Figure 3.2)

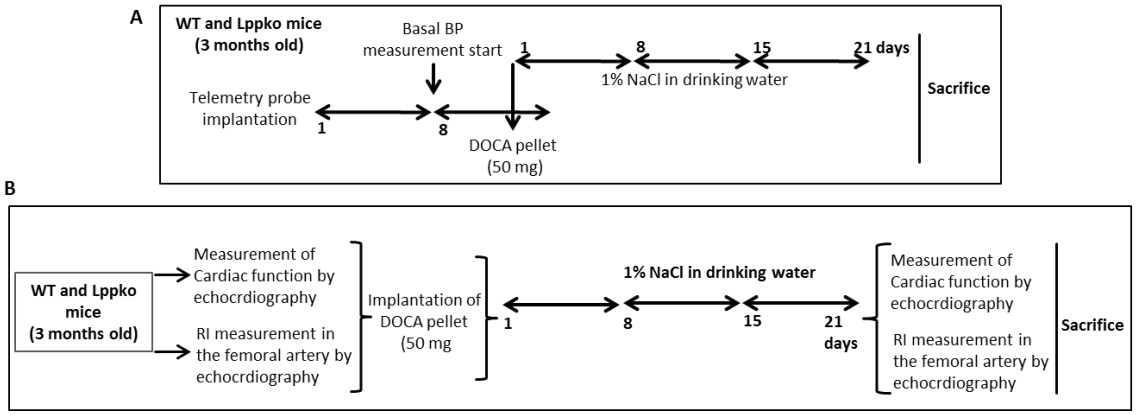

Figure 3.2 Schematic representation of the DOCA-salt model used to induce experimental hypertension and the subsequent analyses performed

(A) Protocol for the blood pressure measurement. (B) Experimental design to measure cardiac function and the resistivity index in the DOCA-salt treated animals. Abbreviations: BP, blood pressure; RI, resistivity index. Each double headed arrow represents a period of seven days.

3.3.1.2 Induction of hypertension by angiotensin II

Aged matched WT and Zyxko mice were anaesthetized using isoflurane. After removing the hair and disinfecting the skin, a paravertebral pocket was created towards the head between the subcutis and the fasciae of the back muscles. The osmotic mini pump filled with Ang II (in a dose of 1.5 mg/kgBW/day, stock was diluted in 0.9% NaCl for specific body weight) was placed in the pocket. The incision was closed with sutures and the animal was allowed to regain consciousness. The body temperature of the animal was maintained at 37 °C during the entire procedure (Figure 3.3).

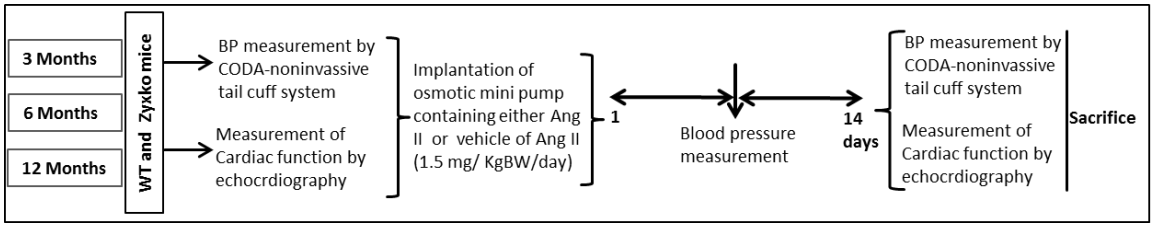

Figure 3.3 Schematic representation of the angiotensin II model to induce experimental hypertension and the subsequent analyses performed
Physiological saline solution (0.9%, w/v, NaCl) was used as vehicle control for the treatment with angiotensin II. Abbreviations: Ang II, angiotensin II; BP, blood pressure. Each double headed arrow represents a period of seven days.

3.3.2 Blood pressure measurements in mice

3.3.2.1 Telemetry

Arterial blood pressure was monitored using radio telemetry probe (PA-C10, DSI) placed at the aortic arch through the left common carotid artery. Briefly, the pain reflex of the isoflurane (1-3% v/v) mediated anaesthetized mouse was tested and the limbs were fixed with tape. The hair was removed from the throat region prior to skin disinfection. The animal was slightly stretched for better visualization of the carotid arteries by placing a thread to the upper incisors. After skin incision, the salivary glands and left common carotid artery were carefully separated from the surrounding fats, nerves and veins. A permanent cranial ligature was placed just below the bifurcation of the carotid artery and a caudal occlusion was made with a micro-vessel clip to temporarily stop the blood flow in this artery segment. The probe was inserted into the artery through a delicate incision and made sure that the tip reached the arch of the aorta and was exposed to the circulating blood. The battery unit of the device was placed in a subcutaneous pocket in the lateral left flank of the mouse. The skin incision was closed and the animal was allowed to regain consciousness. The complete surgical procedure was carried out by placing the mouse on a heating plate at 37 °C. The operated animal was placed inside the cage and kept warm by exposing infra-red light for at least 1 hour. After 7-8 days of post-operative recovery stage, baseline blood pressure was recorded for five days. DOCA (deoxycorticosterone acetate)-salt pellets were implanted afterwards and blood pressure was monitored for next 21 days (Figure 3.2).

3.3.2.2 CODA® tail-cuff method

The tail-cuff method is a non-invasive method for blood pressure measurement in mice. The CODA® tail-cuff system was designed to accurately measure blood pressure in the mouse by utilizing volume pressure recording (VPR) sensor technology to detect the changes in tail volume that correspond to

systolic and diastolic pressures. The mouse was inserted into a small restrainer and placed on a warm platform to comfortably house the mouse while minimizing the movement during the measurement session. The darkened nose cone of the restrainer limit the mouse's view and decreased the level of stress. The rear of the restrainer with the mouse tail was extended outward. The CODA non-invasive blood pressure system relies on two tail cuffs to measure blood pressure, occlusion cuffs (O-cuff) and volume pressure recording cuffs (VPR-cuff). During the measurement cycle, the VPR-cuff inflates first to push blood out of the tail. The O-cuff inflated first to block blood flow back into the tail. The VPR cuff deflates to 30 mmHg pressure to remain snug around the tail to detect changes in tail volume. As the O-cuff deflates and the systolic blood pressure exceeds the O-cuff pressure, blood will flow into the tail and the VPR cuff will detect the increase in tail volume. The O-cuff pressure at the point when tail volume increases is the systolic blood pressure. O-cuff continues to deflate, and the pressure at the point when the rate of tail volume change no longer increases is the diastolic blood pressure. This non-invasive blood pressure measurement protocol can measure systolic, diastolic, and mean arterial blood pressure, heart rate, tail blood volume and blood flow. For each animal, 15 blood pressure reading cycles were performed and recorded (first 5 for acclimatization and the following 10 for regular cycle). Blood pressure recorded in the regular cycle was then used for subsequent analysis.

3.3.3 High resolution ultrasound measurements in mice

3.3.3.1 Echocardiographic image recoding and cardiac function analysis

For cardiac systolic and diastolic function analyses, VisualSonics Vevo 2100 imaging system equipped with MS-550D micro scan transducer (40 MHz) was used to record high resolution ultrasound images. The animal was anaesthetized with isoflurane (1-3% v/v) and positioned on heating platform at supine position. Electrocardiogram (ECG), respiration and body temperature was continuously monitored during the recoding of the images. After removing hair from the chest area, a generous amount of warm ultrasound-compatible gel was applied to record the images.

The morphology and the systolic function of the heart were analyzed in the parasternal long axis view (PLAX). Images were taken in the brightness mode (B-mode) and the motion mode (M-mode). Anatomical structures were identified in B-mode which displayed two-dimensional images of an area of interest. In the M-mode, the movement of the sample volume (vertical line in B-mode) over time was displayed (Figure 3.4 A). The images were analyzed using the analysis software from VisualSonics (Figure 3.4 B). The measurements available in the M-mode include the left ventricular (LV) anterior wall thickness during systole and diastole, LV internal diameter in systole and diastole,

LV posterior wall thickness in systole and diastole, intraventricular septum thickness in systole and diastole. Based on these parameters, the software uses inbuilt algorithms to calculate ejection fraction, fractional shortening, stroke volume and cardiac output of the heart.

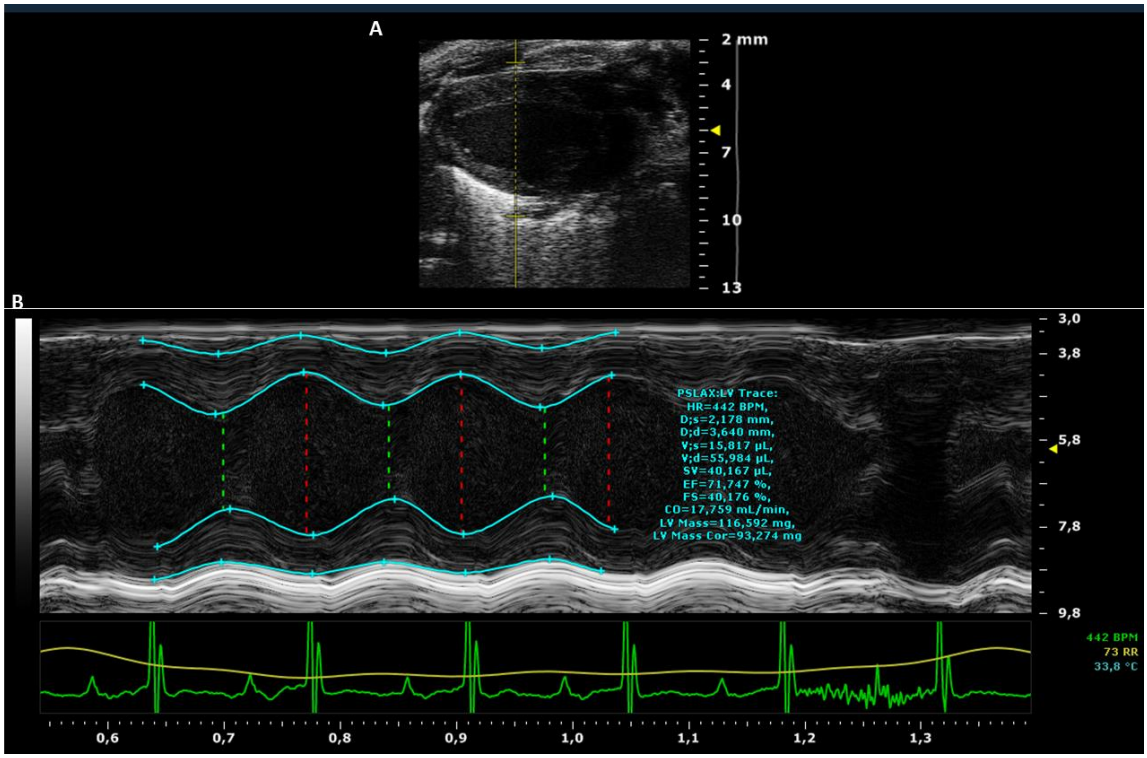

Figure 3.4 Echocardiographic image recoding and cardiac systolic function analysis
(A) Representative echocardiographic image in the parasternal long axis view (PLAX) in M-mode. (B) Measurement of cardiac systolic functional parameters e.g. cardiac output (CO), fractional shortening (FS), ejection fraction (EF), and stroke volume (SV) from the recoded M-mode image. The bottom trace shows the simultaneously recorded electrocardiogram.

The diastolic function of the heart was analyzed in the apical four chamber view (Figure 3.5 A). Images were recorded in color and pulse wave (PW) Doppler mode. In color Doppler mode, the direction of the blood flow was visualized. In PW Doppler mode, velocity of blood flow, which is visualized in color Doppler mode imaging, were measured. For this purpose, the sample volume (square) is placed above the mitral valve and the blood flow was visualized using the color Doppler mode. Using the PW Doppler mode, the velocity for the passive filling of the ventricle (E value) and the active filling of ventricle (A value) were measured (Figure 3.5 B). In addition, the E/A ratio, a common indicator of diastolic function was calculated.

3.3.3.2 Measurement of resistivity index of femoral arteries by ultrasound imaging

The resistivity index (RI) is an important parameter which is determined from the arterial pressure waveform visualized in PW Doppler ultrasonography. To measure the RI towards the blood flow in

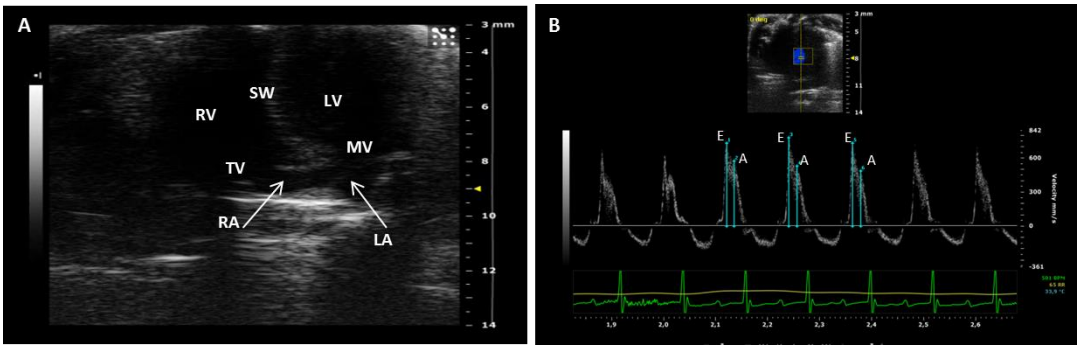

Figure 3.5 Echocardiographic image recoding and cardiac diastolic function analysis
(A) Recorded echocardiographic image in the apical four chamber view in B-mode with the area of view placed over the mitral valve. (B) Measurement for the early passive (E) and late active (A) filling velocities of the left atrium in the Pulse Wave Doppler mode. Abbreviations: SW, intraventricular septal wall; RV, right ventricle; LV , left ventricle; MV, mitral valve; TV, tricuspid valve; RA, right atrium; LA, left atrium.

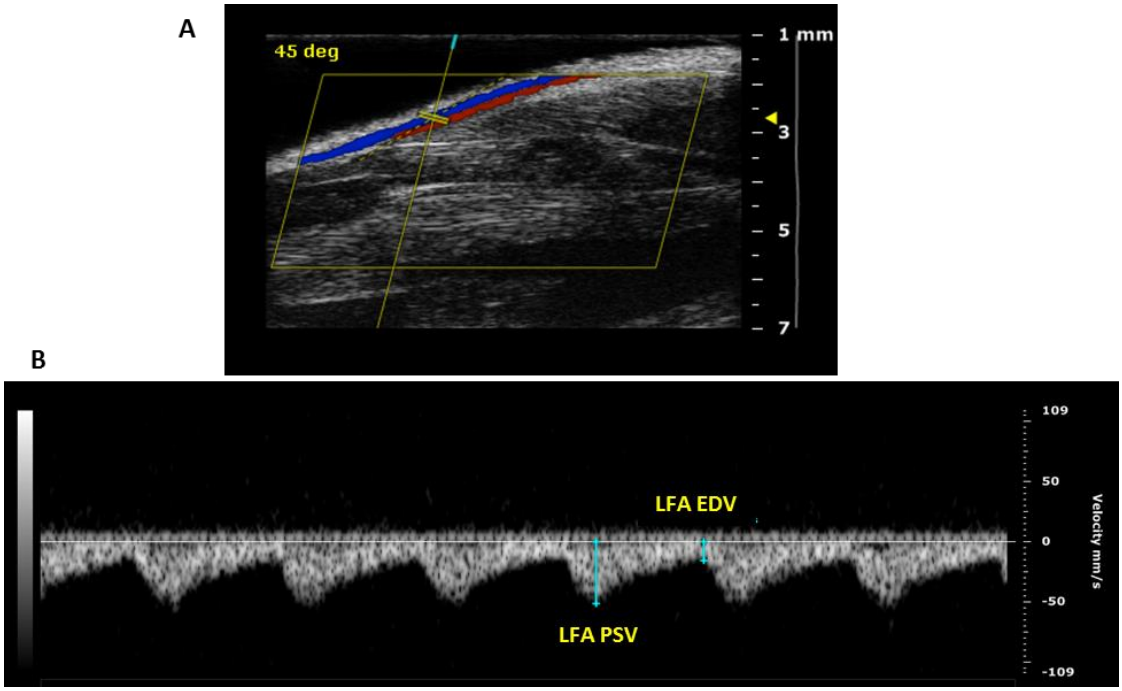

Figure 3.6 Measurement of resistivity index of the femoral arteries by ultrasound imaging
(A) Color Doppler image to locate blood flow in the femoral artery of the mouse. Blood flowing towards the transducer is represented by red and the blood flowing away from the transducer is represented by blue. (B) Measurement of the peak systolic velocity (PSV) and end diastolic velocity (EDV) in the left femoral artery.

the femoral arteries by ultrasound imaging, the animal was prepared on the platform as previously described (section 3.3.3.1). Hair was removed from the hip and the groin region down the left hind limb. A generous amount of warm ultrasound-compatible gel was applied and MS-770D micro scan transducer (70 MHz) head was placed parallel to the femoral artery. The position of the transducer was fine-tuned by using the B-mode and the femoral artery and the vein were distinguished by color Doppler mode (Figure 3.6 A). Blood flowing towards the transducer is represented by red and the blood flowing away from the transducer is represented by blue and in this case representing the vein

and artery, respectively. To acquire the images, the transducer probe was placed in an angle of 45° to the blood flow. The peak systolic velocity and the end diastolic velocities were measured with Vevo 2100 analysis software (Figure 3.6 B). These values were used to calculate the resistivity index (RI) using the formula: (Peak systolic velocity – End diastolic velocity)/ Peak systolic velocity.

3.4 Histochemical methods

3.4.1 Tissue preparation

In euthanized mice, retrograde perfusion was done with ringer solution by puncturing the heart in the left ventricle. Excised organs, after weighing, were preserved according to the subsequent analyses planned, i.e. heart tissue fixed in 4% PFA and isolated femoral artery in zinc fixative. After fixation, tissue samples were dehydrated using a series of increasing concentrations of ethanol (70, 85 and 99%) followed by incubation in Isopropanol. Thereafter, the tissues were embedded in paraffin blocks and stored at room temperature. A fine section of the tissues (5 µm in thickness) were dried and immobilized on the glass slides by drying at 42 °C overnight.

3.4.2 Histological staining

Masson's trichrome and van Gieson's staining protocol were used for the detection of collagen fibers in the heart. The specimens were mounted with a resinous mounting medium (Eukitt®) and imaged using a light microscope. In Masson trichrome staining, collagen stained blue, nuclei appeared black and muscle and cytoplasm appeared red whereas in van Gieson's staining collagen appeared pink, nuclei appeared black and the heart muscle appeared yellow. Slide stained with van Gieson's protocol were analyzed by two blinded persons for the experiment under microscope to calculate the fibrotic score without any biasness. Fibrotic scale was adapted from Beggah et al[118]. Scoring was performed as 0, no collagen at all; 1, only around the blood vessels; 2, at least 2 area of collagen deposition in cardiac tissue; 3, at least 4 area of collagen deposition in cardiac tissue; 4, at least 6 area of collagen deposition in cardiac tissue; 5, more than 6 area of collagen deposition in cardiac tissue[118].

3.4.3 Immunohistochemistry

Prior to immunostaining, the paraffin sections were deparaffinized and rehydrated. Heat mediated antigen retrieval steps were done using steam cocker with 0.1 M citrate buffer at pH 6 for the PFA-fixed samples. The tissue samples were encircled with a DAKO pen by drawing a water repelling

circle around the specimen. Thereafter, the same process of immunostaining was performed as described in section 3.2.4.2.

3.4.4 RNA isolation and cDNA preparation from tissues

Excised tissues were immediately placed in RNA later stabilization reagent (Thermofisher Scientific) for overnight. Tissues were homogenized in lysis solution with gentle MACs dissociator. A RNeasy® mini kit was used for isolating RNA according to manufacturer's instructions from the tissue lysates. Sensiscript® reverse transcription kit was used to synthesize the cDNA from purified RNA according to manufacturer's instructions.

3.4.5 Protein isolation from tissues

After tissue isolation, the samples were snap frozen and stored at -80 °C prior to use. The tissues were lysed with RIPA buffer containing a cocktail of protease inhibitor mixture (PIM), pefabloc® (Roche), sodium orthovanadate and sodium fluoride. Lysate was then cleared by centrifuging at 12,000 rpm at 4 °C for 15 minutes. The supernatant was collected, snap frozen and stored at -80 °C for further protein analysis.

3.5 Image analysis

All the acquired images were post processed and analyzed with ImageJ (https://imagej.net/Fiji/Downloads). To measure the fluorescence intensity of labeled protein, same threshold was used in 8-bit images. To count the nucleus number, batch command was recorded (with specific threshold for 8 bit image and circularity parameter to determine the shape for nucleus) and used. To analyze the fibrotic area in the heart section, randomly numbered images were analyzed by the blinded person for the experiment to record an ImageJ macro which was then further used.

Script of the macro to measure the fibrotic area was as follows

```
if (isOpen("Results")), {selectWindow("Results"); run("Close");}; run("Set Scale...", "distance=0"); run("Set Measurements...", "area redirect=None decimal=3"); run("Duplicate...", "title=RGB"); getRawStatistics(count,mean1,min,max,std1); run("Split Channels"); selectWindow("RGB (red)"); close(); selectWindow("RGB (green)"); setAutoThreshold("Triangle dark");//condition1 setOption("BlackBackground", false); getThreshold(lower1,upper1); if(abs(mean1-lower1)<10){}else{setAutoThreshold("Moments dark");//condition1setOption("BlackBackground", false); getThreshold(lower2,upper2); setThreshold(lower2-100/abs(mean1-lower1),255); setOption("BlackBackground", false);}run("Convert to Mask");run("Create Selection");//CS run("Make Inverse"); roiManager("Add"); roiManager("Select", 0); roiManager("Rename", fibrosis1"); selectWindow("RGB (blue)"); run("Gaussian Blur...", "sigma=2"); setAutoThreshold("Default dark");//condition 2 setOption("BlackBackground", false); run("Convert to Mask"); run("Create Selection"); run("Make Inverse"); roiManager("Add"); roiManager("Select", 1); roiManager("Rename", "tissue1"); close(); close(); run("Select None"); run("Duplicate...", "title=RGB"); roiManager("Select", 0); run("Multiply...", "value=0.000"); roiManager("Select", 1); run("Make Inverse"); run("Multiply...",
```

```
"value=0.000"); run("Split Channels"); imageCalculator("Subtract create", "RGB (green)","RGB (blue)"); selectWindow("Result of RGB (green)"); setAutoThreshold("Triangle dark");//condition 3 setOption("BlackBackground", false); run("Convert to Mask"); run("Create Selection"); roiManager("Add"); roiManager("Select", 2); roiManager("Rename", "muscle1"); close(); selectWindow("RGB (blue)"); close(); selectWindow("RGB (green)"); close(); selectWindow("RGB (red)"); close(); run("Select None"); run("Duplicate...", "title=RGB"); roiManager("Select", 2); run("Multiply...", "value=0.000"); run("Split Channels"); imageCalculator("Subtract create", "RGB (red)","RGB (blue)"); selectWindow("Result of RGB (red)"); setAutoThreshold("IJ_IsoData dark");//condition4 setOption("BlackBackground", false); run("Convert to Mask"); run("Create Selection"); roiManager("Add"); roiManager("Select", 3); roiManager("Rename", "fibrosis2"); roiManager("Select", newArray(0,3)); roiManager("Combine"); roiManager("Add"); roiManager("Select", 4); roiManager("Rename", "fibrosis"); roiManager("Select", newArray(1,2,4)); roiManager("Combine"); roiManager("Add"); roiManager("Select", 5); roiManager("Rename", "tissue"); close(); selectWindow("RGB (blue)"); close(); selectWindow("RGB (green)"); close(); selectWindow("RGB (red)"); close(); roiManager("Select", 0); roiManager("Delete"); roiManager("Select", 0); roiManager("Delete"); roiManager("Select", 0); roiManager("Delete"); roiManager("Select", 0); roiManager("Delete"); roiManager("Select", 1); run("Create Mask"); rename("Mask1"); run("Fill Holes"); run("Outline"); setOption("BlackBackground", false); run("Dilate"); run("Dilate"); run("Dilate"); roiManager("Select", 0); run("Create Mask"); rename("Mask2"); imageCalculator("Multiply create", "Mask1","Mask2"); selectWindow("Result of Mask1"); imageCalculator("Subtract create", "Mask2","Result of Mask1"); selectWindow("Result of Mask2"); run("Create Selection"); roiManager("Add"); close(); selectWindow("Result of Mask1"); close(); selectWindow("Mask2"); close(); selectWindow("Mask1"); close(); roiManager("Select", 0); roiManager("Delete"); roiManager("Select", 1); roiManager("Rename", "fibrosis"); rename("raw"); run("Select None"); run("Duplicate...", "title=tissue"); run("Duplicate...", "title=fibrosis"); selectWindow("tissue"); roiManager("Select", 0); run("Multiply...", "value=0.000"); selectWindow("fibrosis"); roiManager("Select", 1); run("Multiply...", "value=0.000"); run("Images to Stack", "name=Stack title=[] use"); run("Make Montage...", "columns=3 rows=1 scale=1 border=0 label"); selectWindow("Stack"); roiManager("Select", 0); roiManager("Measure"); roiManager("Select", 1); roiManager("Measure"); run("Select None"); setResult("Area", 2, getResult("Area",1)/getResult("Area",0)); setResult("Label", 2, "ratio of fibrosis"); setResult("Label", 0, "area of tissue"); setResult("Label", 1, "area of fibrosis");
```

3.6 Statistical analysis

Data were analyzed by GraphPad Prism7 (GraphPad Software). All the results were represented as means ± SEM of mentioned number of individual mice. For analyzing differences between two individual experimental groups, an unpaired Student's t test was used with $P<0.05$ considered statistically significant. Differences among 3 or more experimental groups were analyzed by one-way ANOVA, followed by a Tukey's multiple comparison test for selected pairs of groups with a probability value of $P<0.05$ considered statistically significant.

4 Results

4.1 Abundance of zyxin family members in the femoral artery of Zyxko mice

Age-dependent variation of the level of two closely related members of the zyxin family of LIM-domain-containing proteins, TRIP6 and LPP, in selected arterial blood vessels of Zyxko mice was determined by RT-qPCR and WB analyses.

4.1.1 Expression (mRNA levels) of TRIP6 and LPP in the femoral artery

In wild type animals, the fold change in TRIP6 and LPP mRNA expression remained similar at the time points studied (6 and 12 months versus the 3 months reference level). In Zxyko mice, mRNA for both gene products peaked at 12 months and then returned to baseline in the 18 months old animals (Figure 4.1 A, B).

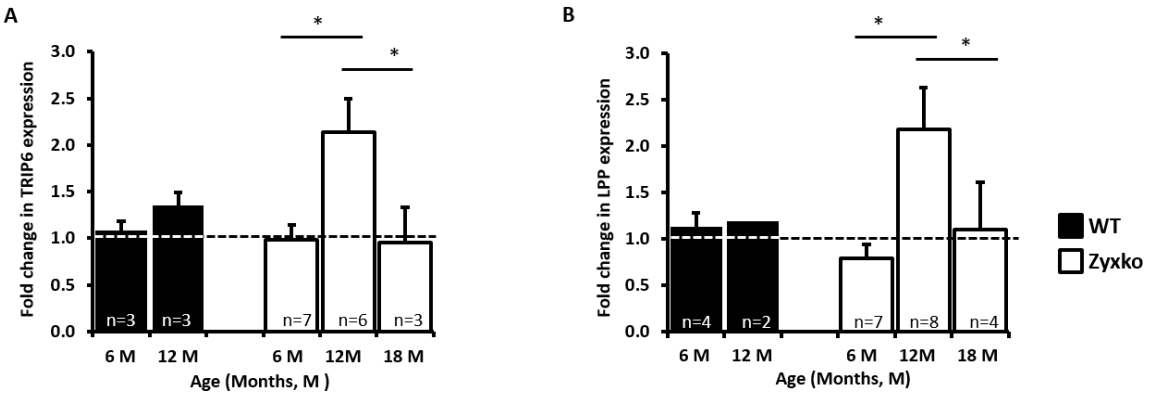

Figure 4.1 TRIP6 and LPP mRNA abundance in the femoral artery of wild type (WT) and zyxin knockout (Zyxko) mice from different age groups

(A, B) Fold change in the expression of TRIP6 and LPP mRNA, respectively. Expression levels were normalized using the reference gene RPL32. The level of expression at 3 months of age in the femoral artery of WT and Zyxko animals was used as calibrator for the respective group (set to 1, indicated by the broken line). Each column represents the mean ± SEM of the indicated number of individual analyses. *p<0.05 as indicated

4.1.2 TRIP6 and LPP protein levels in the femoral artery

TRIP6 protein abundance continuously declined in both WT and Zyxko mice to a comparable degree over time (Figure 4.2 A, C). LPP protein levels also decreased with age in the femoral artery of both WT and Zyxko mice. However, only in Zyxko mice, this decline in LPP protein abundance between 6 and 18 months of age was statistically significant (Figure 4.2 B, D). To rule out the possibility of a blotting variability, LPP protein from both WT and Zyxko mice of corresponding ages was further detected on the same blot. As expected, LPP protein levels remained similar in WT and Zyxko femoral arteries from 6 and 12 months old animals whereas this was significantly decreased in the 18 months old Zyxko animals (Figure 4.3).

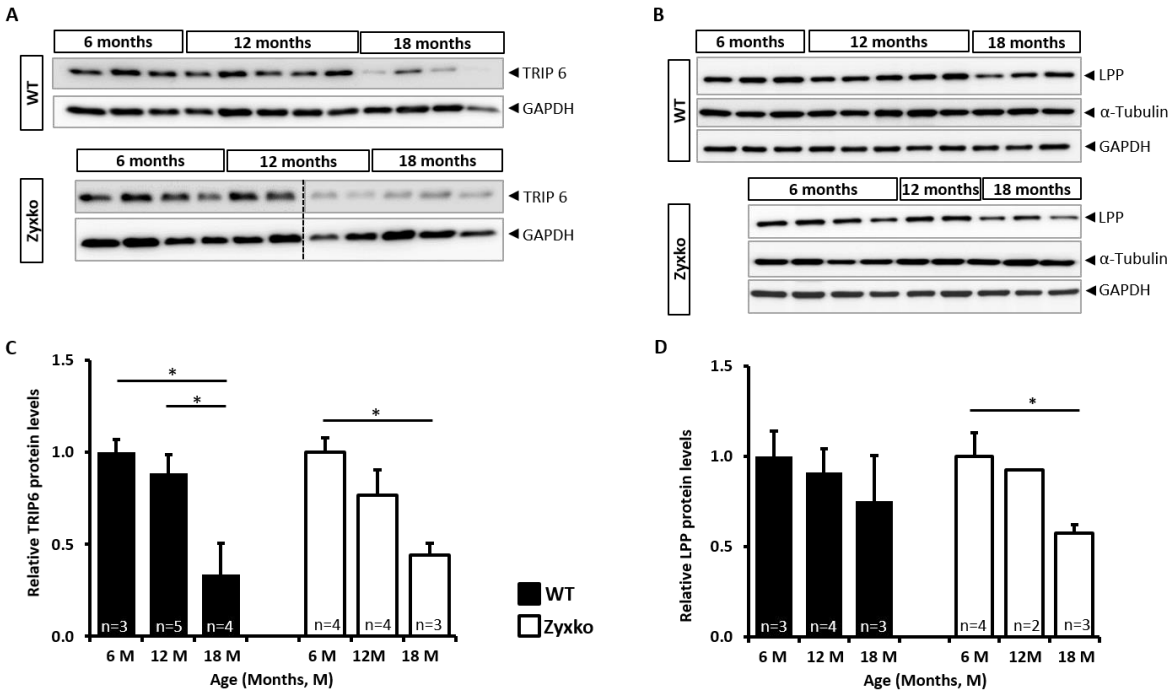

Figure 4.2 TRIP6 and LPP protein levels vary in an age-dependent manner in the femoral artery of Zyxko mice

(A, B) Representative WB images for TRIP6 (A) and LPP (B) in WT and Zyxko femoral artery samples. (C, D) shows quantification of the respective blots from (A) and (B). The individual values were normalized by using the loading controls, GAPDH and/or α-tubulin. The dashed line in (A) indicates an outlier value not included in the analysis. Each column represents the mean ± SEM of the indicated number of individual analyses. *p<0.05 as indicated

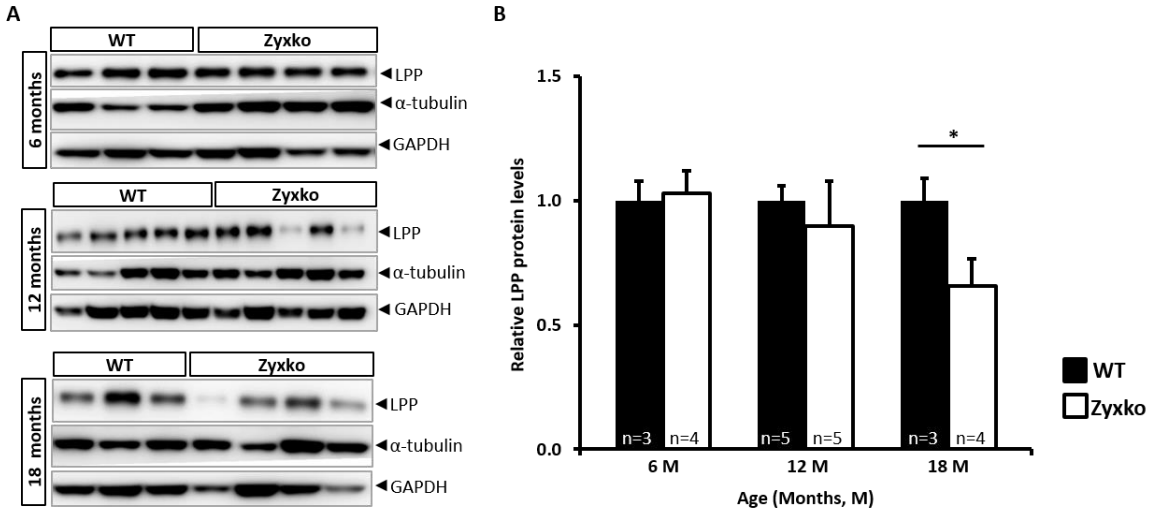

Figure 4.3 LPP protein level significantly declines in the femoral artery of very old (18 months) Zyxko mice

(A) Representative WB images for LPP, α-tubulin and GAPDH abundances in the femoral artery of 6, 12 and 18 months old WT and Zyxko mice. (B) Statistical summary of the relative LPP protein level in the femoral artery of WT and Zyxko mice. The values were normalized by the loading controls, GAPDH and/or α-tubulin. Each column represents the mean ± SEM of the indicated number of individual analyses. *p<0.05 as indicated

4.2 Cellular distribution of TRIP6 and LPP protein in vascular smooth muscle cells

4.2.1 Cellular localization of TRIP6 and LPP protein in mouse VSMCs

TRIP6 protein was mainly localized in the cytosol (perinuclear space) and at cell-cell contacts rather than the nucleus (Figure 4.4 A). On the contrary, LPP protein follows the cellular distribution pattern of zyxin, i.e. it is mainly localized to focal adhesion as well as the nucleus in quiescent, i.e. non-stretched VSMCs from the aorta of WT mice (Figure 4.4 B, C).

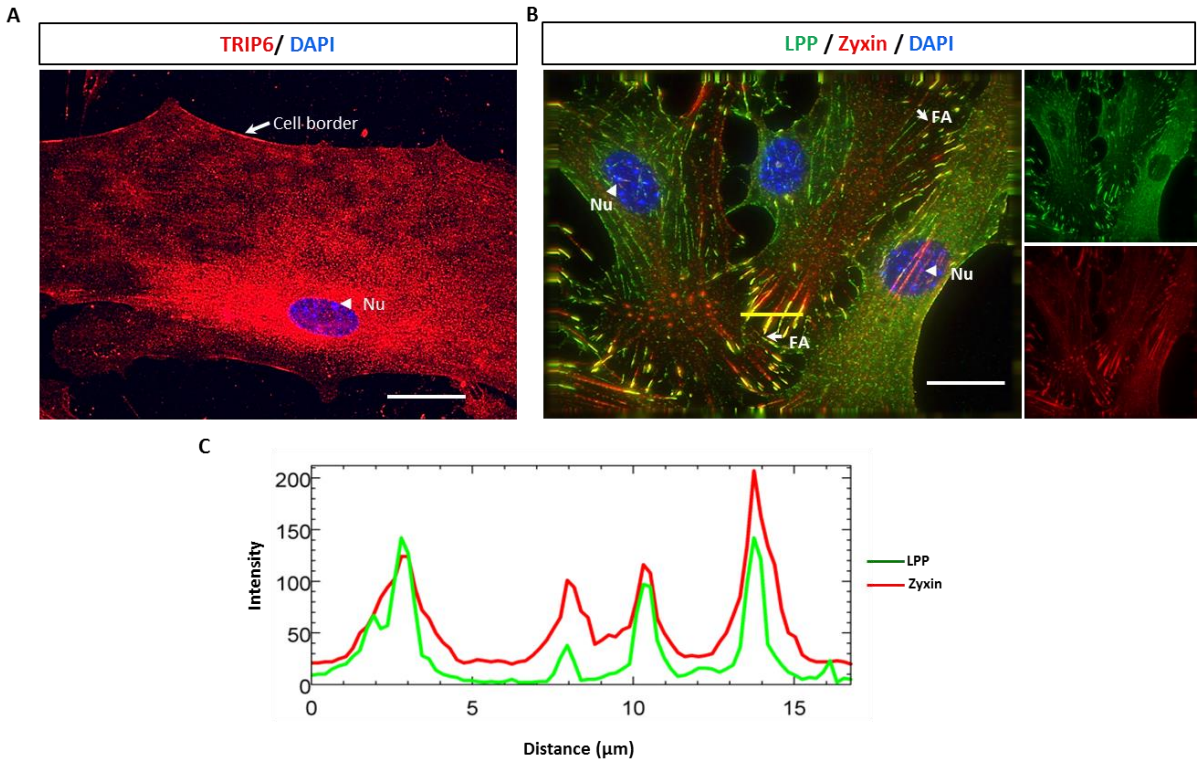

Figure 4.4 Cellular localization of TRIP6 and LPP protein in VSMCs
(A) TRIP6 immunofluorescence analysis, Scale bar, 20 µm. (B, C) LPP and zyxin co-localize in the focal adhesions (FA) but not in the nucleus (Nu). Scale bar, 20 µm (B).The plot profile over the yellow line shows maximum intensity of both zyxin (red) and LPP (green) at the FAs (C). Abbreviations: FA, focal adhesion; Nu, nucleus.

4.2.2 Sub-cellular distribution of TRIP6 and LPP protein in response to stretch

Under static conditions, little LPP or zyxin and no TRIP6 was present in the nucleus of VSMCs (Figure 4.5 A, B, C). TRIP6 appeared largely unresponsive to stretching of the VSMCs for 8 and 24 hours, respectively (Figure 4.5 C). In contrast, LPP like zyxin translocated to the nucleus after 8 hours of stretching and maintained this level for a further 16 hours (Figure 4.5 A, B, D, E).

Similar to zyxin, LPP mainly localized to the focal adhesions under static conditions but appeared to be absent from stress fibers (Figure 4.6 A) in the mouse VSMCs. In response to cyclic stretch, however, LPP like zyxin rapidly translocated to the stress fibers in the mouse VSMCs (Figure 4.6 B).

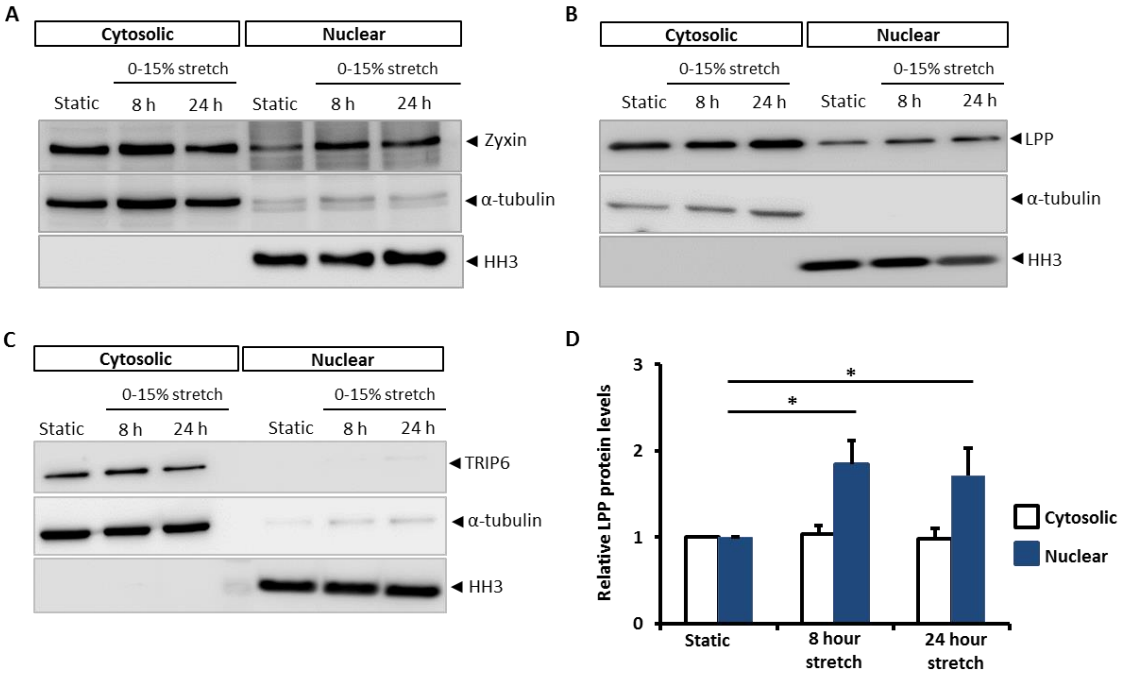

Figure 4.5 Nuclear translocation of zyxin, and LPP but not TRIP6 in response to cyclic stretch in mouse VSMCs

(A, B, C) Representative WB images showing nuclear translocation of zyxin (A) and LPP (B) but not TRIP6 (C) after 8 or 24 hours exposure to cyclic stretch (0-15% stretching at 0.5 Hz). (D) Relative change in LPP abundance in the cytosolic and nuclear fraction after exposure to cyclic stretch over time. Each column represents the mean ± SEM of *n*=3 experiments with individual VSMCs preparation. *p<0.05 as indicated

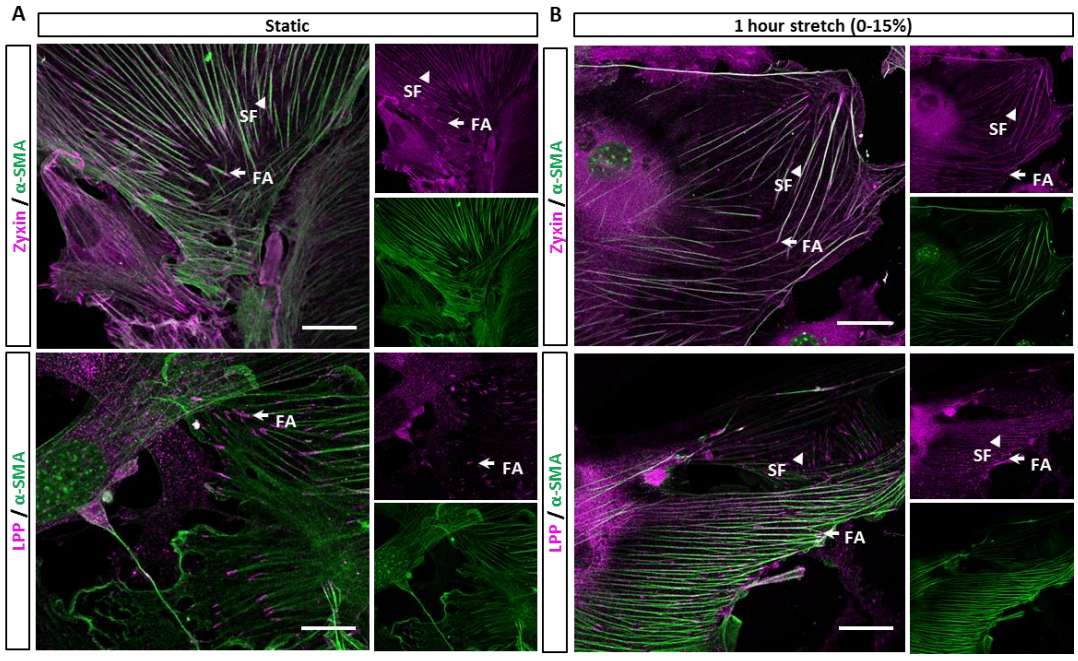

Figure 4.6 Stretch-induced translocation of zyxin and LPP from focal adhesions to stress fibers in mouse VSMCs

(A) Immunofluorescence images for zyxin and LPP in VSMCs under static conditions. (B) Immunofluorescence images showing the localization of zyxin and LPP after one hour exposure to cyclic stretch (0-15% at 0.5 Hz). Scale bar, 20 µm. The arrowheads mark stress fibers whereas focal adhesions are indicated by arrows. Abbreviations: FA, focal adhesion; SF, stress fiber; Nu, nucleus.

4.3 Regulation of VSMC phenotype by LPP and zyxin *in vitro*

As the aforementioned clearly argued against a role of TRIP6 in VSMC mechanotransduction, the following experiments solely focused on LPP and zyxin. VSMCs were analyzed for their three hallmark properties, i.e. migration, proliferation, and contractile capacity both in 2-dimensional (2D) cell culture and 3-dimensional (3D) spheroid culture which more closely reflects the fundamental cellular interactions present in tissues[119].

4.3.1 Phenotype of VSMCs isolated from Lppko mice in 2D cell culture

4.3.1.1 Lppko VSMCs migrate faster than WT VSMCs

In the 2D or lateral sheath migration assay, the ability and speed by which cells close the gap or wound created by insertion of a silicon block was measured. In this setting, VSMCs isolated from 3-months old Lppko mice showed an approximately 2-fold greater speed of migration than their WT counterparts over a 24-hour period (Figure 4.7 A, B).

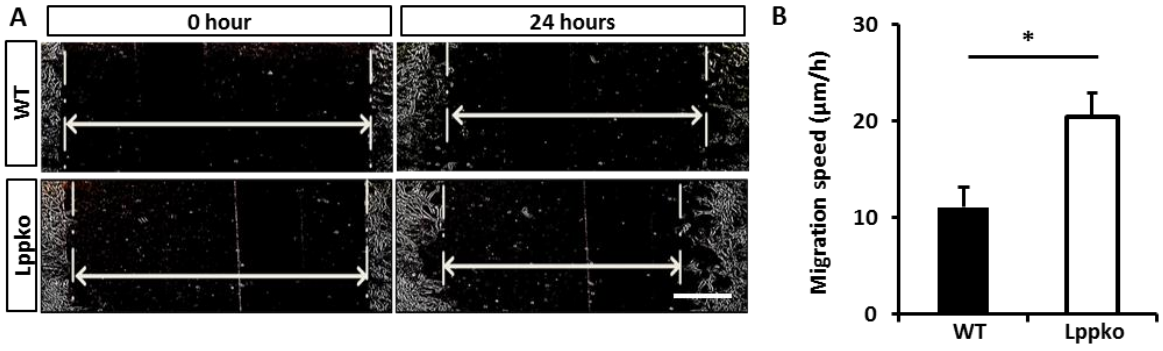

Figure 4.7 2D or lateral sheath migration of WT and Lppko VSMCs
(A) Distance of cell borders around an artificial gap (indicated by double arrow) in the beginning and 24 hours later in a monolayer composed of WT or Lppko VSMCs. (B) Quantitative measurement of the 2D-migration speed. Each column represents the mean ± SEM of n=5 individual VSMC preparation with at least 3 replicates. *p<0.05 as indicated

4.3.1.2 Lppko VSMCs proliferate faster than WT VSMCs

In 2D cell culture proliferation potential was analyzed by counting DAPI-stained nuclei immediately after and 72 hours post seeding. Compared to WT VSMCs, Lppko VSMCs showed higher numbers of DAPI-stained nuclei per optical field of view (Figure 4.8 A) at 72 hours. Approximately a 3-fold increase in cell number was observed in Lppko VSMCs as compared to 1.6-fold in WT VSMCs at this point (Figure 4.8 B).

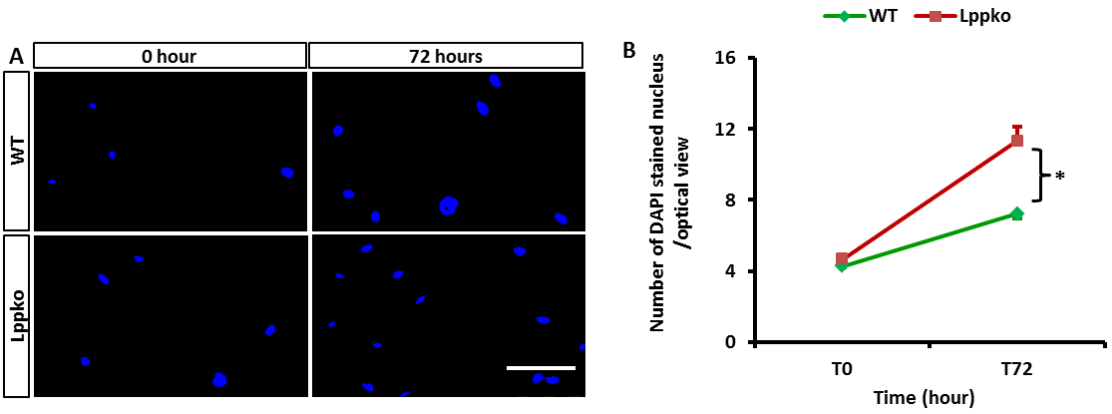

Figure 4.8 2D proliferation analysis by counting DAPI stained nucleus per optical view
(A) DAPI-stained nuclei at 0 and 72 hours post seeding from both WT and Lppko VSMC cultures. Scale bar 100 µm. (B) Statistical summary to estimate the proliferation rate. Here, the data points represent the mean ± SEM of *n*=5 individual VSMC preparations with at least 30 images for each condition counted. *p<0.05 as indicated

4.3.2 Phenotype of VSMCs isolated from Lppko and Zyxko mice in 3D cell culture

To study the migration, proliferation and contractile capacity in 3D cell culture, spheroids was made with VSMCs isolated from the aorta of 3-months old animals. The spheroids were either seeded in collagen gel to study migration or fixed and paraffin embedded to study other properties.

4.3.2.1 Zyxko and Lppko VSMC spheroids show higher invasion capacity than WT

In contrast to WT, both Zyxko and Lppko VSMCs showed a significantly greater degree of sprouting in collagen gels. The cumulative distance travelled by all sprouts derived from a single spheroid was also significantly higher in Zyxko and Lppko VSMCs as compared to WT VSMCs (Figure 4.9 A-H).

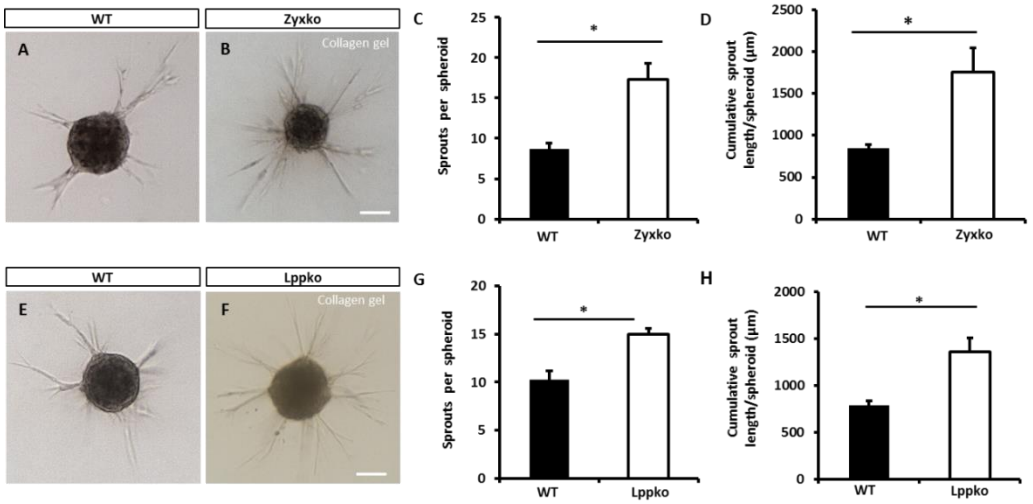

Figure 4.9 Spheroids composed of Zyxko or Lppko VSMCs reveal a higher invasion capacity in collagen gels than WT VSMCs
(A, B, E and F) Representative images of 3D spheroids made from WT, Zyxko and Lppko VSMCs seeded into collagen gels. Scale bar 200 µm (C, G) Average number of sprouts originating from a WT or Zyxko spheroid (C) or

from a WT or Lppko spheroid (G). (D, H) Comparison of the average cumulative sprout length between WT and Zyxko speroids (D) or WT and Lppko spheroids (H). Each column represents the mean ± SEM of n=5 experiments with individual VSMC preparations and at least 15 spheroids analyzed per preparation. *p<0.05 as indicated

4.3.2.2 VSMCs from Zyxko or Lppko mice showed significantly higher degree of proliferation in 3D spheroid culture than VSMCs from WT mice

Of the paraffin embedded spheroids, 5 µm thick sections were prepared and stained for the proliferation marker Ki67 (Figure 4.10 A, C). Spheroids composed of WT VSMCs showed about 4% of cells proliferating whereas spheroids composed of Zyxko or Lppko VSMCs revealed an about 4-fold and 2-fold, respectively, increased number of Ki67-positive cells (Figure 4.10 B, D).

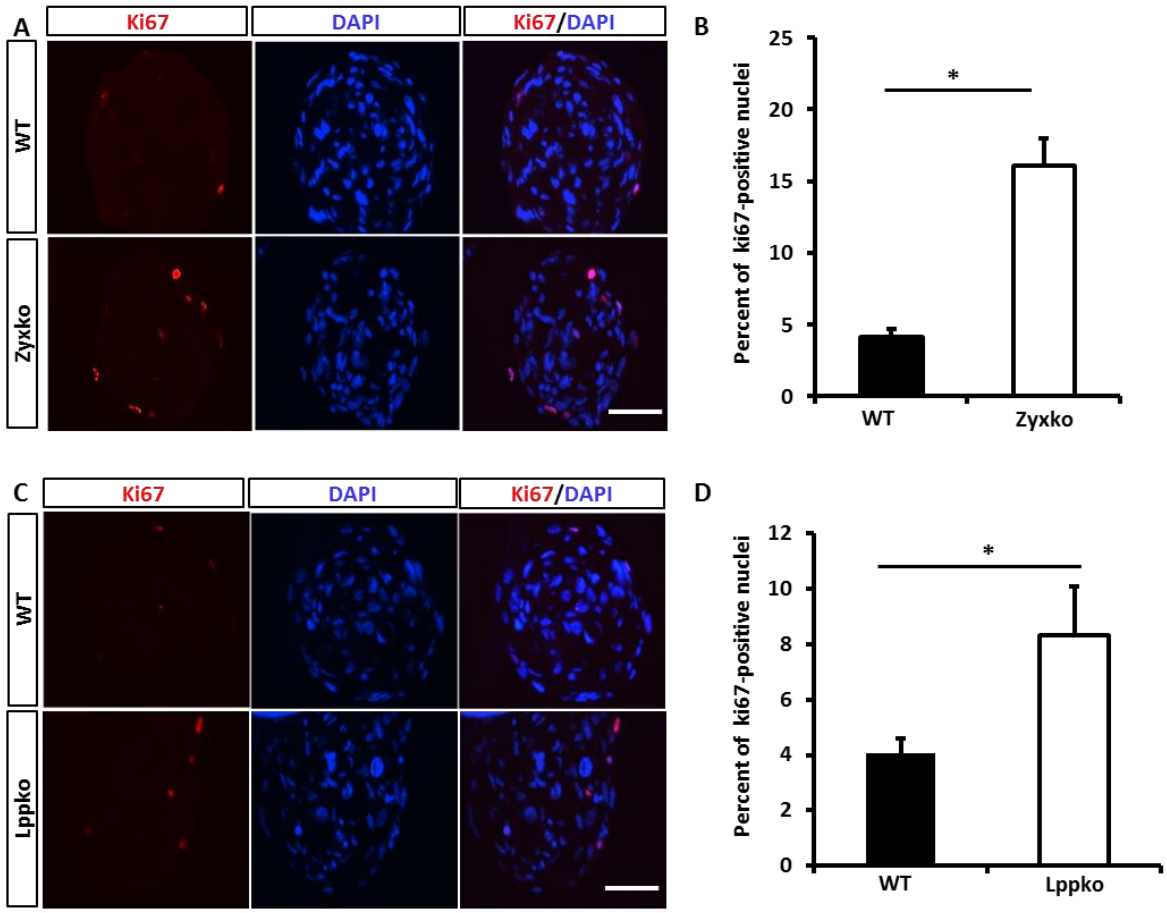

Figure 4.10 VSMCs from Zyxko or Lppko mice seem to proliferate significantly faster than WT VSMCs in 3D spheroid culture

(A, C) Immunofluorescence images of Ki67-positive VSMCs (red), nuclei counterstained with DAPI (blue), in 5-µm sections of spheroids composed of WT and Zyxko VSMCs (A) or WT and Lppko VSMCs (C). Scale bar 50 µm. (B, D) Statistical summary of the number of Ki67-positive VSMCs in WT or Zyxko spheroids (B) and WT or Lppko spheroids (D). Each column represents the mean ± SEM of n=5 individual spheroid preparations with at least 5 spheroids per preparation analyzed. *p<0.05 as indicated

4.3.2.3 VSMCs isolated from Zyxko or Lppko mice rather seem to have a synthetic phenotype as compared to WT VSMCs in 3D spheroid culture

To evaluate the contractile potential of VSMCs isolated from the aorta of 3-months old WT, Zyxko or Lppko mice in 3D culture, 5-µm sections of paraffin embedded spheroids were stained for α-smooth muscle actin (α-SMA) and calponin as contractile markers (Figure 4.11 A,B,C). Fluorescence intensity of the two marker proteins was normalized with DAPI stained nuclei number. Both Zyxko and Lppko VSMCs showed about 3 times lower expression of α-SMA in 3D culture as compared to WT VSMCs (Figure 4.11 D, E). Moreover, Lppko VSMCs revealed an approximately 6 times lower expression of calponin than WT VSMCs in this setting (Figure 4.11 F).

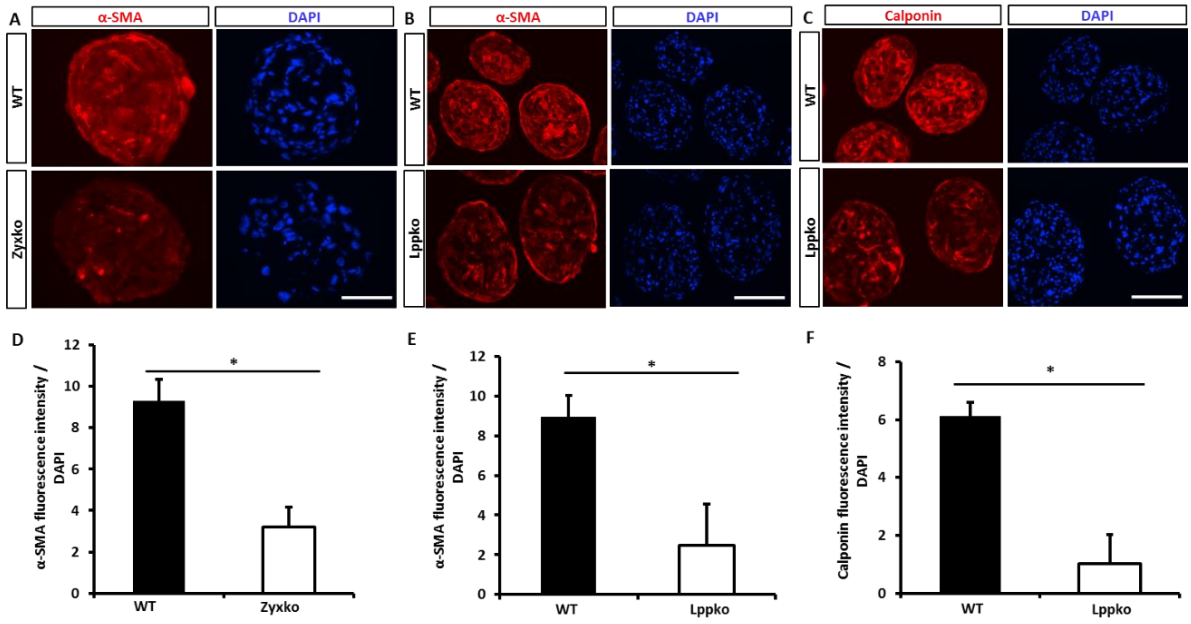

Figure 4.11 VSMCs from Zyxko or Lppko mice express less markers for the contractile phenotype than WT VSMCs in 3D spheroid culture

(A, B) Immunofluorescence images of α-smooth muscle actin (α-SMA, red) positive VSMCs in WT or Zyxko spheroids (A) and WT or Lppko spheroids (B). (C) Immunofluorescence images of calponin (red) positive VSMCs in WT or Lppko spheroids. Nuclei were counterstained with DAPI (blue). Scale bar 50 µm. (D, E, F) Statistical summary of the relative fluorescence intensities for α-SMA (D, E) and calponin (F) in the different types of spheroids. Each column represents the mean ± SEM of n=5 individual spheroid preparations with at least 5 spheroids per preparation analyzed. *p<0.05 as indicated

4.3.3 Matrix metalloproteinase activity of VSMCs isolated from the aorta of WT, Zyxko and Lppko mice *in vitro*

During vascular remodeling processes matrix metalloproteinase (MMP) activity increases to promote migration of vascular VSMCs[32]. Therefore, the relative level of MMP activity in WT, Zyxko and Lppko

VSMCs both in 2D and 3D cell culture was studied by determining fluorescence intensity of the DQ-gelatin substrate in the fixed VSMCs.

4.3.3.1 Zyxko and Lppko VSMCs reveal higher matrix metalloproteinase activity in 2D cell culture than WT VSMCs

Both Zyxko and Lppko VSMCs showed a markedly higher MMP activity as compared to WT VSMCs in 2D cell culture (Figure 4.12). To find the possible contributor for this increased MMP activity, relative abundance of MMP9 and MMP2 was determined in addition by immunofluorescence analysis. In the cultured VSMCs, the majority of the detected MMP activity could be attributed to MMP9 (Figure 4.12 D, E, F).

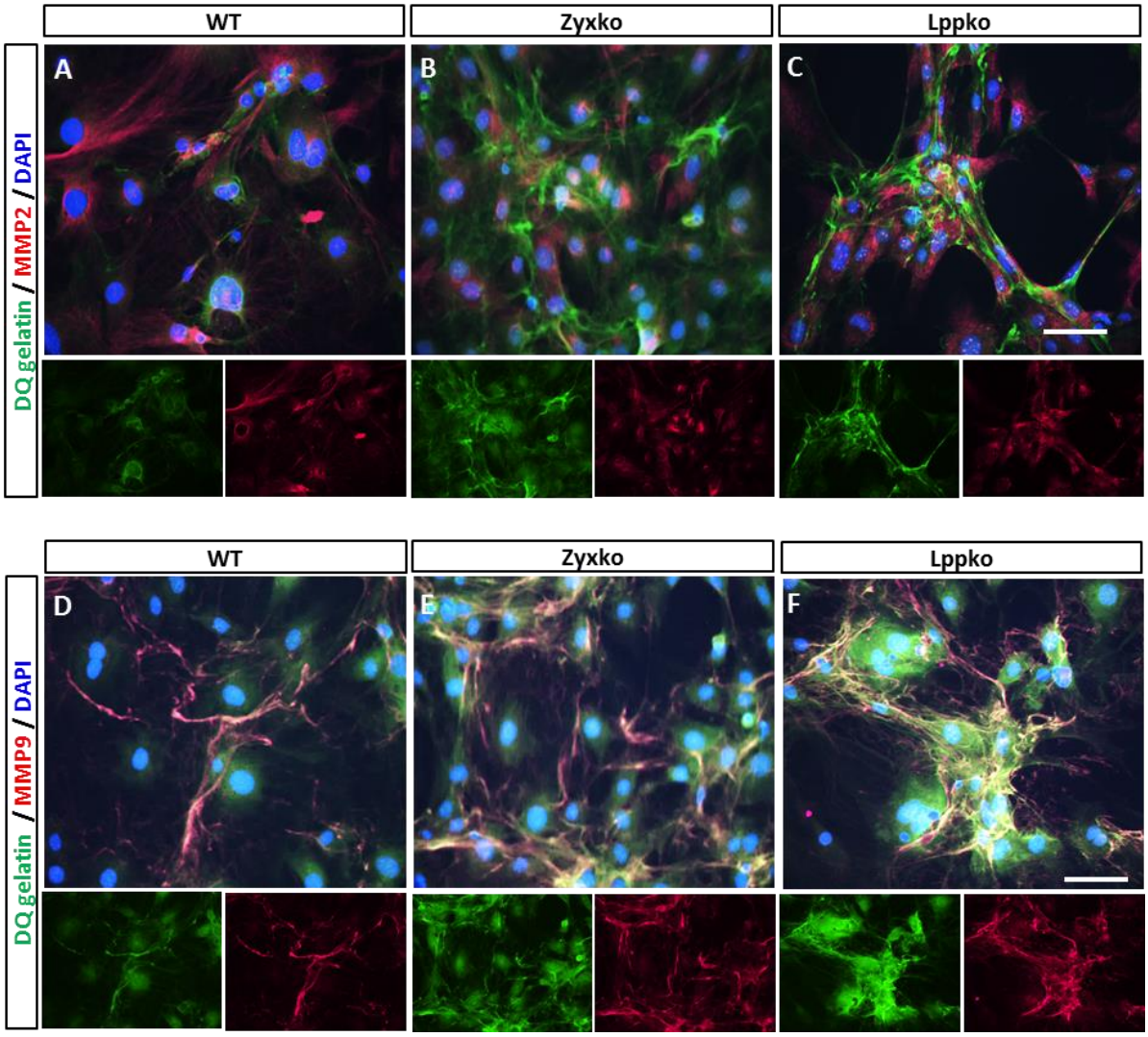

Figure 4.12 Zyxko and Lppko VSMCs in 2D culture display higher MMP activity than WT VSMCs
(A, B, C) Fluorescence intensity of DQ gelatin degradation (green), MMP2 (red) and nuclei (DAPI, blue) in methanol fixed VSMCs isolated from the aorta of 3-months old WT (A), Zyxko (B) or Lppko (C) mice. (D, E, F)

Fluorescence intensity of DQ gelatin (green), MMP9 (red) and nuclei (DAPI, blue) in fixed WT (D), Zyxko (E) or Lppko (F) VSMCs. Scale bar 100 µm (images are representative for n=3 individual VSMC preparations).

4.3.3.2 Significantly higher MMP activity also in VSMCs from Zyxko or Lppko mice in 3D cell culture as compared to VSMCs from WT mice

Essentially the same experimental approach was taken as described before except that the isolated VSMCs were cultured as 3D spheroids which were fixed, cut into 5-µm thin sections and subjected to immunofluorescence analysis. Both Zyxko and Lppko spheroids revealed significantly higher (approximately 2-fold) MMP activity as compared to WT spheroids (Figure 4.13).

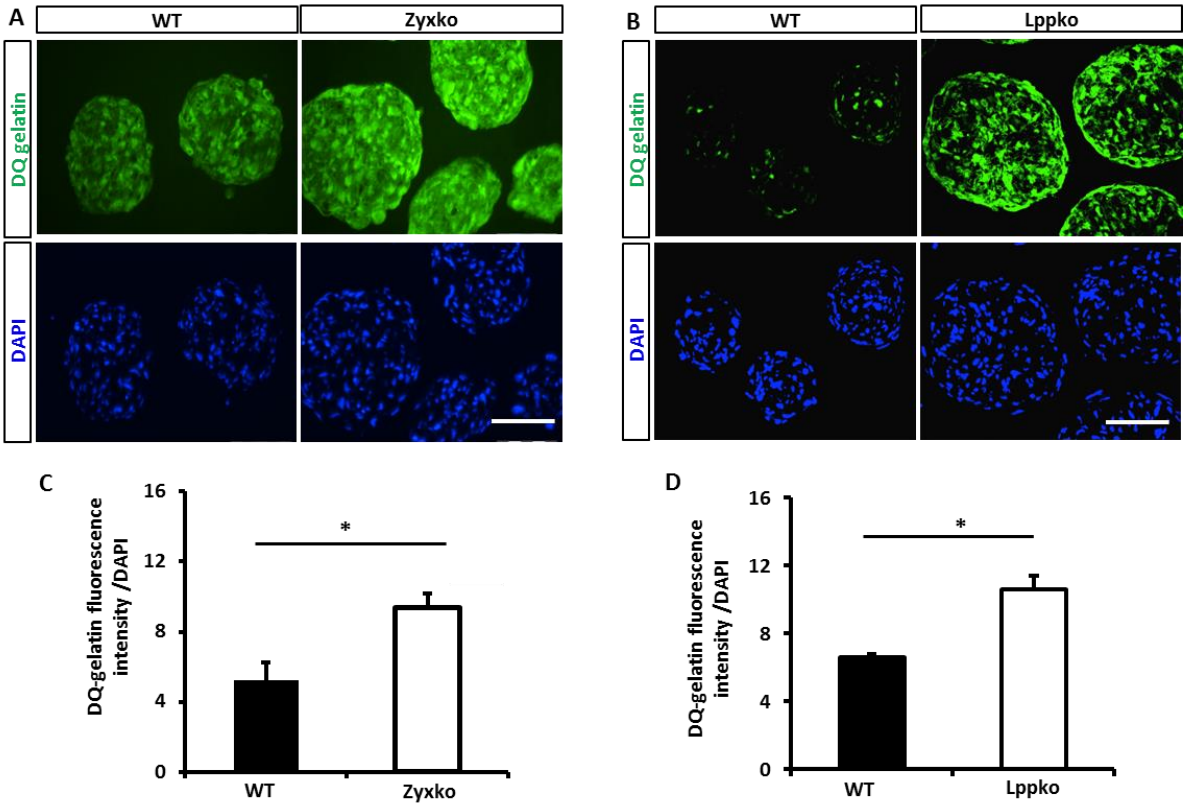

Figure 4.13 Zyxko and Lppko VSMCs in 3D culture display significantly higher MMP activity than WT VSMCs

(A, B) Gelatinase activity (green) and DAPI stained nuclei (blue) in sectioned spheroids composed of WT or Zyxko VSMCs (A) and WT or Lppko VSMCs (B). Scale bar 50 µm. (C, D) Statistical summary of the relative gelatinase activity detected in the aforementioned 3D cultured VSMCs. Each column represents the mean ± SEM, n=5 independent VSMC preparations with at least 5 sectioned spheroids analyzed per preparation. *p<0.05 as indicated

Immunofluorescence intensities for MMP9 and MMP2 were normalized on the basis of the DAPI stained nuclei per spheroid. In 3D cultured Lppko VSMCs namely MMP9 (10-fold increase, Figure 4.14 A, C) but also MMP2 (2.5 fold increase, Figure 4.14 B, D) were significantly more abundant than in WT VSMCs.

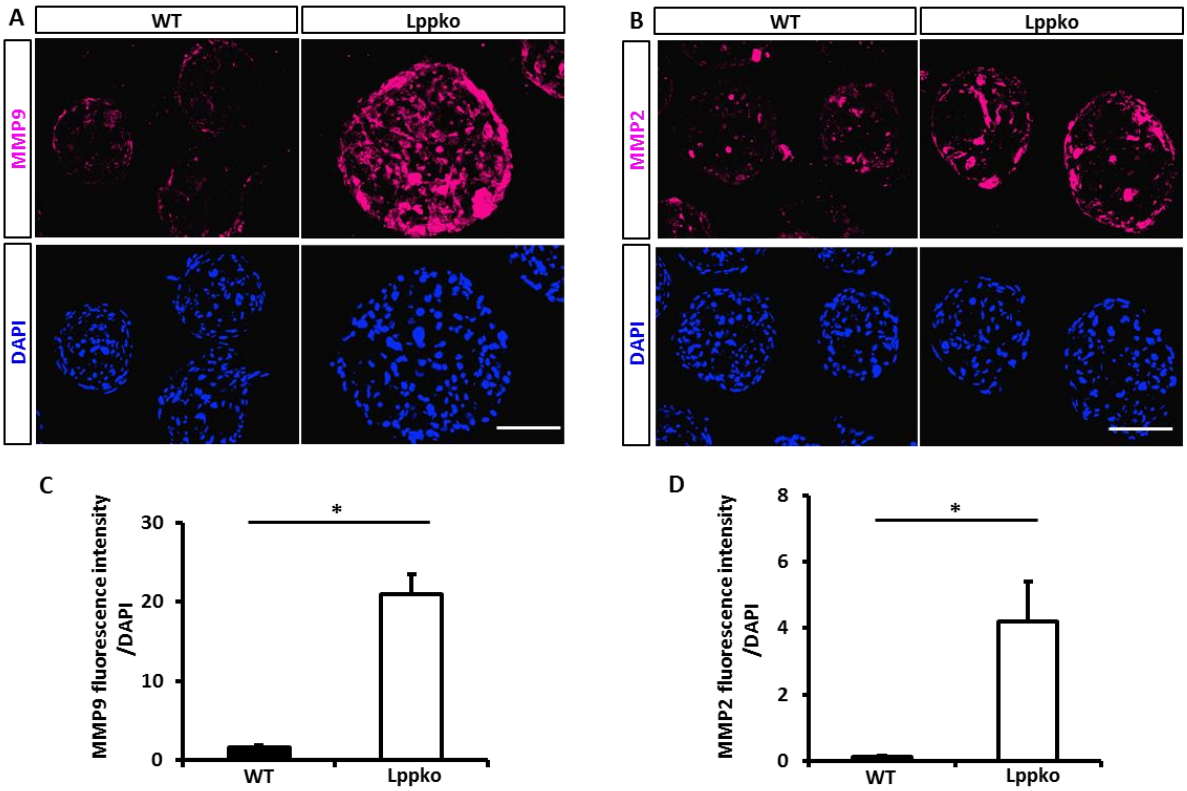

Figure 4.14 Lppko VSMCs reveal a marked increase in MMP9 but also MMP2 expression as compared to WT VSMCs in 3D culture

(A, B) Immunofluorescence images for MMP9 (A) and MMP2 (B) in sectioned (5 µm) spheroids made from WT or Lppko VSMCs. Scale bar, 50 µm. (C, D) Statistical summary of the difference in MMP9 (C) and MMP2 (D) abundance. Each column represents the mean ± SEM, of n=5 individual VSMC preparations with at least 5 spheroids analyzed per preparation. *p<0.05 as indicated

4.4 Functional consequences of the loss of LPP in mice

4.4.1 Young Lppko mice were smaller in size and had higher heart rate at resting conditions

S129 mice with a global loss of LPP were reported to be devoid of any visible phenotype[103]. After backcrossing these mice onto a pure C57Bl6/J background, 3-months old homozygous Lppko mice presented with a smaller body weight (about 10%) than their WT littermates (Figure 4.15 A). Telemetry-based blood pressure (BP) monitoring did not reveal significant differences in systolic or diastolic BP between WT and Lppko mice at baseline (Figure 4.15 B, C). However, their heart rate at rest was significantly increased by about 10% as compared to WT mice, possibly due to their smaller size, while in the active state there was no such difference (Figure 4.15 D). High resolution ultrasound imaging revealed a further difference between Lppko mice and their WT littermates in that they presented with significantly lower early (E) and late (A) diastolic filling velocities but a slightly increased E/A ratio which was not significantly different though (Figure 4.15 E).

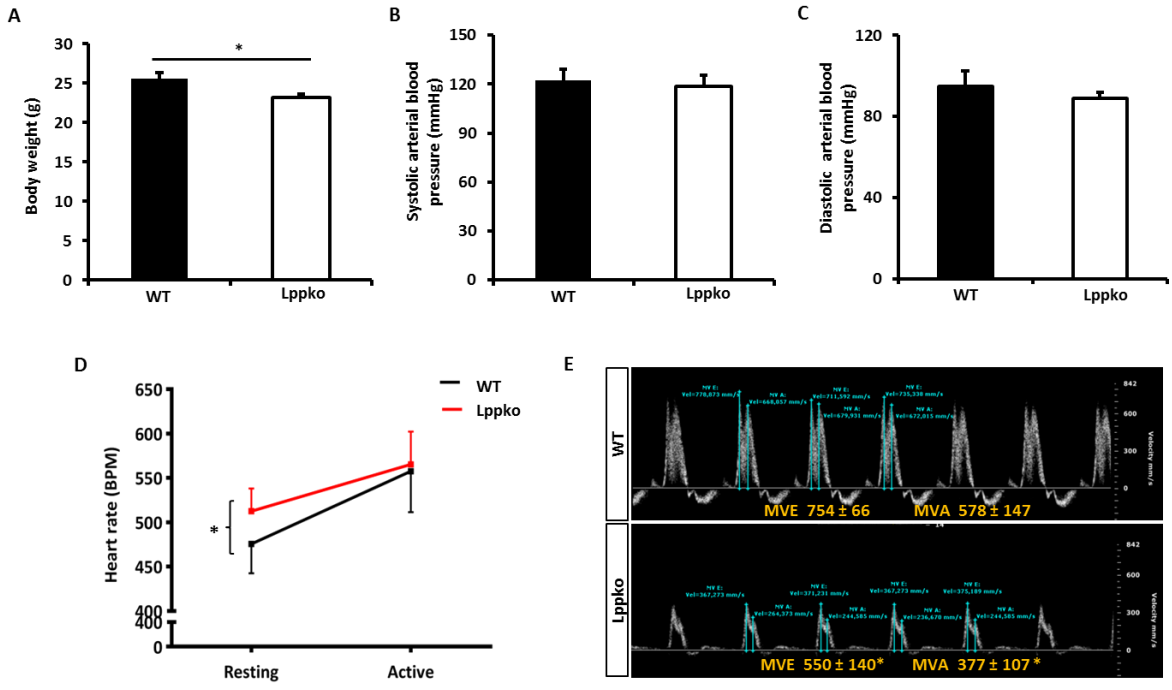

Figure 4.15 Baseline phenotyping of young (3-months old) Lppko mice backcrossed onto the same C57Bl6/J background as the homozygous Zyxko mice

Comparison between age-matched WT and Lppko mice in terms of body weight (A, n=15), systolic (B) and diastolic (C) blood pressure at rest, heart rate (D) in the resting state as compared to the active state (n≥5, *p<0.05 as indicated), and mean velocity for early (MVE) and late filling (MVA) of the left ventricle (E, n≥5, *p<0.05 vs. WT).

4.4.2 DOCA-salt treated young Lppko mice present with a greater blood pressure amplitude and a lower resistivity index as compared to age-matched WT mice

To induce experimental hypertension, the DOCA-salt model was used as described before[58]. Due to a combination of central neurohumoral stimulation and an increased sodium and water retention by the kidneys this murine equivalent of human aldosterone causes a rather prominent increase in blood pressure that is maintained after 10 days on a stable plateau (Figure 4.16 A, B). In this study changes in blood pressure were recorded for 21 days post implantation of the DOCA pellet by radio telemetry. After 5 days of treatment, both WT and Lppko mice showed a significant rise in both systolic and diastolic blood pressure as compared to baseline. This rise in systolic BP was significantly higher in Lppko mice as compared to WT between days 11 and 15 (Figure 4.16 A), while there was no appreciable difference regarding the increase in diastolic BP over time (Figure 4.16 B). However, the resistivity index, recorded in the femoral artery by way of high resolution ultrasound imaging, which is an indirect measure of total peripheral resistance was significantly lower in the Lppko mice as compared to the age-matched WT mice at the end of treatment period (Figure 4.16 C).

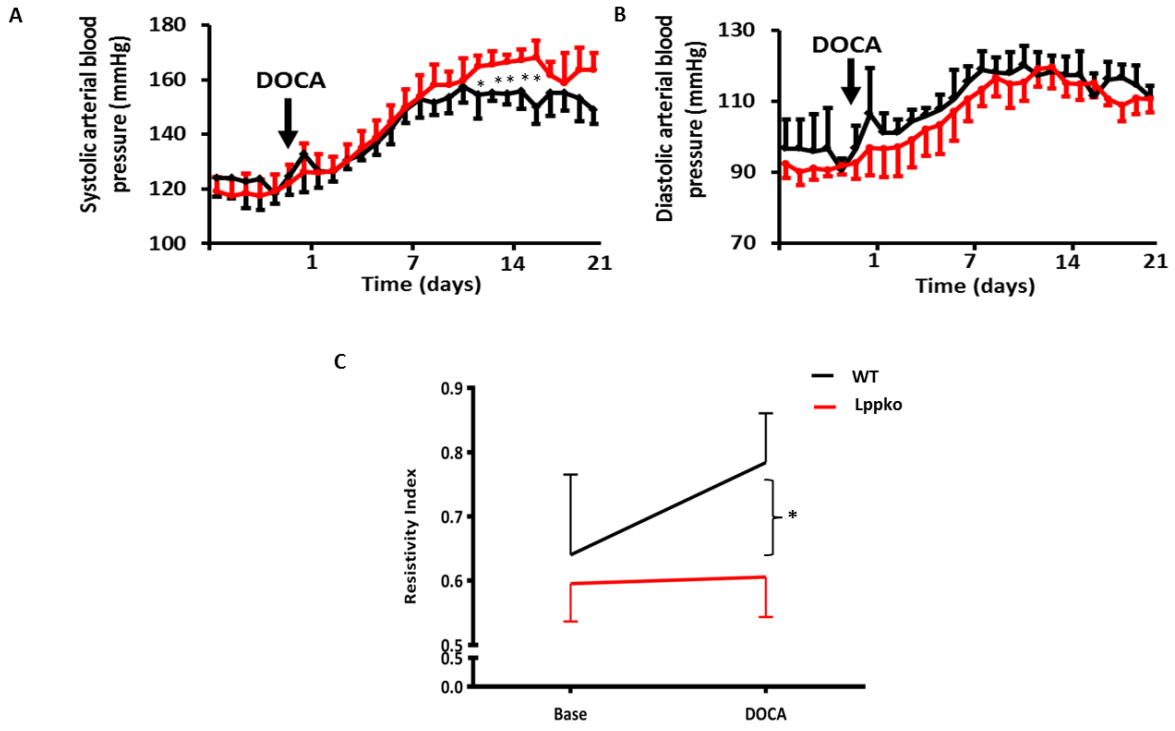

Figure 4.16 DOCA-salt treated Lppko mice reveal a greater blood pressure amplitude but a lower resistivity index as compared to age-matched WT animals

(A, B) During DOCA-salt treatment, systolic blood pressure (A) but not diastolic blood pressure (B) hence blood pressure amplitude is transiently higher in Lppko mice as compared to age-matched WT mice (n≥5, *p<0.05 vs. WT mice). (C) Lppko mice also reveal a reduced resistivity index (measured in the femoral artery) as compared to WT animals at the end of the 21-day treatment period ((n≥5, *p<0.05 vs. WT mice).

4.4.3 VSMCs in the femoral artery of DOCA-salt treated young Lppko and WT mice show a comparable degree of proliferation and contractile marker gene expression

Next, the femoral arteries of these animals were excised at the end of the treatment period and analyzed for the presence of proliferating VSMCs by staining sections of these arteries for proliferating cell nuclear antigen (PCNA). Both WT and Lppko VSMCs in the media revealed similar numbers of PCNA-positive nuclei (Figure 4.17 A, B). Also α-SMA (Figure 4.17 C, D) and calponin (Figure 4.17 E, F), markers for the contractile VSMC phenotype, did not differ in their abundance in the media of these arterial blood vessels, suggesting that in contrast to the isolated VSMCs the native VSMCs do not reveal a vascular phenotype neither at baseline nor following induction of experimental hypertension.

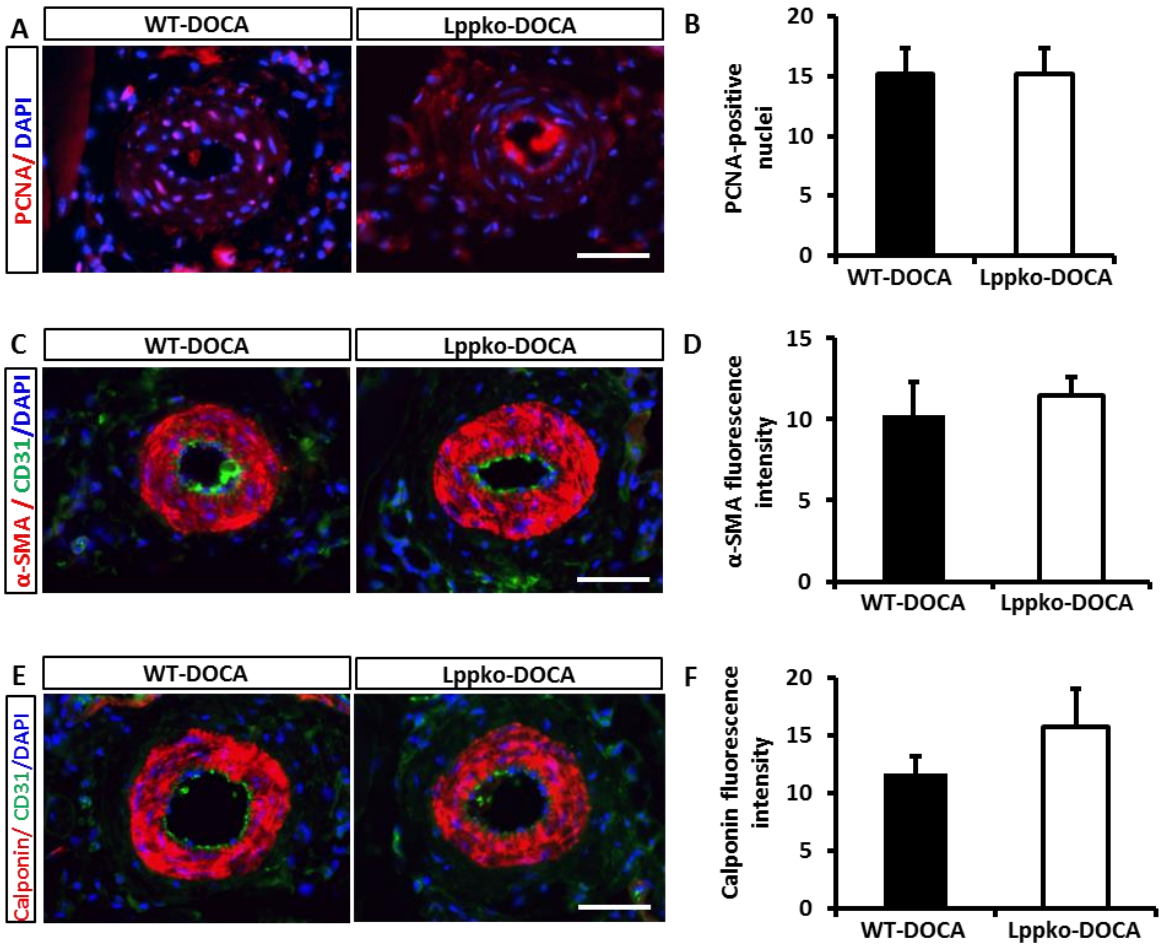

Figure 4.17 No apparent phenotype difference between native WT and Lppko VSMCs following 21 days treatment with DOCA-salt

(A) Immunofluorescence images for PCNA (red) and DAPI (blue), and (B) statistical summary for n≥5 individual animals with 3 femoral artery sections analyzed per animal. Scale bar, 50 µm. (C) Immunofluorescence images for α-SMA (red), CD31 (green) and DAPI (blue), and (D) statistical summary for n≥5 individual animals with 3 femoral artery sections analyzed per animal. Scale bar, 50 µm. (E) Immunofluorescence images for calponin (red), CD31 (green) and DAPI (blue), and statistical summary for n≥5 individual animals with 3 femoral artery sections analyzed per animal. Scale bar, 50 µm.

4.5 Evaluation of the potential of zyxin and LPP to functionally compensate for each other in VSMCs *in vitro*

VSMCs isolated from the aorta of 3-months old Zyxko or Lppko mice similarly exhibited a synthetic phenotype *in vitro* whereas no apparent vascular phenotype could be detected in these animals *in vivo.* To evaluate whether LPP and zyxin can compensate for each other's loss of function in the cultured VSMCs, LPP was transiently overexpressed in Zyxko VSMCs and zyxin *vice versa* in Lppko VSMCs. For this purpose, a plasmid only encoding GFP was used as a transfection control. After successful transfection of these expression constructs into the respective VSMCs, their migration properties both in 2D and 3D cell culture as well as their rate of proliferation in 2D culture was studied.

4.5.1 Overexpression of Lpp in Zyxko VSMCs reverts their migration and proliferation behavior towards the level in WT VSMCs

Transient overexpression of Lpp in Zyxko VSMCs significantly reduces their migration speed compared to that of untransfected Zyxko VSMCs. The migration rate of WT and Lpp-overexpressing Zyxko VSMCs was not significantly different (Figure 4.18 M). In addition Lpp-overexpressing Zyxko VSMCs showed significantly lower number of sprouts originating from 3D spheroids compared to that of untransfected Zyxko VSMCs (Figure 4.19 E). Cumulative sprout length was also significantly reduced in the Lpp-overexpressing Zyxko VSMCs. Both sprout number and cumulative sprout length were not significantly different in Lpp-overexpressing Zyxko and WT VSMCs (Figure 4.19 F).

After Lpp overexpression, Zyxko VSMCs showed an approximately 2-fold increase in cell number after 72 hours, which was significantly lower than their untransfected control counterparts (3.5 fold). Proliferation rate for WT and Lpp-overexpressing Zyxko VSMCs was not significantly different (Figure 4.18 N).

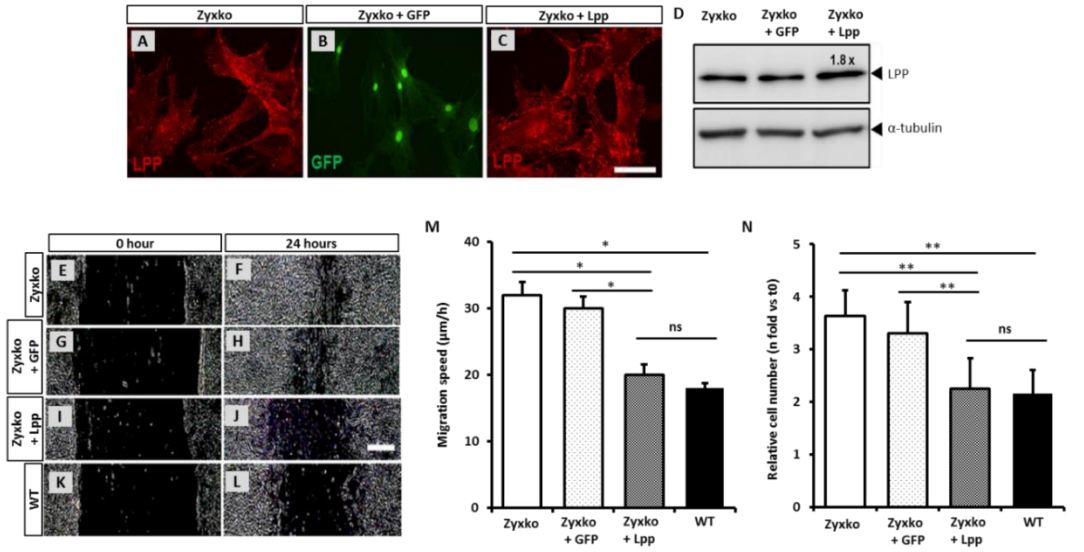

Figure 4.18 Transient overexpression of Lpp in Zyxko VSMCs reverts their migration and proliferation behavior towards the WT level in 2D cell culture

(A, B, C) Immunofluorescence images for LPP (red) and GFP (green) in untransfected (A), control GFP transfected (B) and Lpp-transfected (C) Zyxko VSMCs. Scale bar 100 µm. (D) Representative WB images to check the level of overexpression. (E through L) Light microscopic images for the cell border at the beginning and 24 hours later in untransfected (E,F), control GFP transfected (G,H) and Lpp transfected Zyxko (I,J) and WT VSMCs (K,L). Scale bar 100 µm. (M) Statistical summary for the migration speed observed in differently treated Zyxko and WT VSMCs. (N) Statistical summary for the relative fold changes in Zyxko and WT VSMCs number in the same experimental settings. Each column represents the mean ± SEM of n=3 experiments with individual VSMC preparations with at least 3 technical replicates. **p<0.01, *p<0.05 as indicated

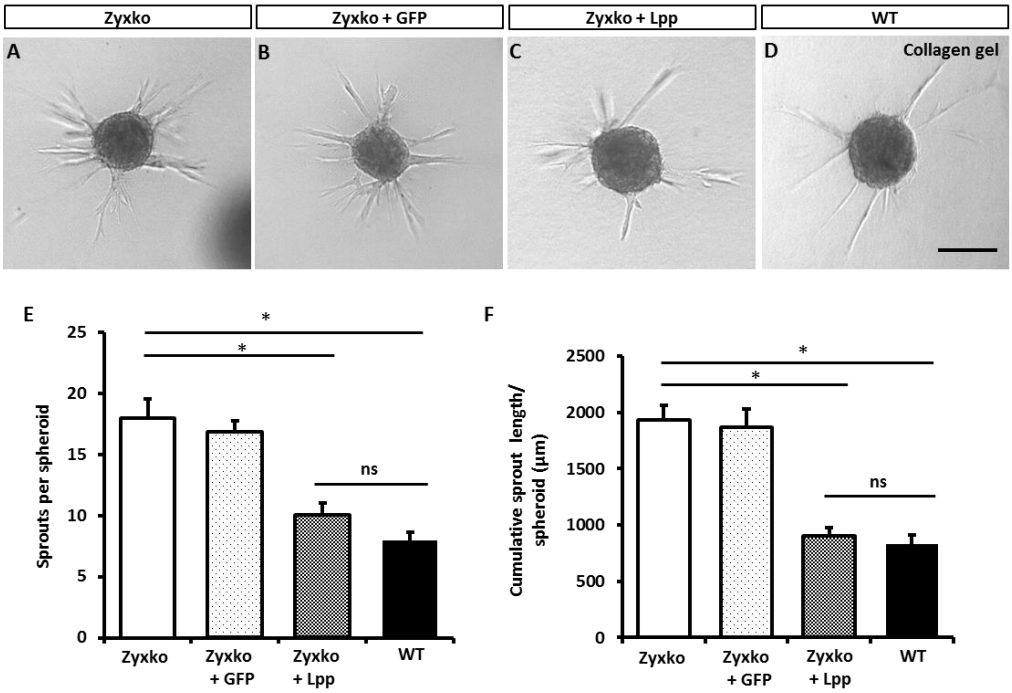

Figure 4.19 Overexpression of Lpp in Zyxko VSMCs reduces their migration rate towards the WT level in 3D spheroids seeded into collagen gel

(A, B, C, D) Images of representative spheroids composed of untransfected (A), control GFP transfected (B), Lpp transfected (C) Zyxko VSMCs and WT VSMCs (D). Scale bar 100 µm. (E, F) Statistical summary for the average number of sprouts (E) and cumulative sprout length (F) originating from a single spheroid in that experimental

settings. Each column represents the mean ± SEM of n=3 experiments with individual VSMC preparations with at least 10 spheroids per condition. Abbreviation: ns, not significant. *p<0.05 as indicated

4.5.2 Zyxin overexpression in Lppko VSMCs reduces their migration and proliferation behavior towards the level in WT VSMCs

Compared to untransfected Lppko VSMCs, Zyx-overexpressing Lppko VSMCs migrated significantly slower in the 2D or lateral sheath migration assay. The migration rate of Zyx-overexpressing Lppko VSMCs was comparable to that of WT VSMSc (Figure 4.20 C, D). Zyx-overexpressing Lppko VSMC spheroids showed significantly lower numbers of sprouts (Figure 4.21 E) as well as a lower average cumulative sprout length (Figure 4.21 F) compared to that of untransfected Lppko VSMC spheroids. Both the sprout number and the cumulative sprout length were comparable in Zyx-overexpressing Lppko and WT VSMC spheroids (Figure 4.21 E, F).

At the starting of the experiment (T0), the number of DAPI-stained nuclei was indifferent for differently transfected Lppko VSMCs and control WT VSMCs. However, after 72 hours, Zyx-overexpressing Lppko VSMCs showed significantly lower number of DAPI-stained nuclei in contrast to untrasfected and GFP control transfected Lppko VSMCs. The number of nuclei was not different between the WT and Zyx-overexpressing Lppko VSMCs (Figure 4.20 E).

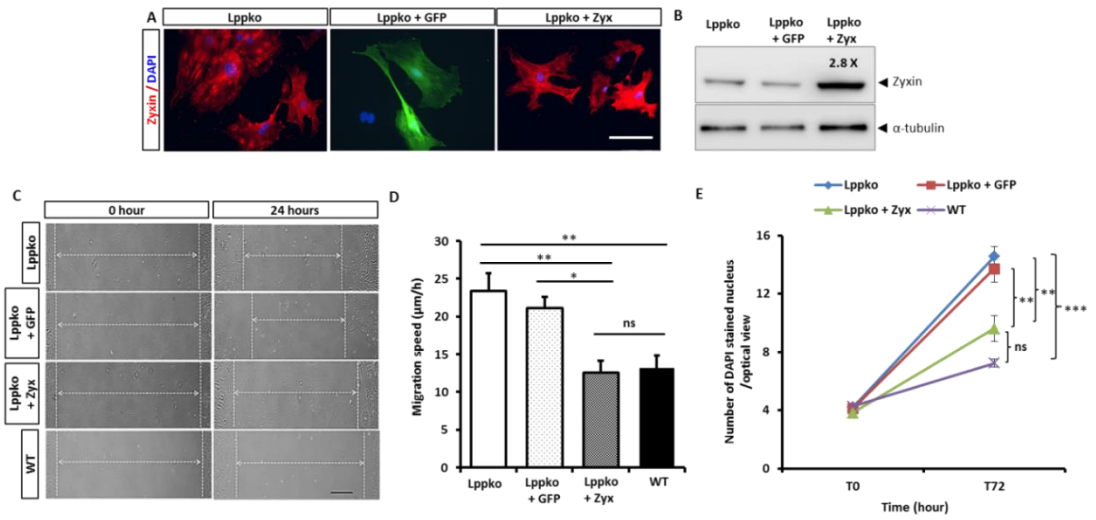

Figure 4.20 Transient overexpression of Zyx in Lppko VSMCs rescues their synthetic phenotype towards the contractile phenotype in WT VSMCs

(A) Immunofluorescence images for zyxin (red) and GFP (green) in untransfected, control GFP transfected and Zyx-overexpressing Lppko VSMCs. Scale bar 100 µm. (B) Representative WB images to check the level of overexpression. (C) Light microscopic images for the cell border at the beginning and 24 hours later in 2D cell culture. Scale bar 100 µm. (D) Statistical summary for the migration speed in the untransfected, control GFP transfected, and Zyx-overexpressing Lppko and WT VSMCs. (E) Statistical summary for the number of DAPI-stained nuclei in the same experimental settings at the beginning (T0) and 72 hours later (T72). Each column represents the mean ± SEM of n=5 experiments with individual VSMC preparations with at least 3 technical replicates. Abbreviation: ns, not significant. ***p<0.001, **p<0.01, *p<0.05 as indicated

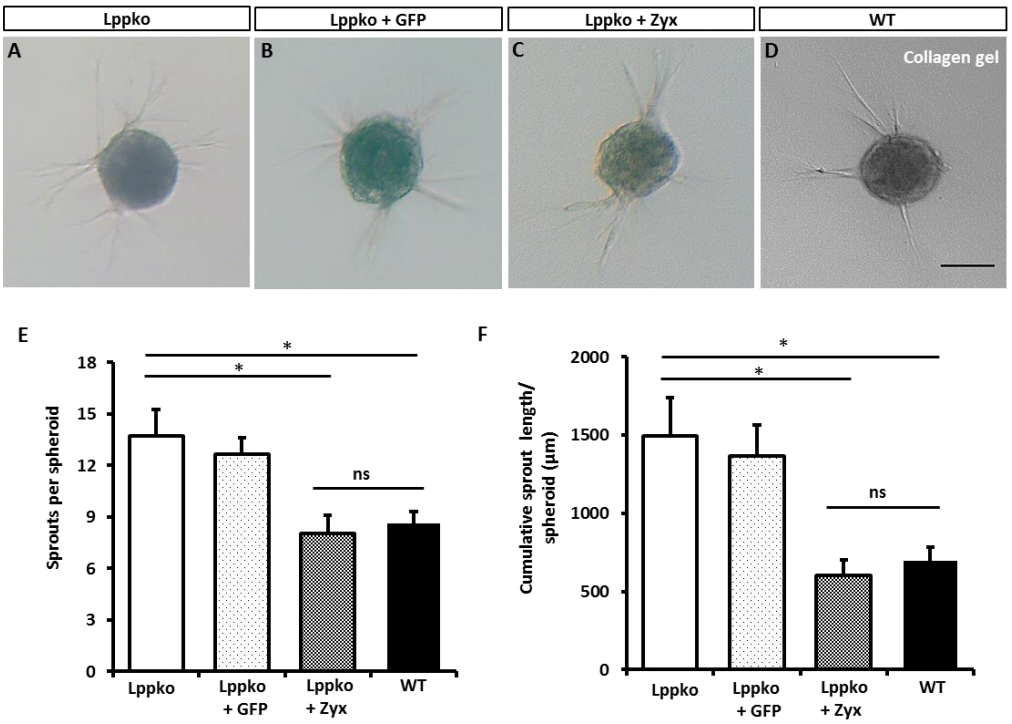

Figure 4.21 In 3D spheroid culture overexpression of Zyx in Lppko VSMCs reduces their migration rate towards the WT level

(A, B, C, D) Images of representative spheroids seeded in collagen gel composed of untransfected (A), control GFP transfected (B), and Zyx transfected (C) Lppko VSMCs as well as non-transfected WT VSMCs (D). Scale bar 100 µm. (E, F) Statistical summary for the average number of sprouts (E) and cumulative sprout length (F) originating from a single spheroid in the same experimental setting. Each column represents the mean ± SEM of n=3 experiments with individual VSMC preparations with at least 10 spheroids per condition. Abbreviation: ns, not significant. *p<0.05 as indicated

4.6 Both systolic and diastolic blood pressure are comparable in WT and Zyxko mice of different age

Blood pressure was monitored in 3, 6 and 12 months old WT and Zyxko mice at baseline by using the CODA-noninvasive tail cuff system. In Zyxko mice, systolic blood pressure was similar to that of WT animals in all age groups. Diastolic blood pressure was also not different among these genotypes (Figure 4.22).

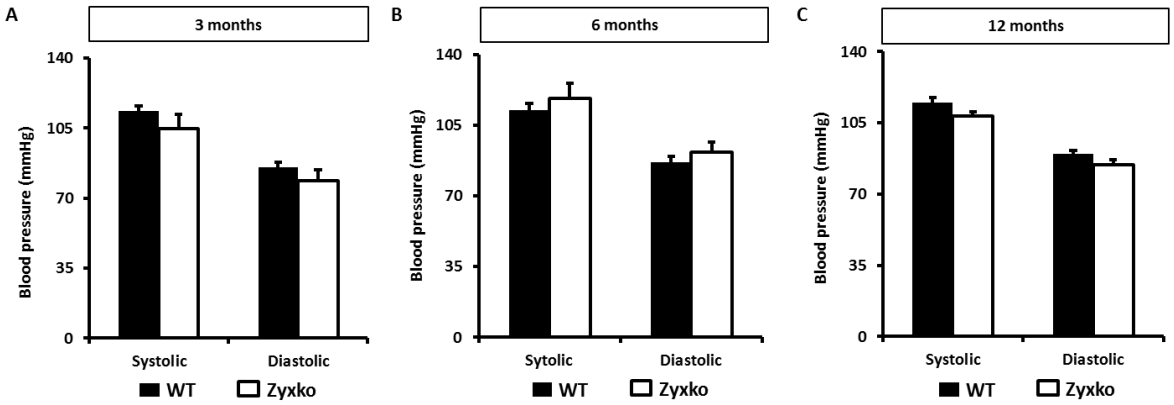

Figure 4.22 Comparable systolic and diastolic blood pressure at baseline in WT and Zyxko mice of different ages

(A, B, C) Systolic and diastolic blood pressure in 3 months (A), 6 months (B) and 12 months (C) old WT and Zyxko mice. Each column represents the mean ± SEM of n =10 mice with 10 individual readings for each mouse.

4.7 Cardiac systolic and diastolic parameters at baseline in WT and Zyxko mice at different ages

Cardiac systolic functional parameters, i.e. cardiac output (CO), stroke volume (SV), ejection fraction (EF) and fractional shortening (FS) were measured from recorded echocardiographic images. All analyzed cardiac systolic parameters were similar in WT and Zyxko mice at 3, 6 and 12-months of age at baseline (Figure 4.23). Unlike cardiac systolic analysis, diastolic functional parameters were significantly different in Zyxko mice as compared to WT animals in all three age groups. Thus, both filling velocities of the left ventricle (early passive filling, E wave and active filling, A wave) during diastole were significantly lower in Zyxko mice as compared to WT mice at 3 and 6-months of age. Although the E wave was significantly lower, reduction of the A wave did not reach statistical significance at 12-months of age in the Zyxko mice (Figure 4.24).

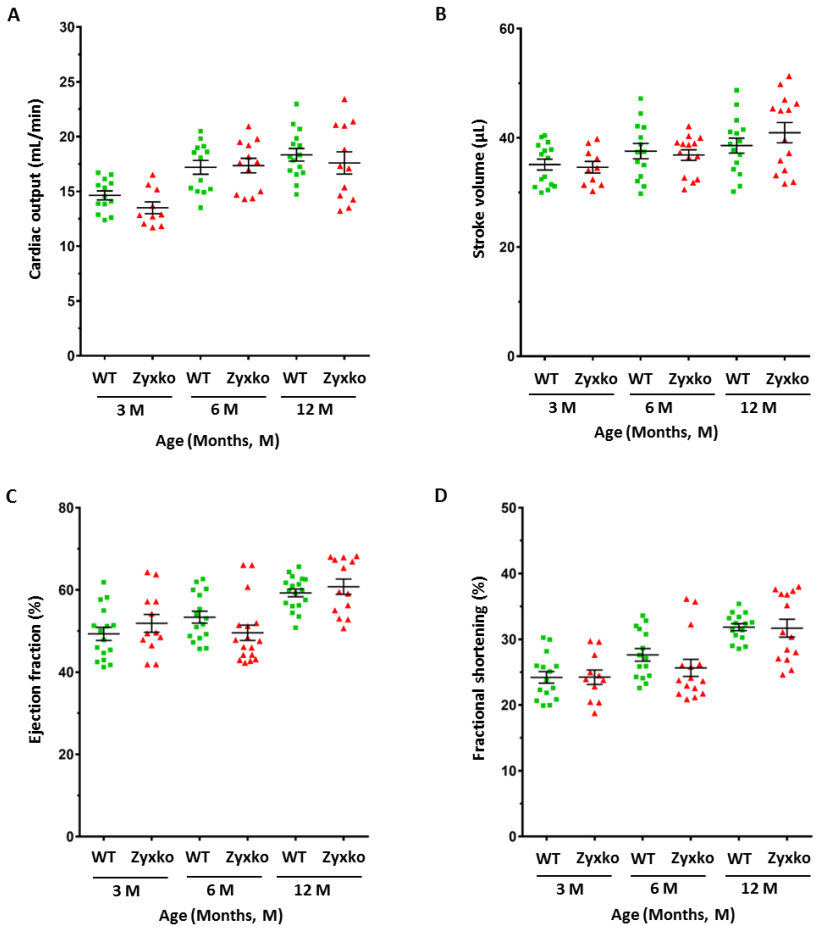

Figure 4.23 Cardiac systolic functional parameters were comparable among WT and Zyxko mice from different age groups at baseline

(A, B, C, D) Cardiac output (A), stroke volume (B), ejection fraction (C) and fractional shortening (D) in WT and Zyxko mice under basal conditions at 3, 6 and 12-months of age. The mean of each group is indicated by a horizontal line ± SEM of n ≥10 mice.

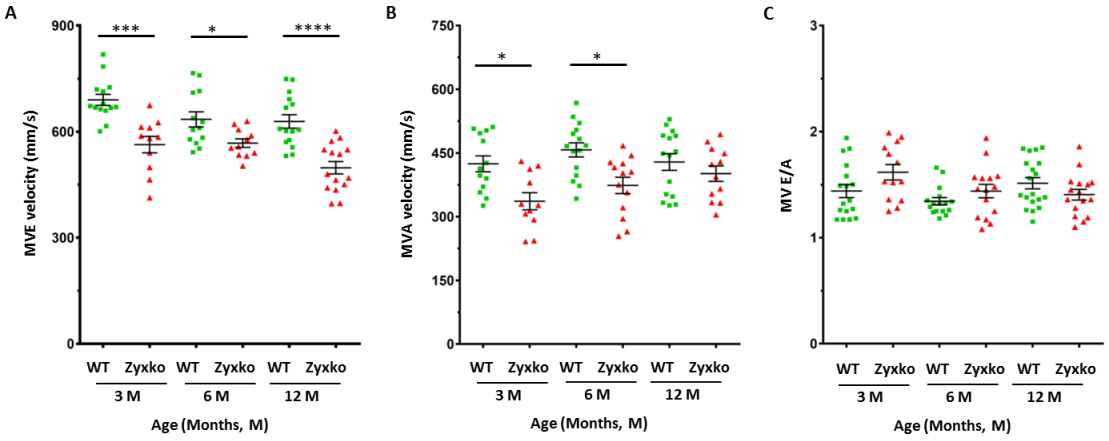

Figure 4.24 Velocities for both early passive and late active filling of the left ventricle were markedly reduced under basal conditions in Zyxko mice as compared to WT mice in all age groups

(A, B) Left ventricular early passive (A) and late active (B) filling during diastole in unchallenged Zyxko and WT mice at 3, 6 and 12-months of age. (C) Ratio for the mitral valve E and A velocities at different ages of WT and Zyxko mice. The mean of each group is indicated by a horizontal line ± SEM of n ≥10 mice. ****p<0.0001, ***p<0.001, *p<0.05 as indicated

4.8 The extent of the rise in blood pressure following angiotensin II treatment is comparable in WT and Zyxko mice

To induce experimental hypertension, both WT and Zyxko mice were treated with angiotensin II (Ang II) at a dose of 1.5 mg/kg body weight/day via subcutaneous implantation of osmotic mini pumps (day 0). Blood pressure elevation was monitored on day 7 and just before terminating the experiment (day 15) by CODA-noninvasive tail cuff system. Elevations of both systolic and diastolic blood pressure were comparable in 3, 6 and 12-months old WT and Zyxko mice after 14 days treatment with Ang II (Figure 4.25). However, in Zyxko mice, the resulting rise in blood pressure appeared to be somewhat delayed as compared to WT mice, i.e. systolic blood pressure took 15 days vs. 7 days to reach its maximum. Treatment of mice with 0.9% NaCl (vehicle control for Ang II) did not show any effect on blood pressure (by comparing vehicle control values in (Figure 4.25) to the basal values shown in (Figure 4.22)).

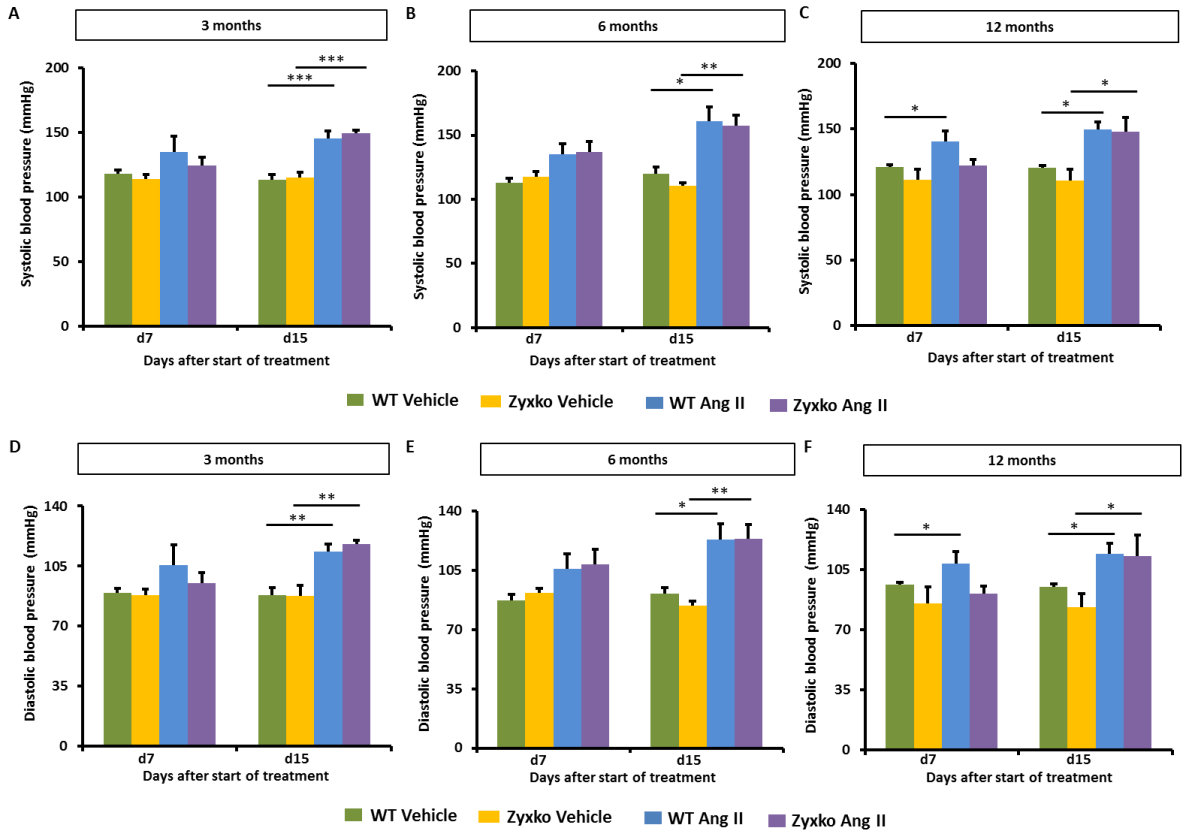

Figure 4.25 Comparable level of blood pressure elevation in WT and Zyxko mice after angiotensin II treatment

(A, B, C) Systolic blood pressure elevation after 7 and 14 days treatment with Ang II or vehicle in WT and Zyxko mice at 3 (A), 6 (B) and 12 (C) months of age. (D, E, F) Elevation in diastolic blood pressure in WT and Zyxko mice receiving the same treatments at 3 (D), 6 (E) and 12 (F) months of age. Each column represents the mean ± SEM of n = 5 mice per treatment condition. ***p<0.001, **p<0.01, *p<0.05 as indicated

4.9 Effect of Ang II treatment on cardiac systolic function of WT and Zyxko mice from different age

4.9.1 Three months old Zyxko mice show comparable cardiac systolic functional parameters after Ang II treatment as age-matched WT mice

Cardiac output (CO), ejection fraction (EF) and fractional shortening (FS) were similar in WT and Zyxko mice after 14 days of Ang II treatment compared to vehicle controls (Figure 4.26 A, C, D). However, stroke volume remained unchanged after treatment (Figure 4.26 B). Treatment of the mice with vehicle control, i.e. physiological saline, did not affect any of these parameters (by comparing vehicle control values (Figure 4.26) to the basal values shown in (Figure 4.24).

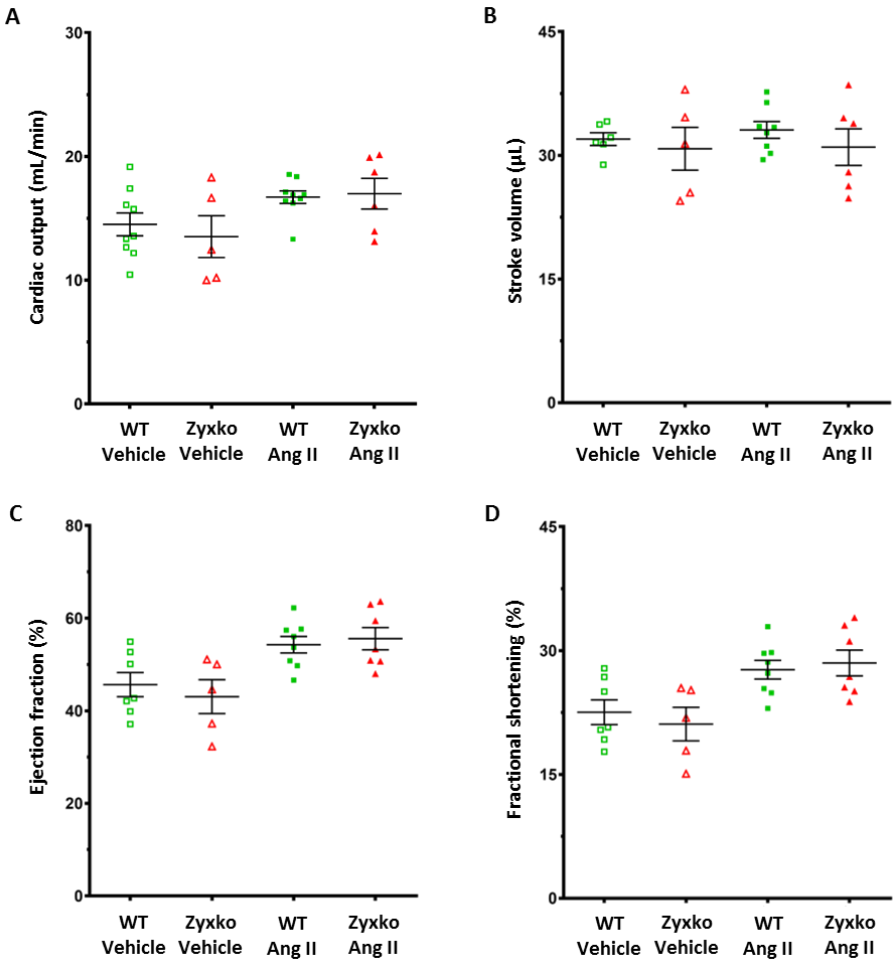

Figure 4.26 Comparable cardiac systolic functional parameters after Ang II treatment in 3-months old WT and Zyxko mice

(A-D) Cardiac output (A), stroke volume (B), ejection fraction (C) and fractional shortening (D) in WT and Zyxko mice after treatment with either Ang II or vehicle control for 14 days. The mean of each group is indicated by a horizontal line ± SEM of n ≥ 5 mice for each treatment.

4.9.2 Ang II treatment of 6-months old WT and Zyxko mice show comparable changes in the cardiac systolic functional parameters

In 6-months old hypertensive WT and Zyxko mice, cardiac output (CO), stroke volume, ejection fraction and fractional shortening were reduced compared to their vehicle treated counterparts (Figure 4.27 A-D). Vehicle treatment did not have any effect on these parameters (when compared to situation at baseline). Ejection fraction and fractional shortening were significantly reduced only in Zyxko mice treated with Ang II but not in WT mice subjected to the same treatment regimen (Figure 4.27 C, D). However, none of the studied cardiac functional parameters were different among WT and Zyxko mice after Ang II treatment.

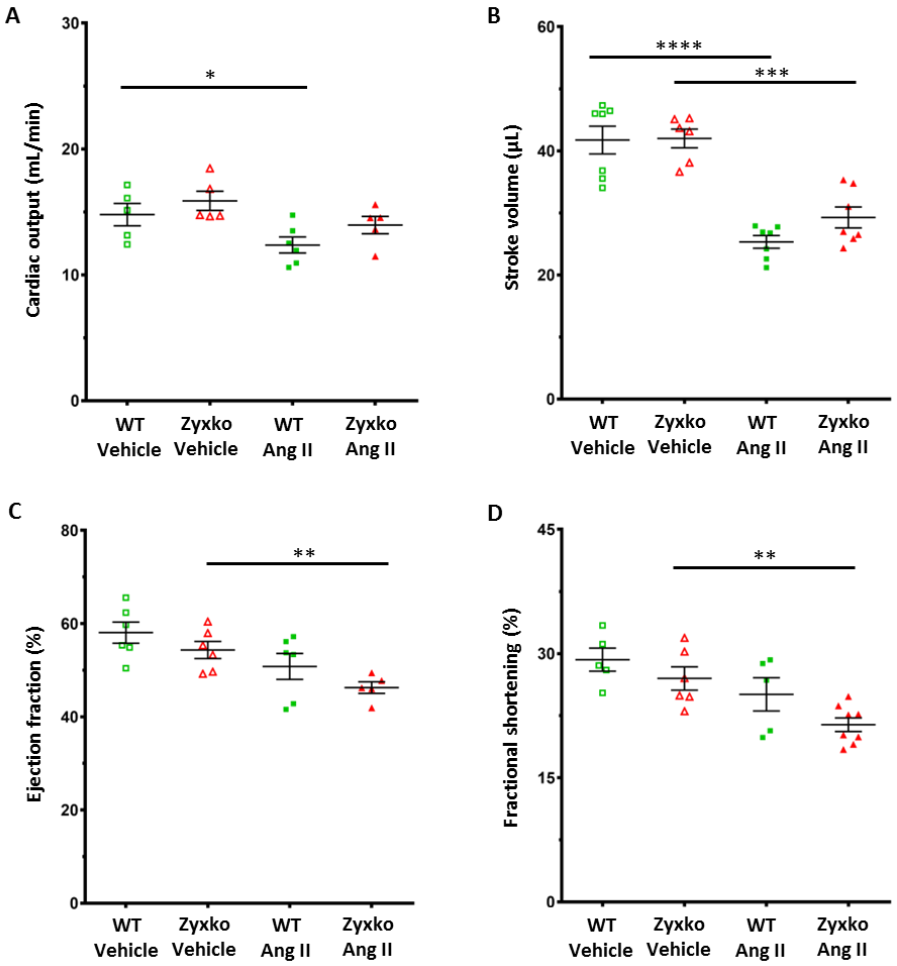

Figure 4.27 Cardiac systolic functional parameters were also comparable in Ang II treated 6 months old WT and Zyxko mice

(A-D) Cardiac output (A), stroke volume (B), ejection fraction (C) and fractional shortening (D) in 6-months old WT and Zyxko mice after treatment with either Ang II or vehicle control. The mean of each group is indicated by a horizontal line ± SEM of n ≥ 5 mice for each treatment. ****p<0.0001, ***p<0.001, **p<0.01, *p<0.05 as indicated

4.9.3 12 months old Zyxko mice show significantly greater differences in cardiac systolic function than WT mice after Ang II treatment

Cardiac output (CO), stroke volume (SV) and ejection fraction (EF) were significantly reduced in Ang II treated Zyxko mice when compared to their vehicle treated counterparts (Figure 4.28 A-C). After Ang II treatment, Zyxko mice showed significantly greater reductions in CO, SV and EF as compared to WT mice. However, the reduction in fractional shortening (FS) after Ang II treatment was statistically insignificant between WT and Zyxko mice (Figure 4.28 D).

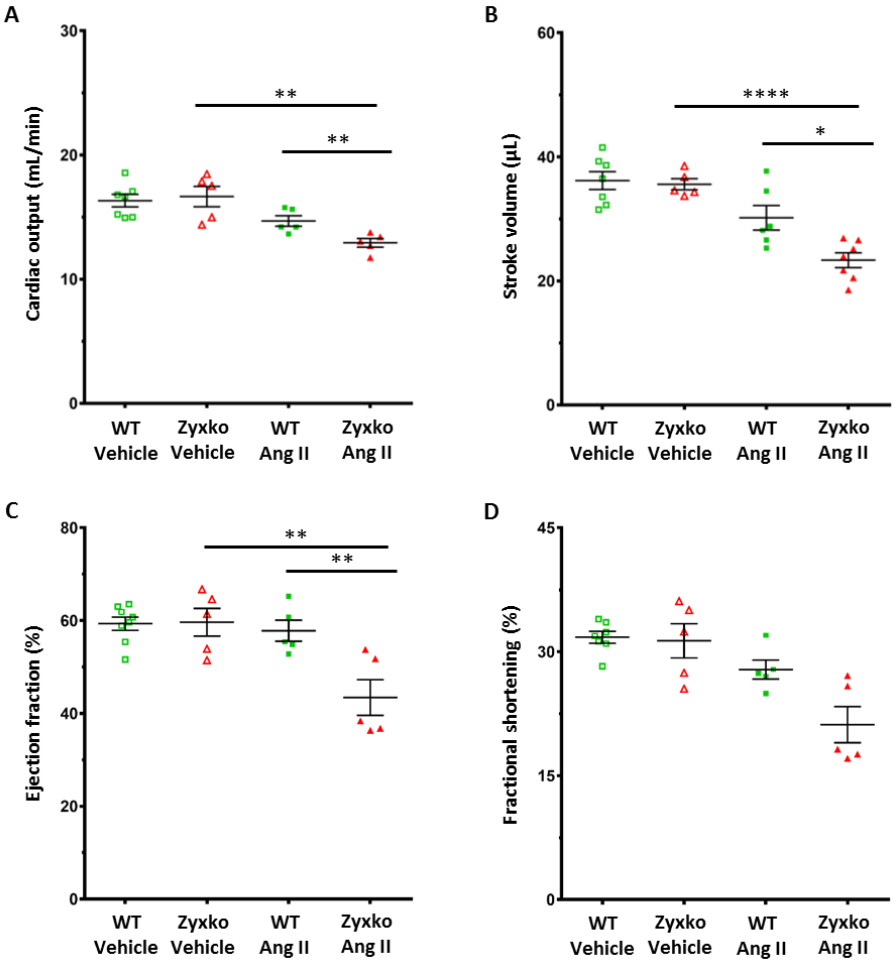

Figure 4.28 Cardiac systolic function was significantly different in Ang II treated WT and Zyxko mice at 12-months of age

(A-D) Cardiac output (A), stroke volume (B), ejection fraction (C) and fractional shortening (D) in 12-months old WT and Zyxko mice after 14 days of treatment with either Ang II or vehicle control. The mean of each group is indicated by a horizontal line ± SEM of n ≥ 5 mice for each treatment. ****p<0.0001, **p<0.01, *p<0.05 as indicated

4.10 Cardiac diastolic functional parameters were similar after Ang II treatment in WT and Zyxko mice of different age

Like under basal conditions, velocities for both the passive filling (E wave) and active filling (A wave) of the left ventricle were significantly lower in vehicle treated Zyxko mice as compared to those of WT at 3 (Figure 4.29), 6 (Figure 4.30) and 12 (Figure 4.31) months of age. After Ang II treatment, both velocities were significantly lower only in WT mice as compared to their vehicle control treated counterparts in all age groups. Like the E/A ratio, velocities for both early passive and late active filling were not significantly different in WT and Zyxko mice after Ang II treatment in all age groups.

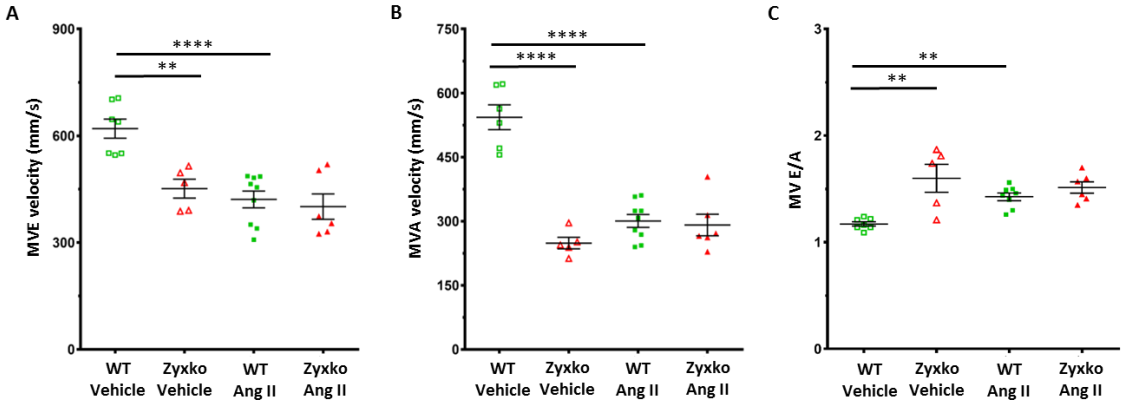

Figure 4.29 Diastolic filling velocities were comparable in Ang II treated WT and Zyxko mice at 3-months of age

(A, B) Velocities for early filling MVE wave (A) and late filling MVA wave (B) in either vehicle or Ang II treated WT and Zyxko mice. (C) Ratio for E and A wave in the same experimental setting. The mean of each group is indicated by a horizontal line ± SEM of n ≥ 5 mice for each treatment. ****p<0.0001, **p<0.01 as indicated

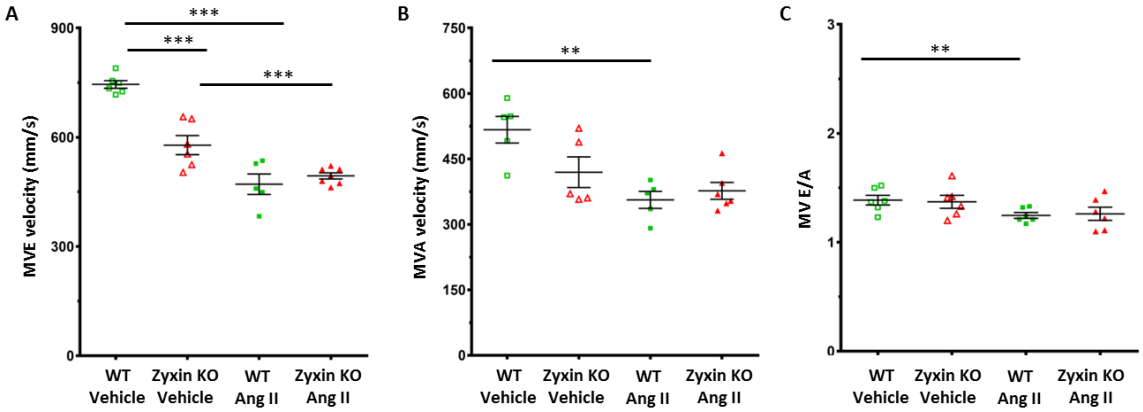

Figure 4.30 Cardiac diastolic functional parameters were not different in Ang II treated WT and Zyxko mice at 6-months of age

(A, B) Early passive, MVE (A) and late active filling, MVA (B) in 6-months old WT and Zyxko mice after 14 days of treatment with either Ang II or its vehicle control. (C) Ratio for E and A wave in the same experimental setting. The mean of each group is indicated by a horizontal line ± SEM of n ≥ 5 mice for each treatment. ***p<0.001, **p<0.01 as indicated

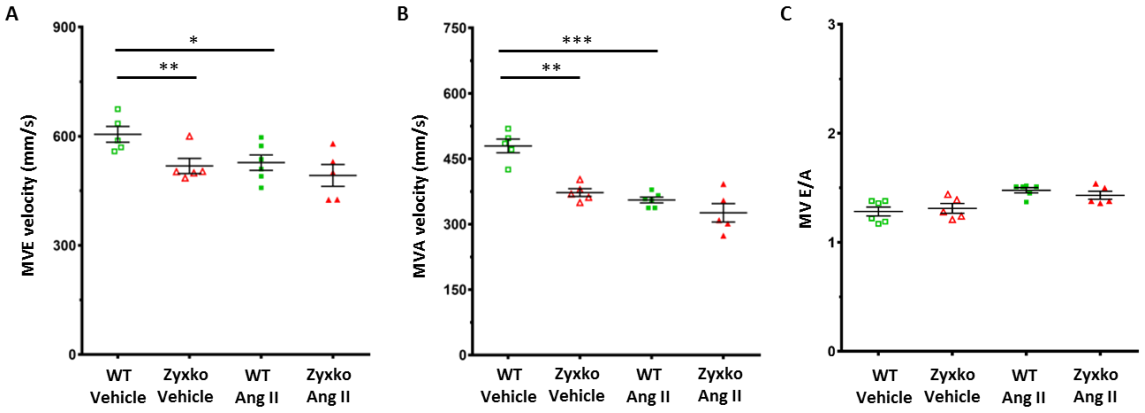

Figure 4.31 Ang II treated Zyxko and WT mice show comparable cardiac diastolic functional parameters at 12-months of age

(A, B) Early passive filling, MVE (A) and late active filling, MVA (B) after 14 days of treatment with either Ang II or vehicle in 12-months old WT and Zyxko mice. (C) Ratio for E and A wave in the same experimental setting. The mean of each group is indicated by a horizontal line ± SEM of n ≥ 5 mice for each treatment. ***p<0.001, **p<0.01, *p<0.05 as indicated

4.11 Angiotensin II treatment induces significant heart hypertrophy only in WT mice

To evaluate the level of heart hypertrophy in WT or Zyxko mice induced by systemic Ang II treatment, left ventricular mass was calculated from the recorded echocardiographic images and normalized with body weight. Only the WT mice showed a significant degree of hypertrophy after Ang II as compared to vehicle control treatment at 3, 6 and 12-months of age (Figure 4.32 A-C). The ratio between heart weight and body weight was also calculated to better evaluate the hypertrophic response of the heart. Ang II treated WT mice showed a significantly higher ratio when compared to vehicle control treated WT animals at 3, 6 and 12-months of age (Figure 4.32 D-E). Judged by this classical parameter, Zyxko mice showed significant induction of hypertrophy at 3 and 6-months of age which, however, was weaker as compared to 3 months old WT mice subjected to the same treatment regimen (Figure 4.32 D-E).

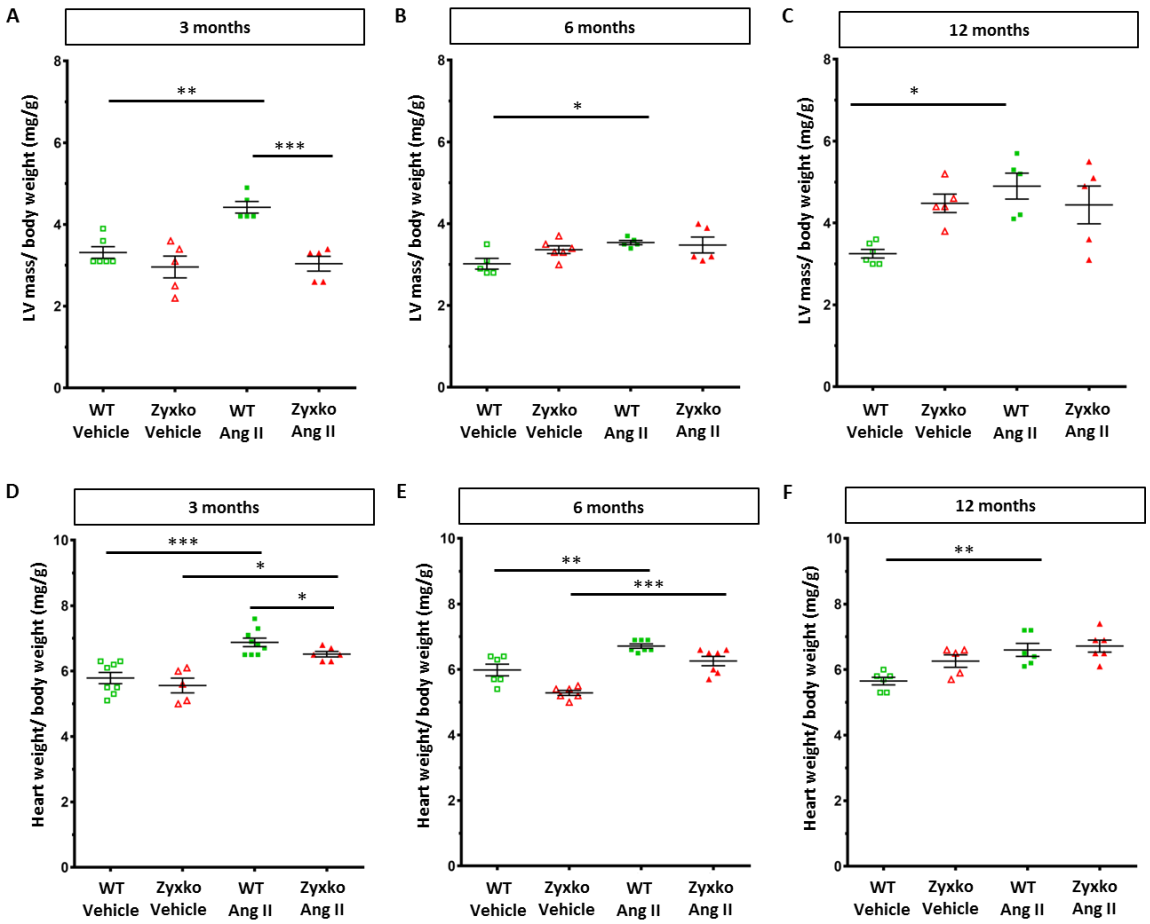

Figure 4.32 Angiotensin II treatment induces significant hypertrophy of the heart primarily in WT mice of different ages

(A, B, C) Normalized left ventricular mass (echocardiography parameter) of vehicle and Ang II treated WT and Zyxko mice at 3 (A), 6 (B) and 12 (C) months of age. (D, E, F) Ratio of heart weight to body weight for vehicle and Ang II treated WT and Zyxko mice at 3 (D), 6 (E) and 12 (F) months of age. The mean of each group is indicated by a horizontal line ± SEM of n ≥ 5 mice for each treatment. ***p<0.001, **p<0.01, *p<0.05 as indicated

4.12 Angiotensin II treatment induces higher expression of CTGF and LOX in the heart of Zyxko mice from different age

As the Ang II treated and thus hypertensive Zyxko mice exhibited signs of systolic dysfunction but only modest cardiac hypertrophy, next their tendency to develop cardiac fibrosis was evaluated by analyzing the expression of connective tissue growth factor (CTGF) and lysyl oxidase (LOX), one of the major collagen cross linking enzymes. In fact, cardiac tissue of Zyxko mice revealed significantly higher levels of both gene products after Ang II treatment at 3, 6 and 12-months of age (Figure 4.33). Cardiac tissue from vehicle treated 6 or 12 months old Zyxko mice showed markedly increased levels of CTGF and LOX mRNA when compared to their WT counterparts. Strikingly, 14 days treatment with Ang II induced expression of these genes in the heart of age-matched WT mice only to a level that is comparable to that of the vehicle control treated Zyxko vehicle control mice.

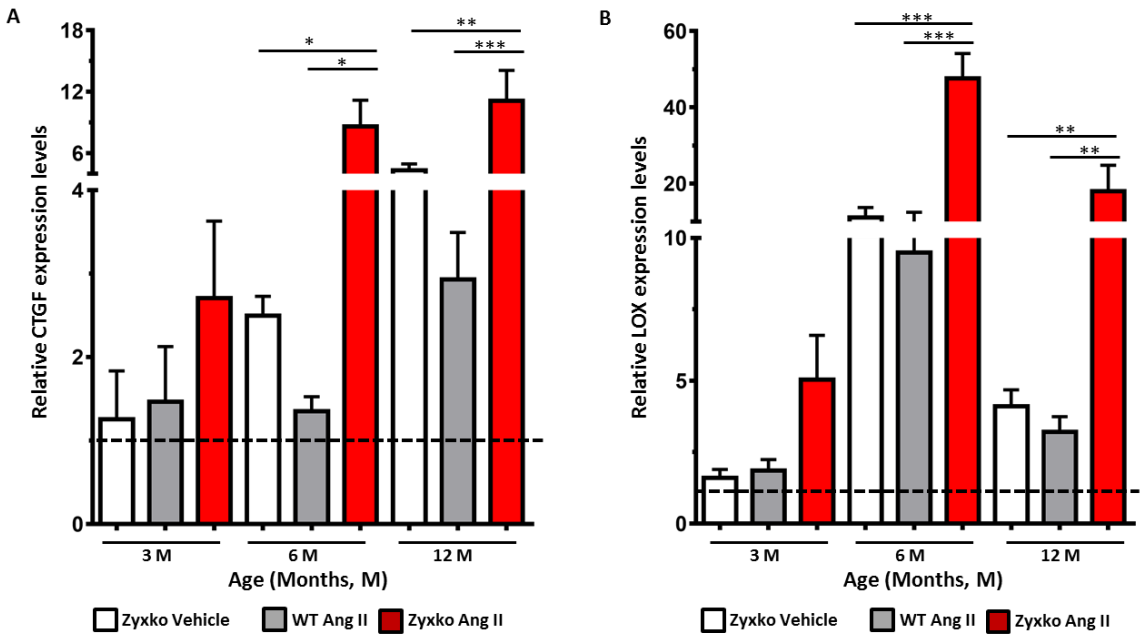

Figure 4.33 Angiotensin II treatment induces higher expression of CTGF and LOX in the heart of Zyxko mice as compared to WT mice irrespective of their age

(A, B, C) Relative mRNA abundance of CTGF in cardiac tissue derived from 3 (A), 6 (B) and 12 (C) months old WT and Zyxko mice after 14 days of treatment with either Ang II or vehicle control. (D, E, F) Relative mRNA level of LOX at same experimental conditions. Relative mRNA abundance was normalized using that of the reference gene RPL32. The level of mRNA in the cardiac tissue of vehicle control treated WT mice was used as a calibrator for the different age groups (set to 1, indicated by the broken line). Each column represents the mean ± SEM of n ≥ 5 mice for each condition. ***p<0.001, **p<0.01, *p<0.05 as indicated

4.13 Angiotensin II treated Zyxko mice show significantly more pronounced cardiac fibrosis in all age groups

The degree of cardiac fibrosis was determined by staining for collagen in the hearts of WT and Zyxko mice after 14 days of Ang II treatment. Collagen fibers were visualized by Masson trichrome and van Gieson's staining protocols. Both protocols revealed significantly higher collagen fiber deposition in the hearts of Ang II treated Zyxko mice as compared to Ang II treated WT mice. After Ang II treatment, perivascular collagen deposition was observed both in WT and Zyxko mouse hearts, whereas interstitial collagen deposition only occurred in the hearts of the Zyxko mice at the age of 3-months (Figure 4.34 A,B), 6-months (Figure 4.35 A,B) and 12-months (Figure 4.36 A,B). To analyze the magnitude of this collagen deposition, numbers of collagen-rich spots were counted under the microscope in a blinded fashion. This way, Ang II treated WT mice get a score for fibrotic collagen deposition of around 1, representing solely perivascular collagen staining, which was similarly found in the vehicle treated WT and Zyxko mice. After Ang II treatment, Zyxko mouse hearts showed significantly higher fibrotic collagen deposition scores in all age groups as compared to WT mice subjected to the same treatment regimen (Figure 4.34 C); (Figure 4.35 C); (Figure 4.36 C). Finally, to avoid any subjective measurement bias, the area of collagen deposition from the captured

microscopic images was quantified by using an image analysis macro in a blinded fashion. Again, only in the hearts of Zyxko mice the fibrotic area was significantly enlarged following Ang II treatment as compared to their vehicle treated counterparts or to WT mice subjected to Ang II treatment in all age groups (Figure 4.34 D); (Figure 4.35 D); (Figure 4.36 D).

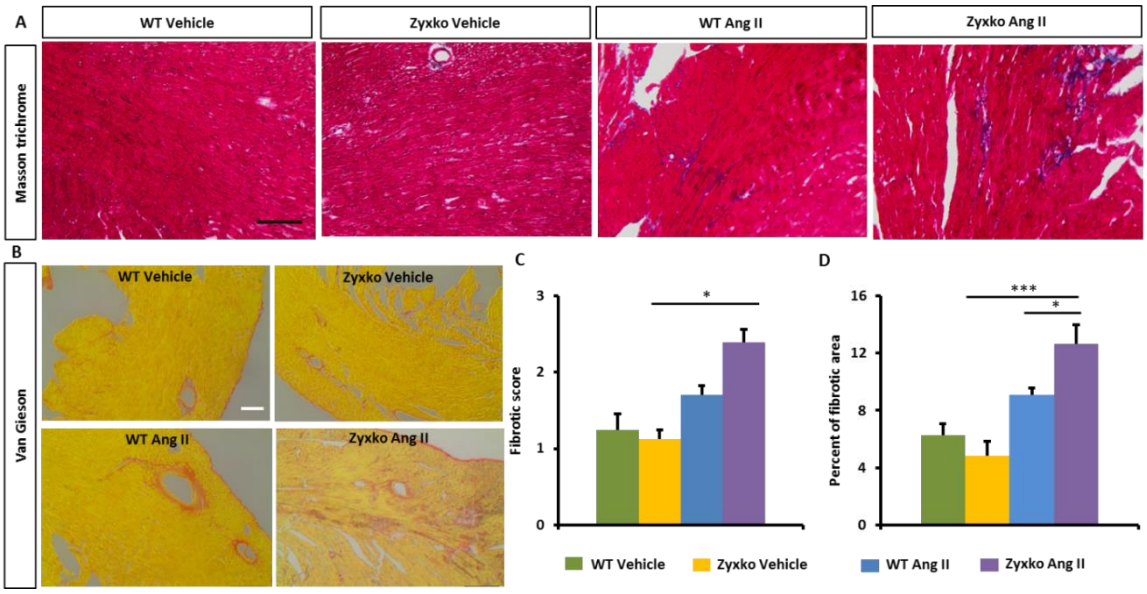

Figure 4.34 Higher cardiac fibrosis is observed in angiotensin II treated Zyxko mice at 3-months of age

(A, B) Masson trichrome (A, red: cardiomyocytes, blue: fibrosis) and van Gieson (B, yellow: cardiomyocytes, pink: fibrosis) staining for collagen fiber deposition in cardiac tissue sections of WT and Zyxko mice subjected to systemic vehicle or Ang II treatment at 3-months of age. Scale bar 200 µm. (C, D) Summarized fibrotic score (C) and area of collagen deposition (D). Each column represents the mean ± SEM of n ≥ 5 mice for each condition with 3 sections for fibrotic score and at least 10 captured images for fibrotic area analyzed per animal. ***p<0.001, *p<0.05 as indicated

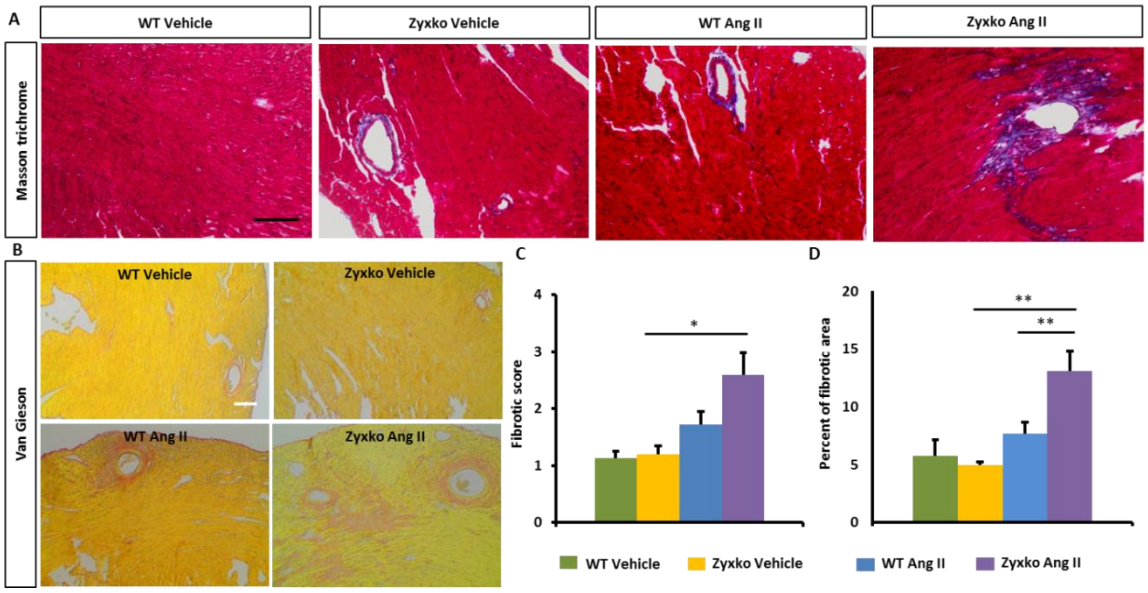

Figure 4.35 Prominent cardiac fibrosis is observed in angiotensin II treated Zyxko mice at 6-months of age

(A, B) Masson trichrome (A, red: cardiomyocytes, blue: fibrosis) and van Gieson (B, yellow: cardiomyocytes, pink: fibrosis) staining for collagen fiber deposition in cardiac tissue sections of WT and Zyxko mice subjected to systemic vehicle or Ang II treatment at 6-months of age. Scale bar 200 µm. (C, D) Summarized fibrotic score (C) and area of collagen deposition (D). Each column represents the mean ± SEM of n ≥ 5 mice for each condition with 3 sections for fibrotic score and at least 10 captured images for fibrotic area analyzed per animal. ***p<0.001, *p<0.05 as indicated

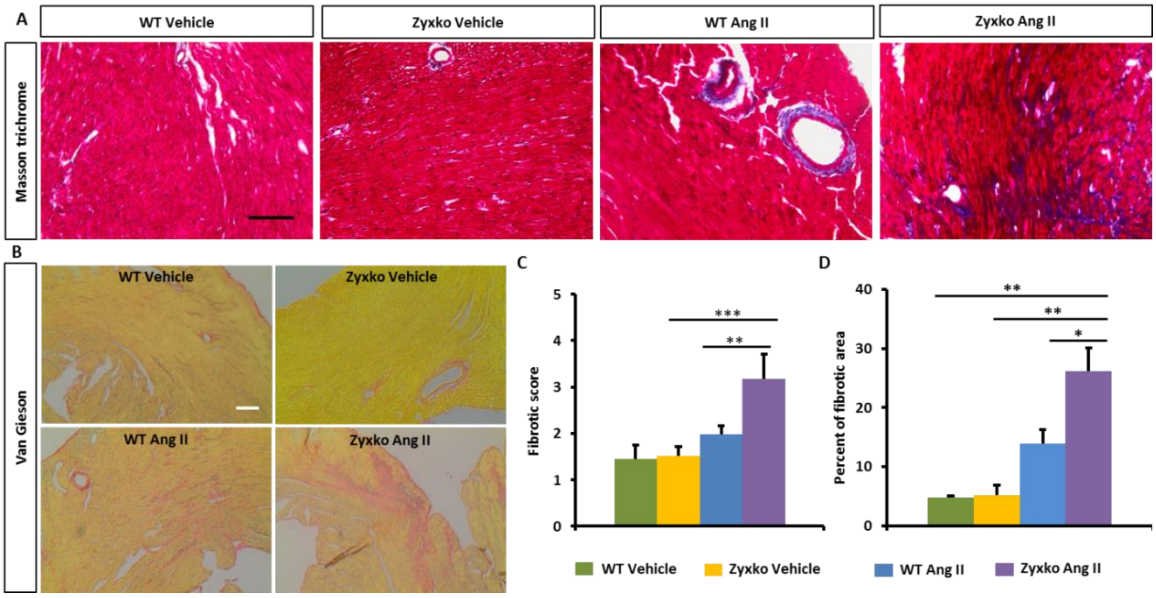

Figure 4.36 Even more prominent cardiac fibrosis is observed in angiotensin II treated Zyxko mice at 12-months of age

(A, B) Masson trichrome (A, red: cardiomyocytes, blue: fibrosis) and van Gieson (B, yellow: cardiomyocytes, pink: fibrosis) staining for collagen fiber deposition in cardiac tissue sections of WT and Zyxko mice subjected to systemic vehicle or Ang II treatment at 12-months of age. Scale bar 200 µm. (C, D) Summarized fibrotic score (C) and area of collagen deposition (D). Each column represents the mean ± SEM of n ≥ 5 mice for each condition with 3 sections for fibrotic score and at least 10 captured images for fibrotic area analyzed per animal. ***p<0.001, *p<0.05 as indicated

4.14 Ang II treated Zyxko mice age-independently show significantly higher levels of lysyl oxidase in the heart than WT mice

Immunofluorescence staining was performed to quantify the level of lysyl oxidase (LOX) in the cardiac tissue sections derived from WT or Zyxko mice at the different ages. After Ang II treatment at 3 and 6 months of age, both WT and Zyxko mouse hearts showed significantly higher levels of LOX compared to those of the respective vehicle controls. Nevertheless, LOX abundance in Ang II treated Zyxko mouse hearts was significantly higher compared to that of WT mouse hearts at 3 and 6-months of age (Figure 4.37 A-C). At 12-months of age, only Zyxko mice showed a significant increase in LOX protein abundance in the heart in Ang II treated animals over vehicle control treated animals as well as Ang II treated WT mice (Figure 4.37 A, D).

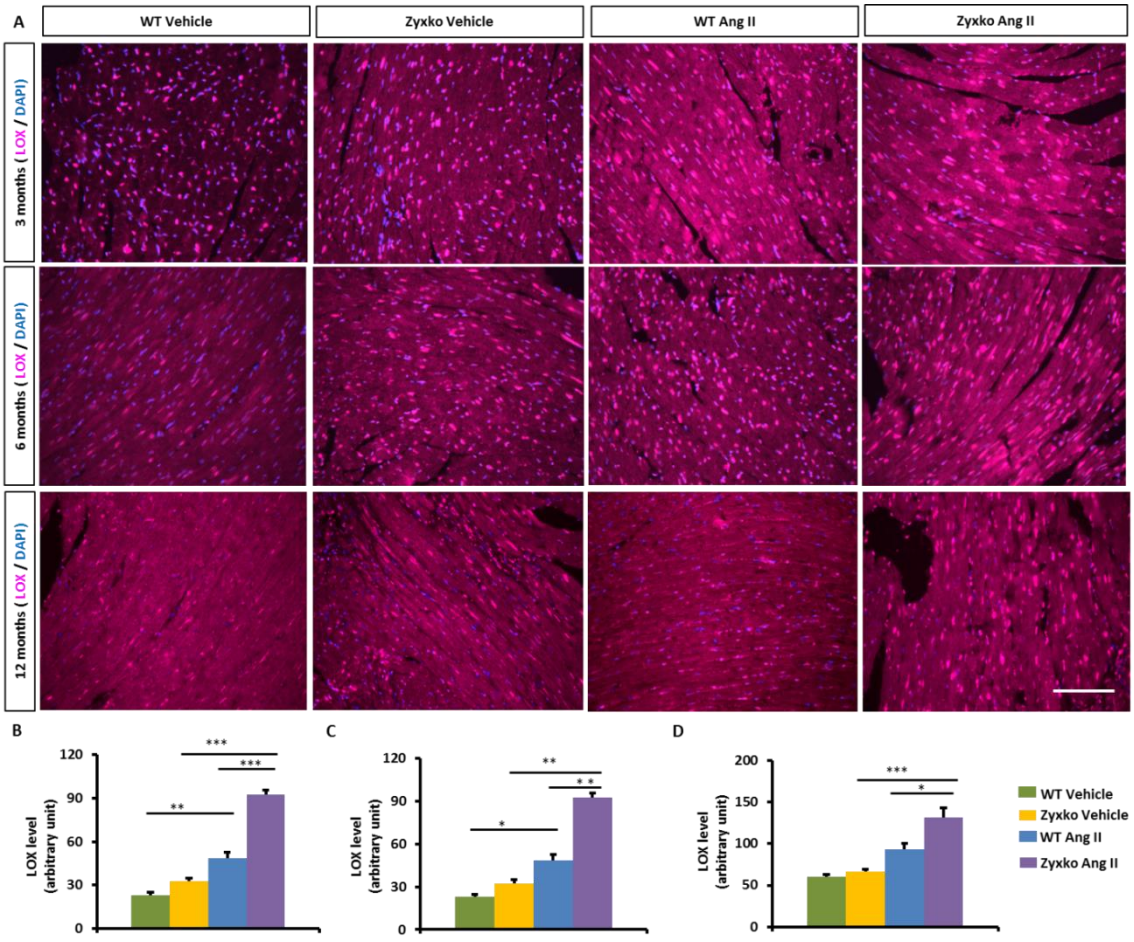

Figure 4.37 Lysyl oxidase level is significantly higher in Ang II treated Zyxko mouse hearts independently of the age of the animals

(A) Immunofluorescence images for lysyl oxidase (LOX) in the cardiac tissue sections of differently treated 3, 6 and 12-month old WT and Zyxko mice. Scale bar 100 µm. (B, C, D) Statistical summary for the LOX-specific fluorescence intensity in 3 (B), 6 (C), and 12 (D) months old animals. Each column represents the mean ± SEM of n ≥ 5 mice for each condition with at least 3 sections analyzed per animal. ***p<0.001, **p<0.01, *p<0.05 as indicated

4.15 Adult cardiac fibroblasts isolated from 3-months old Zyxko mice show significantly higher levels of pro-fibrotic gene expression after TGF-β1 treatment

To investigate the source of the prominent cardiac fibrosis in the heart of Zyxko mice, cardiac fibroblasts isolated from 3 months old WT or Zyxko mice were treated with the pro-fibrotic stimulus TGF-β1. Interestingly, Zyxko cardiac fibroblasts showed a markedly higher expression of CTGF, collagen α1 and lysyl oxidase (LOX) already at baseline when compared to TGF-β1 stimulated WT cardiac fibroblasts. For collagen α3 and integrin-β1, this effect was also clearly visible but did not reach statistical significance. Treatment of the Zyxko cardiac fibroblasts with TGF-β1 approximately doubled the expression of all gene products except integrin-β1, which did not seem to be sensitive to TGF-β1 in these cells. Figure 4.38 summarizes the aforementioned findings.

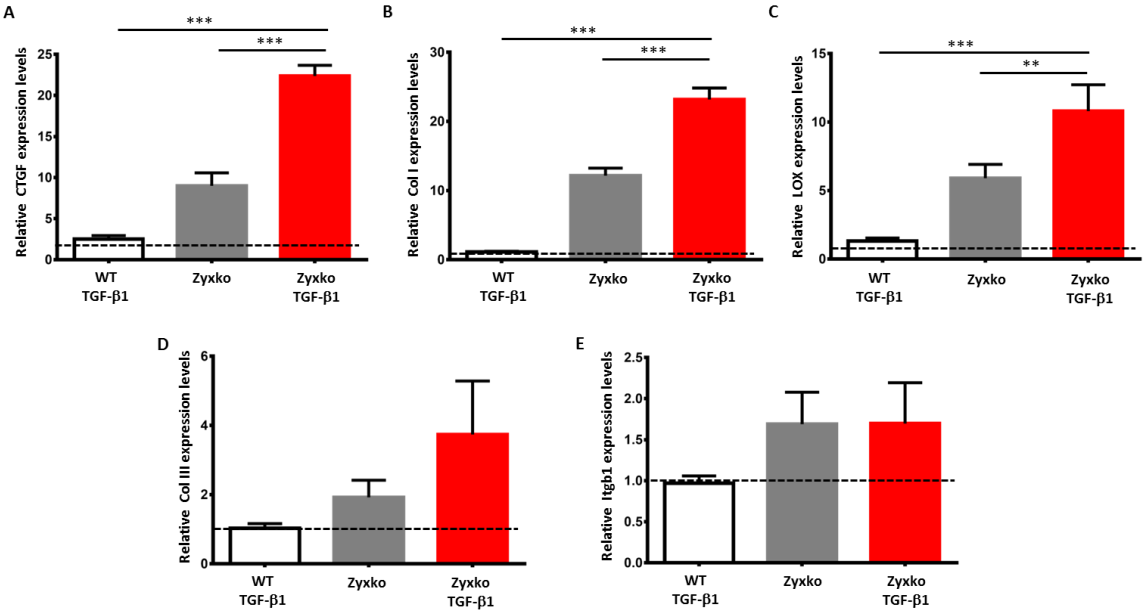

Figure 4.38 Adult cardiac fibroblasts from Zyxko mice showed significantly higher expression of pro-fibrotic genes than cardiac fibroblasts from WT mice

(A-E) Relative expression levels of CTGF (A), Col I (B) LOX (C), Col III (D) and integrin β1 mRNA (E) at baseline and following stimulation with TGF-β1 (10 ng/ml) for 24 hours in adult cardiac fibroblasts isolated from 3 months old WT or Zyxko mice. Expression levels were normalized using the reference gene RPL32. The level of expression in the WT cardiac fibroblasts was used as a calibrator (set to 1, indicated by the broken line). Each column represents the mean ± SEM of n = 5 experiments with individual adult cardiac fibroblast preparations. ***p<0.001, **p<0.01 as indicated

5 Discussion

Hypertension (high blood pressure) is responsible for about 13% of total deaths worldwide and reported to correlate significantly with the risks for, e.g. coronary heart disease, stroke or chronic renal failure. From the clinical standpoint, hypertension is an enigma. It is devoid of any obvious early signs but develops insidiously. Blood pressure (mean arterial pressure) is regulated by cardiac output and total peripheral resistance which is intricately linked to contraction of the medial VSMCs within the vessel wall of the small arteries and arterioles. Together with sympathetic activity, cardiac output is increased at the early stages of hypertension development but normalized once blood pressure has been established at the elevated level. Total peripheral resistance behaves differently and is the physical reason for the persistent (further) rise of blood pressure[25]. Augmented peripheral resistance is inferred to the narrowing of the aforementioned resistance-sized small arteries and arterioles that ensues as part of the (mal)adaptive (cardio)vascular remodelling process to normalize wall stress in the wall of these blood vessels. Vascular smooth muscle cells as well as cardiomyocytes and cardiac fibroblasts elicit functional changes to cope with this local environmental shift by converting the mechanical stimulus to cellular events like alterations in gene expression or even phenotypic shifts. However, the mechanisms underlying mechanotransduction in these cells are not particularly well understood and investigated so far. In the present study, efforts have been made to better understand cytoskeletal proteins associated with focal adhesions (FA) such as zyxin and LPP, their role in mechanotransduction and the control of such cardiovascular remodelling process in response to pathophysiological stress.

5.1 The level of LPP level decreases in arterial blood vessels of aging Zyxko mice to unveil its function as a stabilizer of the VSMC phenotype

A zyxin orthologous cytoskeletal protein has been shown to be required for the viability of drosophila, whereas in C. elegans this orthologous protein is involved in dystrophin-dependent muscle degeneration[120,121]. In contrast, Zyxko mice lack any noticeable abnormalities under basal conditions[110]. Also Lppko mice seem to be free from any definitive phenotype apart from some possible embryonic lethality which might affect the female offspring[103]. In zebrafish, however, Lpp is required for proper embryonic development[100]. A possible explanation for this paradox in mice might be the presence of a functional redundancy between individual members of the zyxin family of LIM-domain containing proteins. The presumption of a compensatory mechanism(s) in mice is further corroborated by the fact that zyxin and its closest homologues LPP and TRIP6 are represented by a single orthologous gene product, Zyx102 in *Drosophila melanogaster* and ZYX-1 in

C. elegans[121,122]. Therefore, in simpler organisms, the loss of this LIM-domain containing protein cannot be compensated and thus has detrimental effects on vital functions. In higher organisms, this effect presumably is lost with the evolutionary emergence of multiple family members with redundant functional roles that can likely replace each other. Moreover, zyxin, LPP and TRIP6 share some interaction partners, which apart from their similar protein structure, is an extra indication that these proteins share one or more functions.

Zyxin has been shown to be involved in regulating the expression of mechanosensitive genes both in endothelial cells and VSMCs[55–58]. It also plays a prominent role in determining the phenotype of VSMCs in vitro[58]. It was therefore quite unexpected that adult Zyxko mice revealed such a vascular phenotype (shift from contractile to synthetic) when subjected to an experimental hypertension model only in very old, i.e. 18 months old animals[111]. By considering this unusual age-dependency, we hypothesized that a possible compensatory mechanism might hinder the younger adult Zyxko mice, precisely the VSMCs within the wall of the arterial blood vessels, to force them into an hypertension induced vascular remodelling process. In this compensatory event, perhaps the two most closely related zyxin homologs LPP and/or TRIP6 conceal the effects of the zyxin deficiency. This notion was tested through analysing their age-dependent abundance in arterial blood vessels of Zyxko mice. Unlike in wild type animals, both LPP and TRIP6 mRNA abundance declined with age in the Zyxko mice but only LPP protein levels significantly dropped by about 50% in the very old Zyxko mice. Further evidence that LPP rather than TRIP6 can compensate for the loss of zyxin in the arterial VSMCs was derived from the very different subcellular distribution of both proteins in these cells at baseline and following exposure to cyclic stretch. In fact, LPP essentially matched the intracellular localisation and stretch-induced redistribution to the nucleus and to the stress fibers of zyxin in a head to head comparison in VSMCs isolated from adult wild type mice. In contrast, TRIP6 only poorly associated with focal adhesions and proved to be essentially insensitive to cyclic stretch. In the present study, the antibody that was used to detect TRIP6 was raised against a peptide positioned close to the N-terminus of TRIP6[110], which is missing in a shorter, strictly nuclear isoform identified at least in humans[79]. Whether such an isoform also exists in mice is yet to be determined. Hence, our analyses did not provide any evidence that full-length TRIP6, like zyxin or LPP, could translocate to the nuclei of murine WT VSMCs upon stretch.

Structurally, LPP is the closest homolog of zyxin while TRIP6 lacks not only the α-actinin but also VASP-binding motif in the pre-LIM region that both LPP and zyxin have[91]. Stretching of VSMCs isolated from VASP knockout mice in fact failed to induce translocation of zyxin to stress fibers or to the nucleus, and failed to control expression of prototypic mechanosensitive genes in these cells (unpublished observation, doctoral thesis of I. Eberhard 2004, University of Goettingen). When

combined these observations suggest that TRIP6, probably because of its lack of interaction with α-actinin and/or VASP, is incapable of transducing mechanical signals perceived by the focal adhesions and transmitted via the actin cytoskeleton to the nuclei of VSMCs. Due to the presence of the corresponding binding motifs (Figure 5.1) as well as its expression profile, on the other hand, LPP looks like the candidate to maintain the quiescent differentiated VSMC phenotype in Zyxko mice up to 12 months of age.

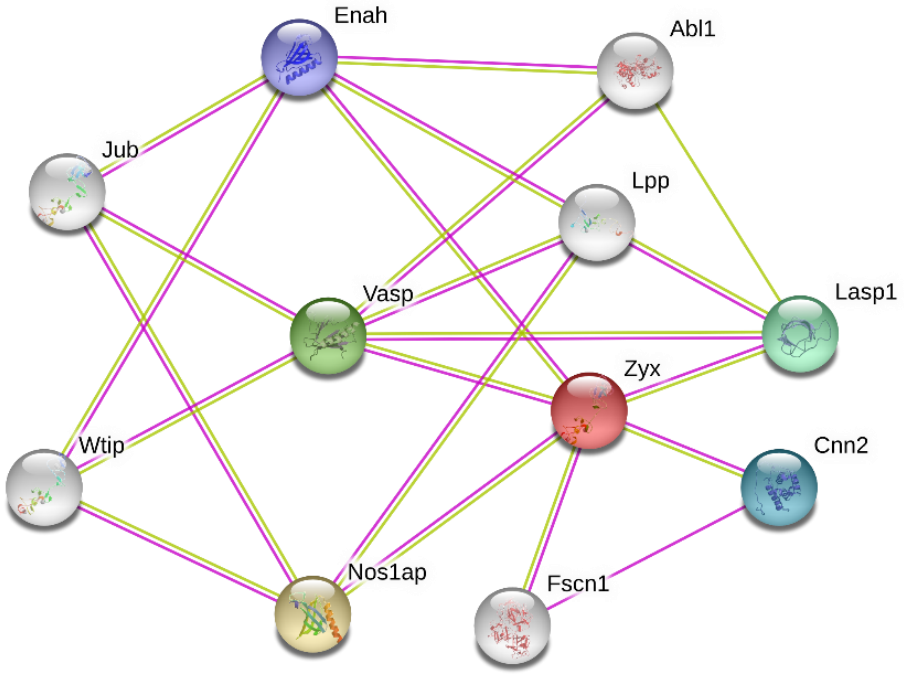

Figure 5.1 Molecular interaction network between mouse Zyxin, LPP and VASP
This protein-protein interaction network was made using the web-based tool STRING (version 10.5, accessed on 14.05.2017). Pink lines denote experimentally determined interactions while the green lines denote interactions based on text mining. Abbreviations: Nos1ap, nitric oxide synthase-1; Fscn1, Fascin Actin-Bundling Protein-1; Abl1, Abelson murine leukemia viral oncogenic homologue-1; Jub, ajuba; Wtip, Wilms tumor-1 interacting protein; Lasp1, LIM and SH3 protein-1; Cnn2, calponin-2; Enah, enabled homolog; Vasp, vasodilator stimulated phosphoprotein.

5.2 VSMCs isolated from adult Lppko mice reveal a synthetic phenotype while the young (3-months old) animals appear to be protected from hypertension-induced arterial remodeling

In adult arterial blood vessels, VSMCs are essentially committed to carry out their contractile function while exhibiting an extremely low rate of proliferation, migration and synthesis of extracellular matrix (ECM) components at the same time. These mature differentiated VSMCs also show extensive phenotypic plasticity under physiological and pathophysiological conditions to confer a survival advantage in higher organisms[123]. Excessive wall stress during hypertension causes switching of their phenotype from this quiescent, contractile state to a proliferative and synthetic

state mainly to normalise any prolonged rise in wall stress[25]. Interestingly, arterial VSMCs isolated from 3 months old Lppko mice mimic the synthetic phenotype of VSMCs isolated from age-matched Zyxko mice[58] with somewhat less pronounced but nonetheless strikingly similar pro-migratory, hyper-proliferative, and poorly contractile characteristics both in 2-dimensional (2D) and 3-dimensional (3D) cell cultures. VSMCs cultured in a 2D environment often behave differently from cells cultured in a 3D matrix in which they are normally embedded in the vessel wall[119].

Moreover, In pathological settings like hypertension, the prolonged rise in wall stress leads to enhanced ECM turnover by humoral factors, thereby triggering VSMC hypertrophy (in conduit arteries) or VSMC hyperplasia (in arterioles) to reinforce the vessel wall[4]. Matrix metalloproteinase (MMP) activity is increased during such vascular remodeling processes for breaching the ECM to support the migration of VSMCs[32]. In fact, VSMCs isolated from both Zyxko and Lppko mice revealed significantly higher MMP activity as compared to that of VSMCs isolated from WT mice both in 2D and in 3D cell cultures. This increased MMP activity was largely attributable to MMP9 rather than MMP2, and this finding correlated well with the higher rate of migration of the VSMCs isolated from Zyxko or Lppko mice while VSMCs isolated from Mmp9ko mice display both impaired migration and proliferation[33].

Since its discovery as a translocation partner in a variety of human cancers, the function of LPP has been studied mainly in the context of cancer development and progression[124]. However, the physiological role of LPP or its significance in other pathological situations, e.g. hypertension, remained elusive so far. In the literature, LPP is mainly referred to as a protooncogene which promotes cancer development by aberrant nuclear translocation together translocation partners like the HMGA2 or MML genes[101,102,125,126]. In contrast, LPP has previously been described as a positive regulator for cellular migration in VSMC[98], in mouse embryonic fibroblasts[103] as well as in lung metastasized breast cancer cells[101,102]. Moreover, LPP has been reported to prevent the migration and tissue invasion of human lung adenocarcinoma cells[125]. The conflicting reports about the role of LPP in cellular migration might be context-dependent or due to heterogeneity of the studied models. This discrepancy could further be explained by the methods employed for knocking down LPP, e.g. by RNA interference.

Thus, fibroblasts isolated from E14.5 Lppko embryos, on a S129 background though, displayed impaired migration and proliferation[103]. In the present study with homozygous adult Lppko mice on a pure C57BL/6J background from which arterial VSMCs were isolated, we noted that these cells in culture clearly present with a synthetic phenotype, i.e. Increased proliferation and migration rates. One reason for such inconsistency could be differences between cell types as well as in terms of

development temporally different roles of LPP. On top of that, choices of method and readout to analyze such functional properties could also be an important source of disagreement. Conventionally, in the 2D migration assay, frequently referred to as scratch-wound assay, closure of the gap is measured rather than counting the number of migrating cells[127]. In their study, Vervenne et al.[103] have generated the wound by scraping away parts of the cell monolayer which may have given rise to possible artifacts due to variable wound size and/or mechanical cell damage (triggering inflammation)[128]. In addition, instead of measuring the gap closure over time by the migrating cell front, they have counted the number of cells migrating to the wounded area. In this study, silicon blocks were used to create nearly identical gaps without any mechanical damage to the cells and measured the distance between the migrating fronts of cells, i.e. gap closure. Moreover, we have also analyzed the 3D invasion capacity of the Lppko VSMCs in the form of a sprouting assay with VSMCs cast as spheroids into collagen gels. To assess their rate of proliferation, we have counted absolute cell numbers over time as well as labeled the proliferating cell with a definitive marker of proliferation, i.e. Ki67, whereas Vervenne et al.[103] have used metabolism-based assay. Furthermore, several lines of evidences have established LPP as a novel marker for the differentiated VSMC phenotype[98,129]. Hence, in the VSMCs isolated from the Lppko mice, lower expression of contractile proteins together with more migration and proliferation did not come as a surprise, but instead reflected their presumed shift towards the synthetic phenotype. Evaluation of the contractile capacity of resistance arteries isolated from these animals would provide additional and solid evidence for our assumption but has not been carried out yet.

Ubiquitous Lppko mice on a pure C57BL/6J background are exclusively raised in our animal facility; they therefore needed to be phenotyped with regard to their cardiovascular status. Young Lppko mice (3-months old) are somewhat smaller in size than their wild type counterparts. Under basal conditions, they do not show any discernible differences in systolic or diastolic blood pressure but present with a significantly higher heart rate at rest that might be associated with their smaller size[130]. Although they have a normal cardiac function in systole at rest, they present with significantly lower diastolic filling velocities of the left ventricle that may indicate an impaired cardiac function in diastole[131]. Although assessment of diastolic dysfunction ideally requires invasive measurements (cardiac catheterization), the left ventricular filling velocities in diastole serve as a non-invasive surrogate parameter with controversial specificity[132,133]. Filling of the left ventricle during diastole is predominantly regulated by the interaction of left atrial compliance and the rate of left ventricular relaxation. The transmitral E wave depends on active left ventricular relaxation, hence a slow or prolonged left ventricular relaxation causes a decrease in E velocity. Although the functional significance of an impaired relaxation of the left ventricle for its refilling is not fully

understood[131], it becomes apparent at an early stage of left ventricular dysfunction which could lead to adverse cardiovascular events[134].

DOCA, the murine equivalent of aldosterone, is used to increase blood pressure inter alia by retention of sodium and water in the kidneys but also by reinforcing central blood pressure control[117]. There are two variants of this experimental hypertension model: one is the renovascular two kidney model whereas the other is the one kidney/one clip model which induces quite a strong increase in blood pressure. In this study, the two kidney model with administration of DOCA and salt loading has been used for maximum animal survival. After induction of experimental hypertension, systolic blood pressure elevation was somewhat higher in the young Lppko mice as compared to their wild type counterparts while diastolic blood pressure elevation was not significantly different. Blood pressure changes in Zyxko mice at this age following DOCA-salt treatment still need to be analyzed but in 6 months old animals no such differences could be observed[111].

The significantly lower resistivity index (RI) in the femoral artery of the Lppko mice, an indirect measure of total peripheral resistance, may indicate an ensuing contraction deficit of the medial VSMCs of the small arteries and arterioles but was not yet reflected by a parallel lower response of diastolic blood pressure to the DOCA-salt treatment regimen. The vascular resistivity and pulsatility indices are calculated from the blood flow velocities during the cardiac cycle to estimate the resistance in arteries. Originally, both indices were introduced to detect peripheral vascular diseases[135–137]. Thus, the relatively reduced change in the resistivity index of the Lppko mice in response to experimental hypertension can be interpreted as indicative for a lower total peripheral vascular resistance in these mice. In this context, it is worth mentioning though that the resistivity index does not solely depend on vascular resistance but also is regulated by vascular compliance which varies from individual to individual[138]. Moreover, the medial VSMCs in the femoral arteries of the hypertensive Lppko mice were not different from those of age-matched wild type animals with respect to proliferation index or the presence of markers of the contractile phenotype. Nonetheless, these first signs of the presence of an altered vascular remodeling in these animals suggest that the arterial VSMCs may switch to the synthetic phenotype much faster than in Zyxko mice, where such a vascular phenotype manifests itself only at 18 months of age[111]. In any case, much older Lppko mice (6, 12 and 18 months old) need and will be analyzed in the near future in this model. Conversely, the fact that the synthetic phenotype of the arterial VSMCs isolated from 3 months old Lppko mice does not reveal itself in form of a vascular phenotype in these animals argues for a compensatory role of zyxin that may be overcome only by analyzing Lpp/Zyx double-knockout mice that are currently being generated.

5.3 Overexpression of either zyxin or LPP in their reciprocal knockout VSMCs fully compensates for their loss of function

VSMCs isolated from age-matched young Zyxko or Lppko mice both revealed synthetic phenotypes *in vitro*. Overexpression of LPP in Zyxko VSMCs and *vice versa* of zyxin in Lppko VSMCs normalized their pro-migratory phenotype in both 2D and 3D cell culture systems, and reversed their increased rates of proliferation towards basal levels. So that these findings strongly argue for the presumed functional redundancy among these two LIM-domain containing members of the zyxin family (Figure 5.2). Although changes in zyxin abundance in 3, 6, 12 and 18 months old Lppko mice still need to be analyzed, we would assume that zyxin does compensate for the loss of LPP in these animals up to a certain age (presumably sooner than in Zyxko mice) where the vascular loss of function phenotype unmasks itself. However, to ultimately proof this functional redundancy, analyses (basal conditions and hypertension) of Lpp/Zyx double-knockout are required; these will commence in due course. Until now, our findings suggest an important protective role for both zyxin family members in hypertension-induced arterial remodeling that may have therapeutic implications.

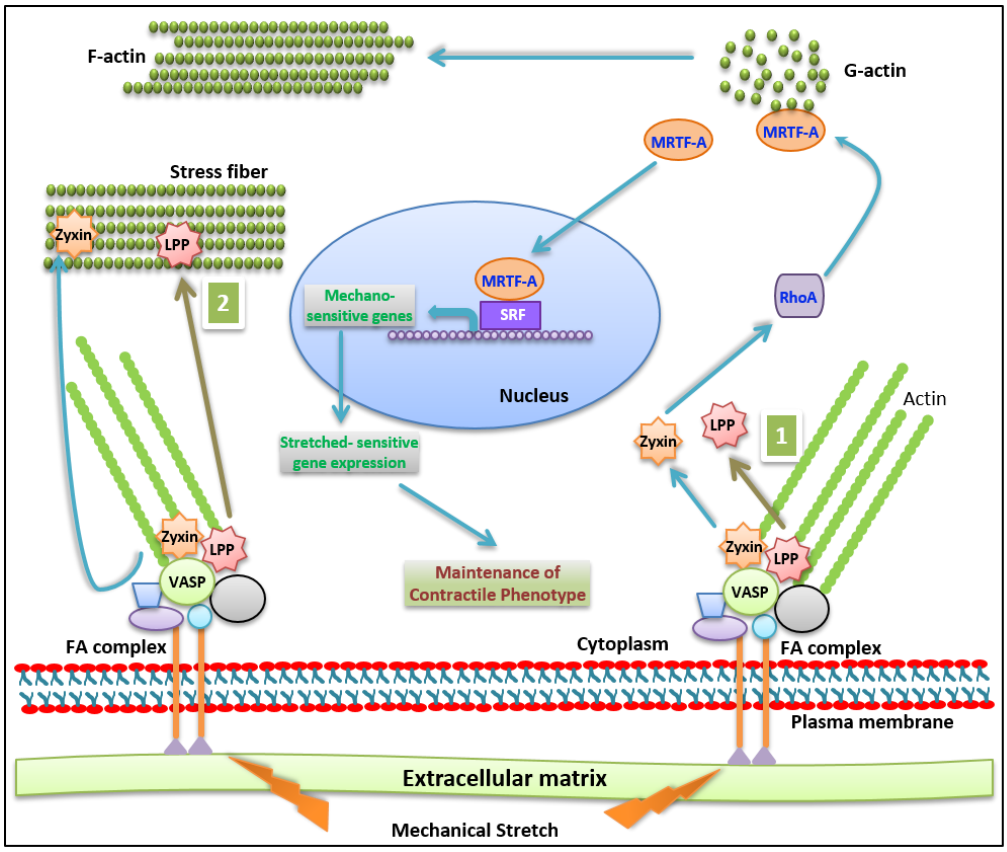

Figure 5.2 Schematic representation of the possible functional redundancy among LPP and zyxin to maintain a quiescent contractile phenotype in arterial VSMCs

Possible interacting fronts are denoted in green squares with white borders: 1. Like zyxin, LPP can regulate the expression of genes to determine the VSMCs phenotype via RhoA- MRTFA signaling pathway similar to zyxin; 2. LPP can also take part in the generation and maintenance of stress fibers in response to stretching. Based on[58].

5.4 Loss of zyxin shifts the balance to a more pro-fibrotic milieu in the heart

Very much like VSMCs in large conduit arteries, terminally differentiated cardiomyocytes respond to arterial hypertension by hypertrophy to neutralize the wall stress[13]. Following compensatory cardiomyocytes hypertrophy, cardiac dysfunction develops due to enhanced loss of cardiomyocytes and increased deposition of extracellular matrix (ECM) proteins by cardiac fibroblasts[14–16]. Zyxin has been reported to protect cardiomyocytes from apoptosis[139]. In a model of experimental hypertension (DOCA-salt treatment), 12 months old Zyxko mice presented with both systolic dysfunction *in vivo* and diastolic dysfunction *in vitro*, increased cardiomyocyte apoptosis, and prominent cardiac fibrosis[111]. Presumably, as a consequence of systolic dysfunction of the left ventricle, the Zyxko mice failed to upregulate systolic blood pressure to the same extent as age-matched wild type control animals[111]. A compromised renal function, as alternative explanation, could be excluded due to an unaltered renal excretion of cystatin C[111].

It has previously been reported that aldosterone in combination with high salt intake upregulates cardiac renin-angiotensin system components to induce a pro-inflammatory as well as pro-fibrotic response in the heart. In this cardiac remodeling situation, the pro-apoptotic signaling intermediate ASK1 (apoptosis signal-regulating kinase-1) serves as a molecular cross-bridge between mineralocorticoid and angiotensin II signaling[140–143]. Nonetheless, the DOCA-salt hypertension model in mice quickly progresses to severe hypertension and requires ingestion of a large amount of NaCl making it a less reliable model for studying the consequences of hypertension in humans like cardiac fibrosis[144,145]. In the present work, we wanted to elucidate the molecular mechanism underlying the development of cardiac fibrosis in Zyxko mice upon angiotensin II-mediated hypertension which is much more pronounced in this model than in the DOCA-salt model. In our previous study employing the DOCA-salt model, the degree of cardiac fibrosis in the 12 months old Zyxko mice may have already been at or beyond the maximum, so that subtle differences or even the onset of fibrosis could not be analyzed properly[111]. Hence, investigation of much younger animals might provide better insight into development of the cardiac phenotype in these animals. As such, mice aged 3, 6 and 12 months were explored for the extent of cardiac fibrosis in the angiotensin II-induced experimental hypertension model.

At baseline, Zyxko and WT mice showed comparable systolic and diastolic blood pressure levels in all three age groups as well as a comparable systolic cardiac function. However, in Zyxko mice both left ventricular filling velocities in diastole were significantly reduced pointing to a possible impairment in diastolic cardiac function[131–134]. This phenotype at baseline, possible diastolic dysfunction with preserved systolic function, is reminiscent of the human condition of restrictive cardiomyopathy

(RCM). RCM is a disease of the myocardium which is characterized by restricted ventricular filling due to increased ventricular stiffness. RCM is not a frequent form of cardiac dysfunction; however, the prognosis is quite poor[146]. RCM in the Zyxko mice might be attributed to a pro-fibrotic myocardium already in young and unchallenged animals.

After the 14-day angiotensin II exposure, changes in blood pressure were comparable in WT and Zyxko mice in all age groups, i.e. they were all clearly hypertensive. Cardiac systolic performance was comparable at 3 months, started to be deregulated at 6 months and was significantly impaired at 12 months of age in Zyxko animals. Interestingly, angiotensin II treatment also significantly reduced both the passive (E) and active (A) left ventricular velocities in diastole both in wild type and Zyxko mice. In the literature, for the same dose of angiotensin II and duration of exposure, only reductions in the A level have been reported[147]. This ambiguity might come from the different genetic backgrounds of the mice under investigation. To analyze cardiac diastolic function, the E/A ratio is the most frequently used indicator. However, after angiotensin II treatment, both wild type and Zyxko mice showed similar E/A ratios between 1 and 2, indicative of a normal diastolic performance. Of note, however, is that the magnitude of reduction of these velocities in angiotensin II-treated Zyxko mice was much less as compared to the wild type control mice. Less reduction in these two velocities in the Zyxko mice might be ascribed to an impairment in left ventricular relaxation in diastole caused by a much stiffer ventricle[131,134]. This assumption is corroborated by the finding in working hearts isolated from DOCA-salt treated 12 months old Zyxko mice that relaxation of the left ventricle in these is about two times slower than in working hearts isolated from age-matched DOCA-salt treated wild type animals[111]. However, to fully prove that diastolic cardiac function in hypertensive Zyxko mice is due to a much stiffer left ventricle further high-resolution ultrasound imaging analyses are necessary.

Somewhat unexpectedly, angiotensin II treatment induced significant cardiac hypertrophy only in wild type mice in all age groups. It was previously shown that angiotensin II type-1 receptor–associated protein (ATRAP) can promote internalization of the AT1 (angiotensin II type-1) receptor and thus prevent development of angiotensin II–induced cardiac hypertrophy, fibrosis, and inflammation[148,149]. However, the rather similar blood pressure elevation in Zyxko and wild type mice essentially eliminates the possibility of a reduced AT1 receptor abundance, e.g. in Zyxko cardiomyocytes. Another possibility could be that Zyxko mice attained the decompensation stage of hypertension-induced cardiac remodeling where the increased loss of cardiomyocyte is compensated by excess cardiac fibrosis[14–16]. This was in fact documented by the quite prominent deposition of fibrillar collagen in the left ventricular myocardium of hypertensive Zyxko mice irrespective of their age. Nonetheless, the overall degree of fibrosis and expression of pro-fibrotic

gene products further increased with age in these animals. This age-dependent pronouncement of cardiac fibrosis might potentiate the development of cardiac dysfunction in older mice.

In pathological settings, alteration of ECM proteins such as collagen in terms of abundance, distribution and degree of crosslinking contributes to the development of both systolic and diastolic heart failure[134]. It has been previously reported that ventricular stiffness positively correlates with the degree of collagen crosslinking in the human failing heart[150–152]. In this context, in Zyxko mouse myocardium there was a quite prominent expression of lysyl oxidase (LOX), one of the major collagen crosslinking enzymes, which further increased with age. LOX is encoded as a pre-proLOX which then undergoes a series of post-translational modifications and finally in the extracellular milieu the active enzyme get secreated[153]. However, catalytically active forms of LOX have also been identified in the cytosolic and nuclear compartments of fibrogenic cells with unspecified substrates[154]. Analogous to extracellular LOX, nuclear LOX also is immunoreactive and sensitive to β-aminopropionitrile (BAPN, broad spectrum LOX inhibitor)[154]. Therefore, in the present study, detection of LOX in the nucleus and cytosol of myocardial cells conforms to the conventional thinking about this enzyme's localization which is associated with its functions.

Distinct LOX expression patterns have been reported to be associated with certain pathological conditions including fibrosis in the heart, lung, liver and kidney in both humans and murine models, tumor progression and metastasis[38,155–158]. In a recent study, it was found that in a mechanically stressed mouse heart LOX can control TGF-β-dependent transformation of fibroblasts to myofibroblasts[37]. Herein, we also observed that cardiac fibroblasts isolated from adult Zyxko mice (3 months old) display significantly higher LOX expression together with that of CTGF and collagen α1 and α3 following TGF-β1 treatment. More strikingly, even in the absence of TGF-β1, Zyxko cardiac fibroblasts revealed a rather high expression of these pro-fibrotic gene products which matched the levels attained in wild type cardiac fibroblasts following TGF-β1 treatment. Higher expression of pro-fibrotic genes under basal condition indicates that the cardiac fibroblasts isolated from Zyxko mice are already committed to transformation into myofibroblasts, and that this process is accentuated in the presence of TGF-β1. A regulatory function of zyxin in epithelial to mesenchymal transition has been reported previously in lung cancer cells. It was found that TGF-β1-dependent expression of zyxin was needed to maintain the balance of integrin α5/β1 thus preventing transition from the epithelial to mesenchymal phenotype[159]. Moreover, in the DOCA-salt model, the left ventricular myocardium of the hypertensive Zyxko mice exhibited an upregulation of TGF-β1 receptor, integrin α5/β1 and the phosphorylated form of focal adhesion kinase (FAK)[111]. During hypertension, mechanical deformation or stretch is directly sensed by integrins and further transduced through signaling molecules attached to the cortical actin cytoskeleton like focal

adhesion kinase (FAK)[160,161]. In fact, the genetic deletion of β-integrin or FAK in mice leads to spontaneous or stress-induced cardiac dysfunction[162–164].

TGF-β1, a locally generated pro-fibrotic cytokine, has been implicated as a major stimulator for the phenotypic modulation of fibroblasts to myofibroblasts. Increased myocardial TGF-β1 expression during cardiac hypertrophy and fibrosis has been shown for humans and experimental animals[165]. Treatment with angiotensin II has been reported to cause upregulation of TGF-β1 in the myocardium to facilitate transformation of cardiac fibroblasts into myofibroblasts[20]. Along these lines, both animal models and clinical studies indicate that the ameliorative effects of ACE inhibitors and AT1 receptor blockers are most likely mediated through antagonism of TGF-β1 and its downstream effects in cardiac cells[166]. Our present findings of an increased pro-fibrotic gene expression in Zyxko cardiac fibroblasts and massive cardiac fibrosis following angiotensin II treatment suggest that zyxin prevents the transformation of cardiac fibroblasts to myofibroblasts. Therefore, in the absence of zyxin, transdifferentiation of cardiac fibroblasts might have been initiated already to get exaggerated in response to angiotensin II to spur cardiac fibrosis and subsequent cardiac dysfunction (Figure 5.3).

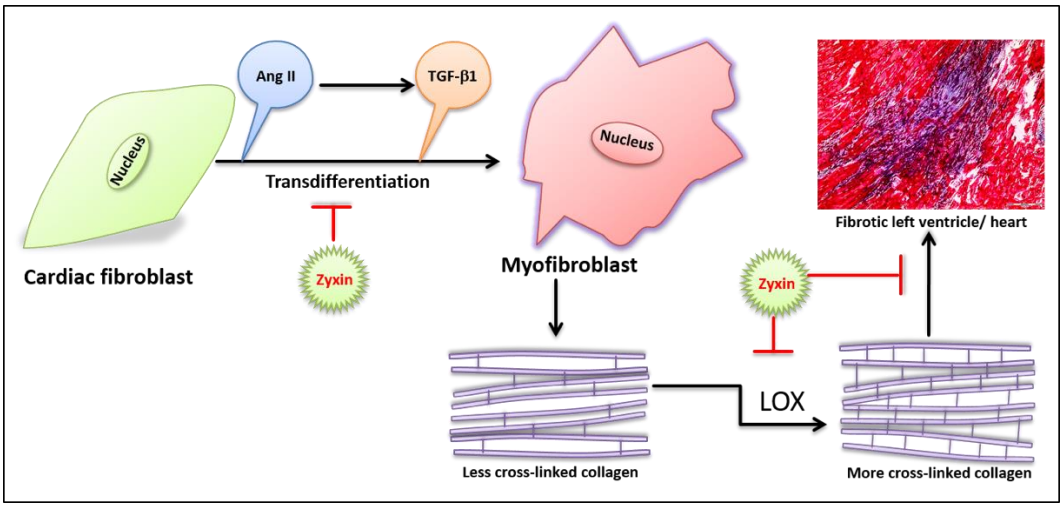

Figure 5.3 Proposed model for the protective role of zyxin in hypertension-induced cardiac fibrosis
Angiotensin II (Ang II) and transformation growth factor β-1 (TGF-β1) can act synergistically to transdiffentiate fibroblasts into myofibroblasts. The newly synthesized collagens by the myofibroblasts can then be further crosslinked to form insoluble collagen fiber deposits. Zyxin may prevent the transdifferentiation as well as the further lysyl oxidase (LOX)-dependent crosslinking of the soluble collagens.

Age-dependent cardiac dysfunction in Zyxko mice might be the consequence of a stiffer left ventricle as a result of this overt collagen deposition. In this context, possible compensatory functions between zyxin and LPP might still be valid, but it is not clear whether this holds true for cardiac myocytes or fibroblasts. Although LPP is denoted as a differentiated smooth muscle cell specific protein and suggested not to be expressed in the heart[96], Hooper *et al.* reported LPP to be present in the myocardium[167,168] . Moreover, it was reported also that LPP expression is higher in cardiac

fibroblasts in comparison to cardiomyocyte, and was upregulated under conditions of pressure overload (transaortic constriction model)[168]. Analyses of older Lppko as well as Lpp/Zyx double-knockout mice will offer a further in-depth understanding of the possible interrelation between LPP and zyxin in cardiac remodeling and the possible target cell for this interaction. In a nutshell, the findings until now suggest the following sequence of events: zyxin-deficient myocardial endothelial cells release increased amounts of CTGF and TGF-β1[57] that prime susceptible zyxin-deficient cardiac fibroblasts to transdifferentiate into myofibroblasts releasing large amounts of collagens and LOX, resulting in a much stiffened ECM which changes the already altered integrin-ECM interaction of the zyxin-null cardiomyocytes so that they undergo increased apoptosis rather than hypertrophy. Further studies will show whether this hypothesis is correct. If so, the mechanotransducer zyxin plays an important role in preventing cardiac remodeling in response to arterial hypertension on several levels and therefore represents an interesting drug target to prevent cardiomyopathies and ultimately heart failure.

6 Concluding remarks

In this study, we have observed a protective role for two members of the zyxin family of LIM-domain containing proteins, zyxin and LPP, in the development of hypertension induced cardiovascular remodeling in a redundant fashion. Although both zyxin and LPP are ubiquitously expressed during embryonic development as well as in adults, a differential tissue distribution of zyxin and LPP was reported. The level of zyxin is five times higher than that of LPP in fibroblasts[91], whereas LPP is highly expressed in smooth muscle tissues[96]. Still controversial, LPP has been reported to be absent in the heart[91]. In experimental hypertension models, mice lacking functional zyxin displayed a vascular phenotype in very old animals (18 months old) but a cardiac phenotype in animals as young as 3 months of age. On the other hand, young Lppko mice (3 months old) reveal some changes as compared to age-matched wild type or zyxin knockout mice that may point to the development of a vascular phenotype.

The differential temporal appearance of these two hypertension-induced phenotypes can be correlated with the degree of zyxin and LPP abundance inside the cells regulating the pathogenesis. To develop a vascular phenotype, VSMCs are the main contributor, hence, LPP may have a stronger potential to suppress the vascular phenotype developing in Zyxko mice until the very old age. Conversely, the higher abundance of LPP and subsequent lack of a complete functional compensation by zyxin in VSMCs may result in the earlier onset of the vascular phenotype in Lppko mice. Cardiac fibroblasts might be the principal regulators of hypertension-dependent cardiac fibrosis. Therefore, Zyxko mice may be more prone to unveil a cardiac phenotype at much younger age due to an insufficient compensation by LPP in this organ. Nevertheless, analysis of much older Lppko and Lpp/Zyx double-knockout mice is necessary to answer the ever emerging questions regarding their functional compensation, at least, in the context of hypertension induced cardiac remodeling.

7 References

1. Lifton, R., Gharavi, A. & Geller, D. Molecular Mechanisms of Human Hypertension. *Cell* **104,** 545–556 (2001).
2. Jeannette Naish, D. S. C. *Medical Sciences E-Book,The cardiovascular system*. (2015).
3. WHO, The top 10 cause 0f death. (2017). Available at: http://www.who.int/mediacentre/factsheets/fs310/en/.
4. Humphrey, J. D. Mechanisms of arterial remodeling in hypertension coupled roles of wall shear and intramural stress. *Hypertension* **52,** 195–200 (2008).
5. Owens, G. K., Kumar, M. S. & Wamhoff, B. R. Molecular Regulation of Vascular Smooth Muscle Cell Differentiation in Development and Disease. *Physiol. Rev.* 767–801 (2004). doi:10.1152/physrev.00041.2003
6. Mulvany, M. J. Small artery remodeling and significance in the development of hypertension. *News Physiol. Sci.* **17,** 105–9 (2002).
7. Lehoux, S., Castier, Y. & Tedgui, A. Molecular mechanisms of the vascular responses to haemodynamic forces. *J. Intern. Med.* **259,** 381–92 (2006).
8. Haga, J. H., Li, Y. J. & Chien, S. Molecular basis of the effects of mechanical stretch on vascular smooth muscle cells. *J. Biomech.* **40,** 947–60 (2007).
9. Regan, C. P., Adam, P. J., Madsen, C. S. & Owens, G. K. Molecular mechanisms of decreased smooth muscle differentiation marker expression after vascular injury. *J. Clin. Invest.* **106,** 1139–1147 (2000).
10. Rensen, S. S. M., Doevendans, P. A. F. M. & van Eys, G. J. J. M. Regulation and characteristics of vascular smooth muscle cell phenotypic diversity. *Netherlands Hear. J.* **15,** 100–8 (2007).
11. Huelsz-Prince, G., Belkin, A. M., Vanbavel, E. & Bakker, E. N. T. P. Activation of extracellular transglutaminase 2 by mechanical force in the arterial wall. *J. Vasc. Res.* **50,** 383–395 (2013).
12. Belo, V. A., Guimarães, D. A. & Castro, M. M. Matrix Metalloproteinase 2 as a Potential Mediator of Vascular Smooth Muscle Cell Migration and Chronic Vascular Remodeling in Hypertension. *J. Vasc. Res.* **52,** 221–231 (2015).
13. Burchfield, J. S., Xie, M. & Hill, J. A. Pathological ventricular remodeling: Mechanisms: Part 1 of 2. *Circulation* **128,** 388–400 (2013).
14. Lips, D. J., DeWindt, L. J., Van Kraaij, D. J. W. & Doevendans, P. A. Molecular determinants of myocardial hypertrophy and failure: Alternative pathways for beneficial and maladaptive hypertrophy. *Eur. Heart J.* **24,** 883–896 (2003).
15. Fan, D., Takawale, A., Lee, J. & Kassiri, Z. Cardiac fibroblasts, fibrosis and extracellular matrix remodeling in heart disease. *Fibrogenesis Tissue Repair* **5,** 1–13 (2012).
16. Leask, A. Getting to the heart of the matter: New insights into cardiac fibrosis. *Circ. Res.* **116,** 1269–1276 (2015).
17. Tomasek, J. J., Gabbiani, G., Hinz, B., Chaponnier, C. & Brown, R. A. Myofibroblasts and mechano-regulation of connective tissue remodelling. *Nat. Rev. Mol. Cell Biol.* **3,** 349–63 (2002).
18. Travers, J. G., Kamal, F. A., Robbins, J., Yutzey, K. E. & Blaxall, B. C. Cardiac fibrosis: The fibroblast awakens. *Circ. Res.* **118,** 1021–1040 (2016).
19. Baum, J. & Duffy, H. S. Fibroblasts and myofibroblasts: what are we talking about? *J. Cardiovasc. Pharmacol.* **57,** 376–9 (2011).
20. Berk, B. C., Fujiwara, K. & Lehoux, S. ECM remodeling in hypertensive heart disease. *J. Clin. Invest.* **117,** 568–575 (2007).
21. Santiago, J. J. *et al.* Cardiac fibroblast to myofibroblast differentiation in vivo and in vitro: Expression of focal adhesion components in neonatal and adult rat ventricular myofibroblasts. *Dev. Dyn.* **239,** 1573–1584 (2010).

22. Zeisberg, E. M. & Kalluri, R. Origins of cardiac fibroblasts. *Circ Res* **107,** 1304–1312 (2010).
23. Leask, A. & Abraham, D. j. TGF- signaling and the fibrotic response. *FASEB J.* **18,** 816–827 (2004).
24. Petrov, V. V, Fagard, R. H. & Lijnen, P. J. Stimulation of collagen production by transforming growth factor-beta1 during differentiation of cardiac fibroblasts to myofibroblasts. *Hypertension* **39,** 258–63 (2002).
25. Mulvany, M. J. Small artery remodelling in hypertension. *Basic Clin. Pharmacol. Toxicol.* **110,** 49–55 (2012).
26. Wang, M., Kim, S. H., Monticone, R. E. & Lakatta, E. G. Matrix metalloproteinases promote arterial remodeling in aging, hypertension, and atherosclerosis. *Hypertension* **65,** 698–703 (2015).
27. Kuzuya, M. & Iguchi, A. Role of matrix metalloproteinases in vascular remodeling. *J. Atheroscler. Thromb.* **10,** 275–282 (2003).
28. Galis, Z. S. & Khatri, J. J. Matrix metalloproteinases in vascular remodeling and atherogenesis: the good, the bad, and the ugly. *Circ. Res.* **90,** 251–262 (2002).
29. Miranti, C. K. & Brugge, J. S. Sensing the environment: a historical perspective on integrin signal transduction. *Nat. Cell Biol.* **4,** 83–90 (2002).
30. Bakker, E. N. T. P. *et al.* Small artery remodeling depends on tissue-type transglutaminase. *Circ. Res.* **96,** 119–126 (2005).
31. Nurminskaya, M. V. & Belkin, A. M. *Cellular functions of tissue transglutaminase*. *International Review of Cell and Molecular Biology* **294,** (2013).
32. Martinez-Lemus, L. a. & Galiñanes, E. L. Matrix metalloproteinases and small artery remodeling. *Drug Discov. Today Dis. Model.* **8,** 21–28 (2011).
33. Cho, A. & Reidy, M. A. Matrix metalloproteinase-9 is necessary for the regulation of smooth muscle cell replication and migration after arterial injury. *Circ. Res.* **91,** 845–851 (2002).
34. Iwanaga, Y. *et al.* Excessive activation of matrix metalloproteinases coincides with left ventricular remodeling during transition from hypertrophy to heart failure in hypertensive rats. *J. Am. Coll. Cardiol.* **39,** 1384–1391 (2002).
35. Janicki, J. S. & Brower, G. L. The role of myocardial fibrillar collagen in ventricular remodeling and function. *J. Card. Fail.* **8,** S319–S325 (2002).
36. Swaney, J. S. *et al.* Inhibition of cardiac myofibroblast formation and collagen synthesis by activation and overexpression of adenylyl cyclase. *Proc. Natl. Acad. Sci. U. S. A.* **102,** 437–42 (2005).
37. Yang, J. *et al.* Targeting LOXL2 for cardiac interstitial fibrosis and heart failure treatment. *Nat. Commun.* **7,** 13710 (2016).
38. González-Santamaría, J. *et al.* Matrix cross-linking lysyl oxidases are induced in response to myocardial infarction and promote cardiac dysfunction. *Cardiovasc. Res.* **109,** 67–78 (2016).
39. Ahmed, S. H. *et al.* Matrix metalloproteinases/tissue inhibitors of metalloproteinases: Relationship between changes in proteolytic determinants of matrix composition and structural, functional, and clinical manifestations of hypertensive heart disease. *Circulation* **113,** 2089–2096 (2006).
40. Matsusaka, H. *et al.* Targeted deletion of matrix metalloproteinase 2 ameliorates myocardial remodeling in mice with chronic pressure overload. *Hypertension* **47,** 711–717 (2006).
41. Heymans, S. *et al.* Loss or inhibition of uPA or MMP-9 attenuates LV remodeling and dysfunction after acute pressure overload in mice. *Am J Pathol* **166,** 15–25 (2005).
42. Hahn, C. & Schwartz, M. A. Mechanotransduction in vascular physiology and atherogenesis. *Nat Rev Mol Cell Biol* **10,** 53–62 (2009).

43. Ye, G. J. C., Nesmith, A. P. & Parker, K. K. The role of mechanotransduction on vascular smooth muscle myocytes cytoskeleton and contractile function. *Anat. Rec.* **297,** 1758–1769 (2014).
44. Humphrey, J. D., Schwartz, M. A., Tellides, G. & Milewicz, D. M. Role of mechanotransduction in vascular biology: Focus on thoracic aortic aneurysms and dissections. *Circ. Res.* **116,** 1448–1461 (2015).
45. Katsumi, A., Orr, W., Tzimas, E. & Schwartz, M. A. Integrins in Mechanotransduction. *J. Biol. Chem.* **279,** 12001–12004 (2003).
46. Kuo, J. C. Focal adhesions function as a Mechanosensor. *Prog. Mol. Biol. Transl. Sci.* **126,** 55–73 (2014).
47. Romer, L. H., Birukov, K. G. & Garcia, J. G. N. Focal adhesions: Paradigm for a signaling nexus. *Circ. Res.* **98,** 606–616 (2006).
48. Schwartz, M. A. Integrins and extracellular matrix in mechanotransduction. *Cold Spring Harb. Perspect. Biol.* **2,** (2010).
49. Hirata, H., Sokabe, M. & Lim, C. T. in *Progress in molecular biology and translational science* 135–154 (2014).
50. Kanchanawong, P. *et al.* Nanoscale architecture of integrin-based cell adhesions. *Nature* **468,** 580–4 (2010).
51. Beckerle, M. C. Zyxin: zinc fingers at sites of cell adhesion. *Bioessays* **19,** 949–957 (1997).
52. Yoshigi, M., Hoffman, L. M., Jensen, C. C., Yost, H. J. & Beckerle, M. C. Mechanical force mobilizes zyxin from focal adhesions to actin filaments and regulates cytoskeletal reinforcement. *J. Cell Biol.* **171,** 209–215 (2005).
53. Hirata, H., Tatsumi, H. & Sokabe, M. Zyxin emerges as a key player in the mechanotransduction at cell adhesive structures. *Commun. Integr. Biol.* **1,** 192–5 (2008).
54. Eriksson, M., Taskinen, M. & Leppä, S. Mechanical forces alter zyxin unbinding kinatics with in focal adhesion of living cells. *J. Cell. Physiol.* **207,** 12–22 (2006).
55. Suresh Babu, S. *et al.* Mechanism of stretch-induced activation of the mechanotransducer zyxin in vascular cells. *Sci. Signal.* **5,** ra91 (2012).
56. Cattaruzza, M., Lattrich, C. & Hecker, M. Focal Adhesion Protein Zyxin is a Mechanosensitive Modulator of Gene Expression in Vascular Smooth Muscle Cells. *Hypertension* **43,** 726–730 (2004).
57. Wójtowicz, A. *et al.* Zyxin mediation of stretch-induced gene expression in human endothelial cells. *Circ. Res.* **107,** 898–902 (2010).
58. Ghosh, S. *et al.* Loss of the Mechanotransducer Zyxin Promotes a Synthetic Phenotype of Vascular Smooth Muscle Cells. *J. Am. Heart Assoc.* **4,** e001712–e001712 (2015).
59. Kadrmas, J. L. & Beckerle, M. C. The LIM domain: from the cytoskeleton to the nucleus. *Nat. Rev. Mol. Cell Biol.* **5,** 920–31 (2004).
60. Smith, M. A., Hoffman, L. M. & Beckerle, M. C. LIM proteins in actin cytoskeleton mechanoresponse. *Trends Cell Biol.* 1–9 (2014). doi:10.1016/j.tcb.2014.04.009
61. Kanungo, J., Pratt, S. J., Marie, H. & Longmore, G. D. Ajuba, a cytosolic LIM protein, shuttles into the nucleus and affects embryonal cell proliferation and fate decisions. *Mol. Biol. Cell* **11,** 3299–3313 (2000).
62. Goyal, R. K. *et al.* Ajuba, a novel LIM protein, interacts with Grb2, augments mitogen-activated protein kinase activity in fibroblasts, and promotes meiotic maturation of Xenopus oocytes in a Grb2- and Ras-dependent manner. *Mol. Cell. Biol.* **19,** 4379–4389 (1999).
63. Pratt, S. J. *et al.* The LIM protein Ajuba influences p130Cas localization and Rac1 activity during cell migration. *J. Cell Biol.* **168,** 813–824 (2005).
64. Shi, X. *et al.* AJUBA promotes the migration and invasion of esophageal squamous cell carcinoma cells through upregulation of MMP10 and MMP13 expression. *Oncotarget* **7,** 36407–36418 (2016).

65. Jagannathan, R. *et al.* AJUBA LIM Proteins Limit Hippo Activity in Proliferating Cells by Sequestering the Hippo Core Kinase Complex in the Cytosol. *Mol. Cell. Biol.* **36,** 2526–42 (2016).
66. Jia, H. *et al.* The LIM protein AJUBA promotes colorectal cancer cell survival through suppression of JAK1/STAT1/IFIT2 network. *Oncogene* **36,** 2655–2666 (2016).
67. Mayank, A. K., Sharma, S., Deshwal, R. K. & Lal, S. K. LIMD1 antagonizes E2F1 activity and cell cycle progression by enhancing Rb function in cancer cells. *Cell Biol. Int.* **38,** 809–817 (2014).
68. Huggins, C. J. & Andrulis, I. L. Cell cycle regulated phosphorylation of LIMD1 in cell lines and expression in human breast cancers. *Cancer Lett.* **267,** 55–66 (2008).
69. Sharp, T. V *et al.* LIM domains-containing protein 1 (LIMD1), a tumor suppressor encoded at chromosome 3p21.3, binds pRB and represses E2F-driven transcription. *Proc. Natl. Acad. Sci. U. S. A.* **101,** 16531–6 (2004).
70. Srichai, M. B. *et al.* A WT1 Co-regulator Controls Podocyte Phenotype by Shuttling between Adhesion Structures and Nucleus. *J. Biol. Chem.* **279,** 14398–14408 (2004).
71. James, V. *et al.* LIM-domain proteins, LIMD1, Ajuba, and WTIP are required for microRNA-mediated gene silencing. *Proc. Natl. Acad. Sci. U. S. A.* **107,** 12499–12504 (2010).
72. Wu, C. Migfilin and its binding partners: from cell biology to human diseases. *J. Cell Sci.* **118,** 659–64 (2005).
73. Tu, Y., Wu, S., Shi, X., Chen, K. & Wu, C. Migfilin and Mig-2 link focal adhesions to filamin and the actin cytoskeleton and function in cell shape modulation. *Cell* **113,** 37–47 (2003).
74. Brahme, N. N. *et al.* Kindlin binds migfilin tandem LIM domains and regulates migfilin focal adhesion localization and recruitment dynamics. *J. Biol. Chem.* **288,** 35604–35616 (2013).
75. Akazawa, H. *et al.* A novel LIM protein Cal promotes cardiac differentiation by association with CSX/NKX2-5. *J. Cell Biol.* **164,** 395–405 (2004).
76. Haubner, B. J. *et al.* In vivo cardiac role of migfilin during experimental pressure overload. *Cardiovasc. Res.* **106,** 398–407 (2015).
77. Gkretsi, V., Stylianou, A. & Stylianopoulos, T. Vasodilator-Stimulated Phosphoprotein (VASP) depletion from breast cancer MDA-MB-231 cells inhibits tumor spheroid invasion through downregulation of Migfilin, β-catenin and urokinase-plasminogen activator (uPA). *Exp. Cell Res.* **352,** 281–292 (2017).
78. Wang, Y. & Gilmore, T. D. LIM domain protein Trip6 has a conserved nuclear export signal, nuclear targeting sequences, and multiple transactivation domains. *Biochim. Biophys. Acta - Mol. Cell Res.* **1538,** 260–272 (2001).
79. Kassel, O. *et al.* A nuclear isoform of the focal adhesion LIM-domain protein Trip6 integrates activating and repressing signals at AP-1- and NF-kappaB-regulated promoters. *Genes Dev.* **18,** 2518–2528 (2004).
80. Wang, Y., Dooher, J. E., Koedood Zhao, M. & Gilmore, T. D. Characterization of mouse Trip6: a putative intracellular signaling protein. *Gene* **234,** 403–9 (1999).
81. Bai, C., Ohsugi, M., Abe, Y. & Yamamoto, T. ZRP-1 controls Rho GTPase-mediated actin reorganization by localizing at cell-matrix and cell-cell adhesions. *J. Cell Sci.* **120,** 2828–37 (2007).
82. Yi, J. *et al.* Members of the zyxin family of LIM proteins interact with members of the p130Cas family of signal transducers. *J. Biol. Chem.* **277,** 9580–9589 (2002).
83. Lin, V. T. G. & Lin, F. TRIP6: an adaptor protein that regulates cell motility, antiapoptotic signaling and transcriptional activity. *Cell. Signal.* **23,** 1691–7 (2011).
84. Lin, F.-T., Lin, V. Y., Lin, V. T. & Lin, W.-C. TRIP6 antagonizes the recruitment of A20 and CYLD to TRAF6 to promote the LPA2 receptor-mediated TRAF6 activation. *Cell Discov.* **2,** 15048 (2016).

85. Kemler, D., Dahley, O., Roßwag, S., Litfin, M. & Kassel, O. The LIM domain protein nTRIP6 acts as a co-repressor for the transcription factor MEF2C in myoblasts. *Sci. Rep.* **6,** 27746 (2016).
86. Diefenbacher, M. *et al.* Restriction to Fos family members of Trip6-dependent coactivation and glucocorticoid receptor-dependent trans-repression of activator protein-1. *Mol Endocrinol* **22,** 1767–1780 (2008).
87. Sheppard, S. A., Savinova, T. & Loayza, D. TRIP6 and LPP, but not Zyxin, are present at a subset of telomeres in human cells. *Cell Cycle* **10,** 1726–1730 (2011).
88. Dahlen, A. Fusion, Disruption, and Expression of HMGA2 in Bone and Soft Tissue Chondromas. *Mod. Pathol.* **16,** 1132–1140 (2003).
89. Petit, M. M., Mols, R., Schoenmakers, E. F., Mandahl, N. & Van de Ven, W. J. LPP, the preferred fusion partner gene of HMGIC in lipomas, is a novel member of the LIM protein gene family. *Genomics* **36,** 118–29 (1996).
90. Dahéron, L. *et al.* Human LPP gene is fused to MLL in a secondary acute leukemia with a t(3;11) (q28;q23). *Genes Chromosomes and Cancer* **31,** 382–389 (2001).
91. Petit, M. M. *et al.* LPP, an actin cytoskeleton protein related to zyxin, harbors a nuclear export signal and transcriptional activation capacity. *Mol. Biol. Cell* **11,** 117–29 (2000).
92. Guo, B. *et al.* The LIM Domain Protein LPP Is a Coactivator for the ETS Domain Transcription Factor PEA3. *Mol. Cell. Biol.* **26,** 4529–4538 (2006).
93. Petit, M. M. R., Meulemans, S. M. P. & Van de Ven, W. J. M. The focal adhesion and nuclear targeting capacity of the LIM-containing lipoma-preferred partner (LPP) protein. *J. Biol. Chem.* **278,** 2157–68 (2003).
94. Li, B., Zhuang, L., Reinhard, M. & Traueb, B. The lipoma preferred partner LPP interacts with alpha-actinin. *J. Cell Sci.* **116,** 1359–1366 (2003).
95. Hansen, M. D. H. & Beckerle, M. C. alpha-Actinin links LPP, but not zyxin, to cadherin-based junctions. *Biochem. Biophys. Res. Commun.* **371,** 144–8 (2008).
96. Gorenne, I. *et al.* LPP, a LIM protein highly expressed in smooth muscle. *Am. J. Physiol. Cell Physiol.* **285,** C674-85 (2003).
97. Nelander, S., Mostad, P. & Lindahl, P. Prediction of Cell Type-Specific Gene Modules : Identification and Initial Characterization of a Core Set of Smooth Muscle-Specific Genes. *Genome Res.* 1838–1854 (2003). doi:10.1101/gr.1197303
98. Gorenne, I. *et al.* LPP expression during in vitro smooth muscle differentiation and stent-induced vascular injury. *Circ. Res.* **98,** 378–385 (2006).
99. Petit, M. M. R. *et al.* Smooth muscle expression of lipoma preferred partner is mediated by an alternative intronic promoter that is regulated by serum response factor/myocardin. *Circ. Res.* **103,** 61–9 (2008).
100. Vervenne, H. B. V. K. *et al.* Lpp is involved in Wnt/PCP signaling and acts together with Scrib to mediate convergence and extension movements during zebrafish gastrulation. *Dev. Biol.* **320,** 267–277 (2008).
101. Ngan, E., Northey, J. J., Brown, C. M., Ursini-Siegel, J. & Siegel, P. M. A complex containing LPP and α-actinin mediates TGFβ-induced migration and invasion of ErbB2-expressing breast cancer cells. *Journal of cell science* **126,** 1981–91 (2013).
102. Ngan, E. *et al.* LPP is a Src substrate required for invadopodia formation and efficient breast cancer lung metastasis. *Nat. Commun.* **8,** 15059 (2017).
103. Vervenne, H. B. V. K. *et al.* Targeted disruption of the mouse Lipoma Preferred Partner gene. *Biochem. Biophys. Res. Commun.* **379,** 368–373 (2009).
104. Hoffman, L. M., Jensen, C. C., Chaturvedi, A., Yoshigi, M. & Beckerle, M. C. Stretch-induced actin remodeling requires targeting of zyxin to stress fibers and recruitment of actin regulators. *Mol. Biol. Cell* **23,** 1846–59 (2012).
105. Macalma, T. *et al.* Molecular characterization of human zyxin. *J. Biol. Chem.* **271,** 31470–8 (1996).

106. Drees, B. *et al.* Characterization of the interaction between zyxin and members of the Ena/vasodilator-stimulated phosphoprotein family of proteins. *J. Biol. Chem.* **275,** 22503–22511 (2000).
107. Smith, M. a *et al.* A zyxin-mediated mechanism for actin stress fiber maintenance and repair. *Dev. Cell* **19,** 365–76 (2010).
108. Han, X. *et al.* Zyxin regulates endothelial von Willebrand factor secretion by reorganizing actin filaments around exocytic granules. *Nat. Commun.* **8,** 14639 (2017).
109. Nix, D. A. & Beckerle, M. C. Nuclear-cytoplasmic shuttling of the focal contact protein, zyxin: a potential mechanism for communication between sites of cell adhesion and the nucleus. *J. Cell Biol.* **138,** 1139–47 (1997).
110. Hoffman, L. M. *et al.* Targeted Disruption of the Murine zyxin Gene. *Mol. Cell. Biol.* **23,** 70–79 (2003).
111. Ghosh, S. Role of the focal adhesion protein zyxin in hypertension-induced cardiovascular remodelling. *PhD Diss.* (2015).
112. Korff, T. & Augustin, H. G. Integration of endothelial cells in multicellular spheroids prevents apoptosis and induces differentiation. *J. Cell Biol.* **143,** 1341–1352 (1998).
113. Arnold, C. *et al.* RGS5 promotes arterial growth during arteriogenesis. *EMBO Mol. Med.* **6,** 1075–89 (2014).
114. Livak, K. J. & Schmittgen, T. D. Analysis of relative gene expression data using real-time quantitative PCR and the 2(-Delta Delta C(T)) Method. *Methods* **25,** 402–8 (2001).
115. Scherer, C. *et al.* Arterial wall stress controls NFAT5 activity in vascular smooth muscle cells. *J. Am. Heart Assoc.* **3,** (2014).
116. Hadler-Olsen, E. *et al.* Gelatin in situ zymography on fixed, paraffin-embedded tissue: zinc and ethanol fixation preserve enzyme activity. *J. Histochem. Cytochem.* **58,** 29–39 (2010).
117. Johns, C., Gavras, I., Handy, E. D., Salomao, A. & Gavras, H. Models of experimental hypertension in mice. *Hypertension* **28,** 1064–1069 (1996).
118. Beggah, A. T. *et al.* Reversible cardiac fibrosis and heart failure induced by conditional expression of an antisense mRNA of the mineralocorticoid receptor in cardiomyocytes. *Proc. Natl. Acad. Sci. U. S. A.* **99,** 7160–7165 (2002).
119. Pampaloni, F., Reynaud, E. G. & Stelzer, E. H. K. The third dimension bridges the gap between cell culture and live tissue. *Nat. Rev. Mol. Cell Biol.* **8,** 839–845 (2007).
120. Renfranz, P. J., Blankman, E. & Beckerle, M. C. The cytoskeletal regulator zyxin is required for viability in Drosophila melanogaster. *Anat. Rec.* **293,** 1455–1469 (2010).
121. Lecroisey, C. *et al.* ZYX-1, the unique zyxin protein of Caenorhabditis elegans, is involved in dystrophin-dependent muscle degeneration. *Mol. Biol. Cell* **24,** 1232–1249 (2013).
122. Renfranz, P. J., Siegrist, S. E., Stronach, B. E., Macalma, T. & Beckerle, M. C. Molecular and phylogenetic characterization of Zyx102, a Drosophila orthologue of the zyxin family that interacts with Drosophila Enabled. *Gene* **305,** 13–26 (2003).
123. Owens, G. K., Kumar, M. S. & Wamhoff, B. R. Molecular Regulation of Vascular Smooth Muscle Cell Differentiation in Development and Disease. *Physiol. Rev.* **84,** 767–801 (2004).
124. Grunewald, T. G., Pasedag, S. M. & Butt, E. Cell Adhesion and Transcriptional Activity - Defining the Role of the Novel Protooncogene LPP. *Transl. Oncol.* **2,** 107–16 (2009).
125. Kuriyama, S. *et al.* LPP inhibits collective cell migration during lung cancer dissemination. *Oncogene* **35,** 952–964 (2015).
126. Janssens, V. *et al.* PP2A binds the LIM-domains of Lipoma Preferred Partner via its PR130/B" subunit to regulate cell adhesion and migration. *J. Cell Sci.* **129,** 1605–1618 (2016).
127. Liang, C. C., Park, A. Y. & Guan, J. L. In vitro scratch assay: a convenient and inexpensive method for analysis of cell migration in vitro. *Nat. Protoc.* **2,** 329–33 (2007).

128. Kramer, N. *et al.* In vitro cell migration and invasion assays. *Mutat. Res.* 10–24 (2013). doi:10.3791/51046
129. Spin, J. M. *et al.* Transcriptional profiling of in vitro smooth muscle cell differentiation identifies specific patterns of gene and pathway activation. *Physiol Genomics* 292–302 (2005). doi:10.1152/physiolgenomics.00148.2004
130. Simone, G. *et al.* Relation of heart rate to left ventricular dimensions in normotensive, normal-weight children, adolescents and adults. *Ital Hear. J. I* 599–604. (2001).
131. Mottram, P. M. & Marwick, T. H. Assessment of diastolic function: what the general cardiologist needs to know. *Heart* **91,** 681–95 (2005).
132. Garcia, M. J., Thomas, J. D. & Klein, A. L. New doppler echocardiographic applications for the study of diastolic function. *J. Am. Coll. Cardiol.* **32,** 865–875 (1998).
133. Kass, D. A., Bronzwaer, J. G. F. & Paulus, W. J. What mechanisms underlie diastolic dysfunction in heart failure? *Circ. Res.* **94,** 1533–1542 (2004).
134. Zile, M. R. & Brutsaert, D. L. New concepts in diastolic dysfunction and diastolic heart failure: Part II. Causal mechanisms and treatment. *Circulation* **105,** 1503–1508 (2002).
135. Calabia, J. *et al.* The relationship between renal resistive index, arterial stiffness, and atherosclerotic burden: The link between macrocirculation and microcirculation. *J. Clin. Hypertens.* **16,** 186–191 (2014).
136. Viazzi, F., Leoncini, G., Derchi, L. E. & Pontremoli, R. Ultrasound Doppler renal resistive index: a useful tool for the management of the hypertensive patient. *J. Hypertens.* **32,** 149–53 (2014).
137. dos Reis, G. F. M. *et al.* Spectral analysis of femoral artery blood flow waveforms of conscious domestic cats. *J. Feline Med. Surg.* **16,** 972–8 (2014).
138. Bude, R. O. & Rubin, J. M. Relationship between the Resistive Index and Vascular Compliance and Resistance. *Radiology* **211,** 411–417 (1999).
139. Kato, T. *et al.* Atrial natriuretic peptide promotes cardiomyocyte survival by cGMP-dependent nuclear accumulation of zyxin and Akt. *J. Clin. Invest.* **115,** (2005).
140. Nakamura, T. *et al.* Critical role of apoptosis signal-regulating kinase 1 in aldosterone/salt-induced cardiac inflammation and fibrosis. *Hypertension* **54,** 544–551 (2009).
141. Kurdi, M. & Booz, G. W. New take on the role of angiotensin II in cardiac hypertrophy and fibrosis. *Hypertension* **57,** 1034–1038 (2011).
142. Zhang, A. Di *et al.* Cross-talk between mineralocorticoid and angiotensin II signaling for cardiac remodeling. *Hypertension* **52,** 1060–1067 (2008).
143. Izumiya, Y. *et al.* Apoptosis Signal-Regulating Kinase 1 Plays a Pivotal Role in Angiotensin II-Induced Cardiac Hypertrophy and Remodeling. *Circ. Res.* **93,** 874–883 (2003).
144. Dornas, W. C. & Silva, M. E. Animal models for the study of arterial hypertension. *J. Biosci.* **36,** 731–737 (2011).
145. Leong, X. F., Ng, C. Y. & Jaarin, K. Animal Models in Cardiovascular Research: Hypertension and Atherosclerosis. *Biomed Res. Int.* **2015,** (2015).
146. Jean-Charles, P. Y., Li, Y. J., Nan, C. L. & Huang, X. P. Insights into restrictive cardiomyopathy from clinical and animal studies. *J. Geriatr. Cardiol.* **8,** 168–183 (2011).
147. Glenn, D. J. *et al.* Cardiac Steatosis Potentiates Angiotensin II Effects in the Heart. *Am. J. Physiol. Heart Circ. Physiol.* H339–H350 (2014). doi:10.1152/ajpheart.00742.2014
148. Wakui, H. *et al.* Cardiac-specific activation of angiotensin II type 1 receptor-associated protein completely suppresses cardiac hypertrophy in chronic angiotensin II-infused mice. *Hypertension* **55,** 1157–1164 (2010).
149. Cai, J. *et al.* Targeted expression of receptor-associated late transducer inhibits maladaptive hypertrophy via blocking epidermal growth factor receptor signaling. *Hypertension* **53,** 539–548 (2009).
150. Badenhorst, D. *et al.* Cross-linking influences the impact of quantitative changes in

myocardial collagen on cardiac stiffness and remodelling in hypertension in rats. *Cardiovasc. Res.* **57,** 632–641 (2003).
151. Norton, G. R. *et al.* Myocardial Stiffness Is Attributed to Alterations in Cross-Linked Collagen Rather Than Total Collagen or Phenotypes in Spontaneously Hypertensive Rats. *Circulation* **96,** 1991–1998 (1997).
152. Mäki, J. M. Lysyl oxidases in mammalian development and certain pathological conditions. *Histol. Histopathol.* **24,** 651–660 (2009).
153. Smith-Mungo, L. I. & Kagan, H. M. Lysyl oxidase: Properties, regulation and multiple functions in biology. *Matrix Biol.* **16,** 387–398 (1998).
154. Li, W. *et al.* Localization and activity of lysyl oxidase within nuclei of fibrogenic cells. *Proc. Natl. Acad. Sci. U. S. A.* **94,** 12817–12822 (1997).
155. Rodríguez, C. *et al.* Regulation of lysyl oxidase in vascular cells: Lysyl oxidase as a new player in cardiovascular diseases. *Cardiovasc. Res.* **79,** 7–13 (2008).
156. Hermida, N. *et al.* A synthetic peptide from transforming growth factor-beta 1 type III receptor prevents myocardial fibrosis in spontaneously hypertensive rats. *Cardiovasc. Res.* **81,** 601–609 (2009).
157. Stefanon, I. *et al.* Left and Right Ventricle Late Remodeling Following Myocardial Infarction in Rats. *PLoS One* **8,** (2013).
158. McCormick, R. J., Musch, T. I., Bergman, B. C. & Thomas, D. P. Regional differences in LV collagen accumulation and mature cross-linking after myocardial infarction in rats. *Am. J. Physiol.* **266,** H354-9 (1994).
159. Mise, N. *et al.* Zyxin is a transforming growth factor-beta (TGF-beta)/Smad3 target gene that regulates lung cancer cell motility via integrin alpha5beta1. *J Biol Chem* **287,** 31393–31405 (2012).
160. Heineke, J. & Molkentin, J. D. Regulation of cardiac hypertrophy by intracellular signalling pathways. *Nat. Rev. Mol. Cell Biol.* **7,** 589–600 (2006).
161. Ross, R. S. & Borg, T. K. Integrins and the myocardium. *Circ. Res.* **88,** 1112–9 (2001).
162. Peng, X. *et al.* Inactivation of focal adhesion kinase in cardiomyocytes promotes cardiac eccentric hypertrophy and fibrosis in mice. *Circulation* **112,** U60–U60 (2005).
163. Katsumi, A., Naoe, T., Matsushita, T., Kaibuchi, K. & Schwartz, M. A. Integrin activation and matrix binding mediate cellular responses to mechanical stretch. *J. Biol. Chem.* **280,** 16546–16549 (2005).
164. Manso, A. M., Elsherif, L., Kang, S. M. & Ross, R. S. Integrins, membrane-type matrix metalloproteinases and ADAMs: Potential implications for cardiac remodeling. *Cardiovasc. Res.* **69,** 574–584 (2006).
165. Kuwahara, F., Kai, H., Tokuda, K. & Kai, M. Transforming Growth Factor-β Function Blocking Prevents Myocardial Fibrosis and Diastolic Dysfunction in pressure overloaded rats. *Circulation* 130–135 (2002). doi:10.1161/01.CIR.0000020689.12472.E0
166. Khan, R. & Sheppard, R. Fibrosis in heart disease: Understanding the role of transforming growth factor-beta 1 in cardiomyopathy, valvular disease and arrhythmia. *Immunology* **118,** 10–24 (2006).
167. Hooper, C. L., Dash, P. R. & Boateng, S. Y. Lipoma preferred partner is a mechanosensitive protein regulated by nitric oxide in the heart. *FEBS Open Bio* **2,** 135–44 (2012).
168. Hooper, C. L., Paudyal, A., Dash, P. R. & Boateng, S. Y. Modulation of stretch-induced myocyte remodeling and gene expression by nitric oxide: a novel role for lipoma preferred partner in myofibrillogenesis. *Am. J. Physiol. Heart Circ. Physiol.* **304,** H1302-13 (2013).

8 Acknowledgements

I would like to express my deepest gratitude to Prof. Dr. Markus Hecker for providing me with this precious opportunity to conduct my doctoral training at the Institute of Physiology and Pathophysiology. This thesis would not have been possible without his mentorship. Thanks for his guidance, support and assurance of a nice working environment throughout my research work.

I would also like to thank Prof. Dr. Thomas Wieland and Prof. Dr. Johannes Backs for their valuable feedback on my work and stimulating discussions during my annual thesis advisory committee (TAC) meetings. Thanks to all principal investigators of the Department of Cardiovascular Physiology, PD Dr. Andreas Wagner, Prof. Dr. Thomas Korff, Dr. Oliver Drews and Dr. Nina Ullrich, for their thought-provoking discussions and experienced advice.

Very big appreciation for Dr. Subhajit Ghosh for his early training at the onset of my doctoral study. I am also grateful to Dr. Caroline Arnold not only for teaching me all the difficult animal surgeries but also for her ready-to-help approach. I thank all my colleagues for their affection during my time in Heidelberg. My present and former colleagues Ake, Anca, Andrea, Anne-Sophie, Anja, Carla, Cheryl, Christoph, Christian, Cordula, Eda, Fan, Felix, Florian, Franziska, Hanna, Hannes, Iva, Johannes, Julian, Laura-Ines, Larissa, Lexiao, Max, Maren, Martin, Miruna, Moritz, Nikolai, Phillip, Prisca, Sebastian, Sibgha, Synje, Tanja are all part of my cherish memories. My special thanks to the technicians, Anita, Gudrun, Franziska, Lidya, Maria, Marie, Nadine and Yvonne. Big thanks for Felicia, for her great technical assistance in the project. My kind regards for Dr. Gerd Koenig, Jan Simon, and Michaela Neidig for their great support. Very big thanks for Barbara Richards, for her smiling face, friendliness and all sorts of official helps to make our life easier.

I am deeply indebted to Renate (my lab mother) for being more than a technical assistant rather being like family. Her smiling face meant a lot to me. I will also take this opportunity to thank all my friends, whom I meet in Heidelberg long away from Bangladesh, for their inspiration, support and make our stay comfortable here. No words would be enough for expressing my thanks and gratitude to my parents and sister, Nurun Nahar, Tajul Islam and Tajmun Nahar Leepa. Thanks for being supportive and make my path always smoother.

Finally, my utmost gratitude is reserved for my husband, Borhan Uddin, for being part of this difficult journey. Thanks for supporting me all the way through this PhD training. I would not have made it without him. I forget all the hardship of life after seeing my daughter Lubaba Borhan Manha‘s face. Thanks to all my friends and colleagues for showing their love and affection to my little ‘princess’.

Last but not least, thanks to almighty ALLAH for considering me worthy of this rich experience and showing me the way.